

UNIVERSIDAD DE INGENIERÍA Y TECNOLOGÍA

BIOENGINEERING DEGREE PROGRAM



**SYNTHESIS AND CHARACTERIZATION OF A
NANO GEL ENCAPSULATING SILICON QUANTUM
DOTS (SIQDS) FOR ENHANCED TARGETED
PHOTODYNAMIC THERAPY IN HELA CANCER
CELLS**

THESIS

To obtain the Professional Engineering Degree in Bioengineering

AUTHOR

Ariana Fernanda Ponce Bohórquez 

SUPERVISOR(S)

Ravin Narain 

ADVISOR(S)

Artjima Ounkaew 

Karen Gonzales Rojas 

Lima - Peru

2024

DECLARACIÓN JURADA

Yo, Karen Nonaquina Gonzales Rojas, identificado con DNI N° 47528581, en mi condición de persona responsable de validar la autenticidad de los trabajos de investigación y tesis de la Universidad de Ingeniería y Tecnología (en adelante, la Universidad), **declaro bajo juramento** lo siguiente:

Que el trabajo de investigación/tesis denominado: "Synthesis and Characterization of a Nanogel Encapsulating Silicon Quantum Dots (SiQDs) for Enhanced Targeted Photodynamic Therapy in HeLa Cancer Cells" ha sido elaborado bajo mi asesoría, por Ariana Ponce Bohórquez, identificado con DNI N° 70656316, para obtener el título profesional de Bioingeniería.

El trabajo de investigación/tesis antes mencionado ha sido sometido a los mecanismos de control y sanciones anti plagio previstos en la normativa interna de la Universidad, encontrándose un porcentaje de similitud de 0%.

En fe de lo cual firmo la presente.

En Barranco, el 09 de enero de 2025

Nonaquina

Firma del asesor

Dedication:

To my family, for encouraging me to follow my dreams and supporting me in every step of my personal and academic journey. Especially to my mom Rosario, for always giving me wise advice and teaching me the value of perseverance through her example. To my dad Tomás, for always being there for me.

Also, to my dear brother Rubén, for accompanying me in my studies in Tacna and Lima. To my cousins Benjamín, Juan Diego, and Leonardo, for motivating me to be a good example for them. To my grandparents for believing in me.

To my friends Augusto, Sebastian C., Rosario, Harold, Edir, Sebastian G., and Mauricio, whom I met at university and who constantly inspire me to be a better version of myself, as well as to my best friends since childhood, Camila and Gabriela, for encouraging me at every stage of my life.

Finally, to my supervisor and advisors from the University of Alberta and UTEC, for their guidance, knowledge, and patience, and for cultivating in me the aspiration to continue in academic research.

Acknowledgements:

I would like to express my most sincere gratitude to all those who played a fundamental role in the completion of this thesis. First, I am profoundly thankful for the Emerging Leaders in the Americas Program (ELAP) scholarship, which allowed me to work as a research assistant under the guidance of exceptional professionals. I am especially grateful to Artjima Ounkaew for her patience and instruction, particularly in silicon quantum dots at the University of Alberta. Her dedication as a researcher has been a continual source of inspiration and guidance for me. Additionally, I extend my gratitude to Ravin Narain for giving me the opportunity to be his intern in the Department of Chemical and Materials Engineering at the University of Alberta. His confidence in my abilities have allowed me to grow both academically and professionally.

I would also like to acknowledge the Provost scholarship from UTEC, which provided financial support for my research project. This scholarship reflects the university's commitment to fostering the development of students' ideas during their academic journey.

I am also thankful to the Internationalization Office at UTEC for providing the necessary tools for students to take advantage of opportunities abroad, thus fostering personal and professional development.

My deepest thanks go to my parents, whose unconditional support and constant encouragement have been fundamental pillars in all my endeavors and dreams. I cannot fail to mention my friends, who have been a constant source of motivation and emotional support throughout this process.

Finally, I express my sincere appreciation to my professors at UTEC, Karen Gonzales, Andrés Arias, and Alberto Donayre. Their dedication, knowledge, and guidance have been crucial in enhancing this thesis and contributing to my formation as a bioengineer.

Contents

| | Page |
|--|-----------|
| RESUMEN | 2 |
| ABSTRACT | 3 |
| CHAPTER I INTRODUCTION | 4 |
| 1.1 Problem formulation | 9 |
| 1.2 Research objectives | 10 |
| 1.3 Hypothesis | 11 |
| 1.4 Justification | 12 |
| 1.5 Scope and limitations | 14 |
| 1.6 Bases of the Bioengineering curriculum | 16 |
| CHAPTER II CRITICAL REVIEW OF THE LITERATURE | 21 |
| CHAPTER III THEORETICAL FRAMEWORK | 28 |
| 3.1 Cancer | 28 |
| 3.2 Conventional Treatments for Cancer | 29 |
| 3.2.1 Chemotherapy | 29 |
| 3.2.2 Radiotherapy | 30 |
| 3.2.3 Surgery | 31 |
| 3.3 Photodynamic Therapy (PDT) | 31 |
| 3.3.1 Principles of Photodynamic Therapy | 31 |
| 3.3.2 Mechanism of Action | 32 |

| | | |
|---------|---|----|
| 3.3.3 | Photosensitizers | 33 |
| 3.3.4 | Administration of Photosensitizers (PSs) | 35 |
| 3.3.4.1 | Administration of PSs via Targeting | 35 |
| 3.3.4.2 | Passive Targeting | 37 |
| 3.3.4.3 | Active Targeting | 38 |
| 3.4 | Administration of PSs by Responses | 39 |
| 3.4.1 | Light Delivery and Dosimetry | 40 |
| 3.4.1.1 | Light Sources for PDT | 41 |
| 3.4.1.2 | Light Delivery Techniques | 41 |
| 3.4.1.3 | Near-Infrared Radiation | 43 |
| 3.4.2 | Reactive Oxygen Species (ROS) | 44 |
| 3.4.2.1 | Types of Reactive Oxygen Species | 45 |
| 3.5 | Silicon Quantum Dots (SiQDs) | 47 |
| 3.5.1 | Properties of Silicon Quantum Dots | 48 |
| 3.5.1.1 | Bright Light Emission | 48 |
| 3.5.1.2 | Long-Term Stability in Photoluminescence (PL) | 48 |
| 3.5.1.3 | Less Toxicity to Cells | 49 |
| 3.5.1.4 | Theranostics | 50 |
| 3.5.2 | SiQD Preparation | 50 |
| 3.5.2.1 | Physical Routes to Synthesizing SiQDs | 50 |
| 3.5.2.2 | Chemical Routes to SiQDs | 51 |
| 3.5.3 | Functionalization of SiQDs | 52 |
| 3.5.4 | SiQDs as Photosensitizers for ROS Production | 53 |
| 3.5.4.1 | Photosensitization Mechanism | 53 |
| 3.5.4.2 | Factors Affecting ROS Generation | 54 |
| 3.6 | Nanogel | 54 |
| 3.6.1 | Types of Nanogels | 55 |
| 3.6.2 | Synthesis of Nanogels | 56 |

| | | |
|-------------------------------|---|-----------|
| 3.6.2.1 | Physical Methods for Nanogel Formation | 56 |
| 3.6.2.2 | Chemical Methods for Nanogel Formation | 56 |
| 3.6.3 | Properties of Nanogels | 58 |
| 3.6.3.1 | Size and Morphology | 58 |
| 3.6.3.2 | High Water Content | 58 |
| 3.6.3.3 | Stimuli-Responsiveness | 58 |
| 3.6.3.4 | High Loading Capacity | 59 |
| 3.7 | RAFT Polymerization Technique | 60 |
| 3.7.1 | Key Elements of RAFT Polymerization | 61 |
| 3.7.1.1 | Crosslinking Agent | 61 |
| 3.7.1.2 | Chain Transfer Agent | 61 |
| 3.7.1.3 | Free Radical Initiator | 61 |
| 3.7.2 | Monomers | 62 |
| 3.7.2.1 | Di(ethylene glycol) methyl ether methacrylate (DEGMA) | 63 |
| 3.7.2.2 | 2-(Methacryloyloxy)ethyl phosphorylcholine (MPC) | 63 |
| 3.7.3 | Polymer | 64 |
| 3.7.4 | Copolymers | 65 |
| 3.8 | Cellular Analysis | 66 |
| 3.8.1 | MTT Assay | 66 |
| CHAPTER IV METHODOLOGY | | 68 |
| 4.1 | Development of Alternatives | 68 |
| 4.1.1 | Nanogel Copolymer Materials | 68 |
| 4.1.1.1 | Polyethylene Glycol (PEG) and Trimethyl Chitosan (TMC) | 68 |
| 4.1.1.2 | DEGMA (Di(ethylene glycol) methyl ether methacrylate) and MPC (2-(Methacryloyloxy)ethyl phosphorylcholine) | 69 |
| 4.1.2 | Nanogel Method of Synthesis | 70 |
| 4.1.2.1 | Atom Transfer Radical Polymerization (ATRP) | 70 |

| | | |
|---------|---|----|
| 4.1.2.2 | Reversible Addition-Fragmentation Chain Transfer (RAFT) Polymerization | 71 |
| 4.2 | Evaluation of Alternative Solutions Based on Engineering Criteria and Characteristics | 71 |
| 4.2.1 | Nanogel Copolymer Materials Analysis | 71 |
| 4.2.2 | Analysis of Nanogel Synthesis Methods | 73 |
| 4.3 | Description of the Research Methodology | 75 |
| 4.4 | Research Characterization | 77 |
| 4.5 | Synthesis and Characterization of Copolymer Nanogel | 79 |
| 4.5.1 | Materials for the Nanogel Structure | 79 |
| 4.5.2 | RAFT Polymerization Process | 79 |
| 4.5.2.1 | Preparation of MPC-macroCTA | 79 |
| 4.5.2.2 | DEGMA Purification | 80 |
| 4.5.2.3 | Nanogel Synthesis | 80 |
| 4.6 | SiQDs Encapsulation and Efficiency Assessment | 83 |
| 4.6.1 | Encapsulation of SiQDs | 83 |
| 4.6.1.1 | Preparation of SiQDs Solution | 83 |
| 4.6.1.2 | Encapsulation Procedure for Acid-SiQDs | 85 |
| 4.6.1.3 | Encapsulation Procedure for Acid-PEO-SiQDs | 86 |
| 4.6.2 | Loading Efficiency Determination | 88 |
| 4.6.2.1 | Encapsulation Efficiency for Acid-SiQDs | 88 |
| 4.6.2.2 | Encapsulation Efficiency for Acid-PEO-SiQDs | 89 |
| 4.6.2.3 | Fluorescence Analysis Protocol | 91 |
| 4.7 | Characterization of Nanogel and SiQDs Encapsulation | 93 |
| 4.7.1 | Dynamic Light Scattering (DLS) | 93 |
| 4.7.2 | Thermogravimetric Analysis (TGA) | 94 |
| 4.7.3 | Nuclear Magnetic Resonance (NMR) | 95 |
| 4.7.3.1 | NMR Sample Preparation | 96 |

| | | |
|--------------------------|--|------------|
| 4.7.3.2 | NMR Spectroscopy Procedure | 97 |
| 4.8 | Biocompatibility Assessment of SiQDs-loaded Nanogel | 98 |
| 4.8.1 | Cell Culture Preparation | 98 |
| 4.8.2 | MTT Assays for Cytotoxicity | 99 |
| 4.8.2.1 | MTT Assay Protocol for HDFa | 99 |
| 4.9 | <i>In vitro</i> Delivery and Photodynamic Therapy Efficacy | 101 |
| 4.9.1 | Cell Culture Preparation | 101 |
| 4.9.2 | Preparation of Nanogel-SiQDs Concentration | 101 |
| 4.9.3 | Photodynamic Therapy Application | 101 |
| 4.9.3.1 | NIR Light Application Protocol | 102 |
| 4.9.4 | MTT Assays for Photodynamic Efficacy | 104 |
| 4.9.4.1 | MTT Assay Protocol for HeLa Cells | 104 |
| 4.9.4.2 | Data Collection and Analysis for Therapeutic Efficacy | 105 |
| 4.10 | Ethical Considerations | 106 |
| CHAPTER V RESULTS | | 108 |
| 5.1 | Synthesis and Characterization of Nanogel | 108 |
| 5.1.1 | Gel Permeation Chromatography (GPC) of MPC-macroCTA Results | 109 |
| 5.1.2 | Synthesis of Copolymer Nanogel | 109 |
| 5.2 | Encapsulation of SiQDs | 111 |
| 5.2.1 | Encapsulation of Acid-SiQDs in the Nanogel | 111 |
| 5.2.2 | Encapsulation of Acid-PEO-SiQDs in the Nanogel | 112 |
| 5.2.3 | Fluorescence Analysis for Acid-SiQDs | 113 |
| 5.2.3.1 | Encapsulation Efficiency for Acid-SiQDs | 116 |
| 5.2.4 | Fluorescence Analysis for Acid-PEO-SiQDs | 117 |
| 5.2.4.1 | Encapsulation Efficiency for Acid-PEO-SiQDs | 119 |
| 5.2.4.2 | Comparison of Encapsulation Efficiencies for Acid-SiQDs and Acid- PEO-SiQDs | 120 |
| 5.3 | Physicochemical Characterization of SiQDs-loaded Nanogel | 121 |

| | |
|--|------------|
| 5.3.1 Particle Size Distribution | 121 |
| 5.3.1.1 Dynamic Light Scattering (DLS) Results of the Nanogel at 25°C | 122 |
| 5.3.1.2 Dynamic Light Scattering (DLS) Results of the Nanogel at 37°C | 123 |
| 5.3.2 Comparison of DLS Results of Nanogel at Different Temperatures | 124 |
| 5.3.2.1 Dynamic Light Scattering (DLS) Results of Acid-SiQDs-loaded Nanogel at 25 °C | 126 |
| 5.3.2.2 Dynamic Light Scattering (DLS) Results of Acid-SiQDs-loaded Nanogel at 37 °C | 128 |
| 5.3.2.3 Comparison of DLS Results for Acid-SiQDs-loaded Nanogel at Different Temperatures | 129 |
| 5.3.3 Thermal Stability | 131 |
| 5.3.3.1 Thermogravimetric Analysis (TGA) Results | 131 |
| 5.3.4 Chemical Structure Analysis | 133 |
| 5.3.4.1 Nuclear Magnetic Resonance (NMR) of Nanogel (NG) | 133 |
| 5.3.4.2 Nuclear Magnetic Resonance (NMR) of Acid-SiQDs | 135 |
| 5.3.4.3 Nuclear Magnetic Resonance (NMR) of Nanogel Encapsulating Acid-Functionalized SiQDs | 137 |
| 5.4 Cell Viability Assessment | 139 |
| 5.4.1 MTT Assay Results for HDFa Cells | 139 |
| 5.5 <i>In Vitro</i> Delivery and Photodynamic Therapy Efficacy | 140 |
| 5.5.1 MTT Assay Results for HeLa Cells | 141 |
| CHAPTER VI DISCUSSION | 143 |
| CONCLUSIONS | 152 |
| RECOMMENDATIONS | 153 |
| ANNEXES | 155 |
| 6.1 Annex 1. Protocol - Gel Permeation Chromatography (GPC) of MPC-macroCTA155 | |
| 6.1.1 Steps for GPC Analysis | 155 |
| 6.1.1.1 Sample Preparation | 155 |

| | | |
|---------|--|-----|
| 6.1.1.2 | Column Selection | 155 |
| 6.1.1.3 | Injection and Elution | 156 |
| 6.1.1.4 | Detection | 156 |
| 6.1.1.5 | Data Analysis | 156 |
| 6.2 | Annex 2. Differential Scanning Calorimetry (DSC) | 157 |
| 6.3 | Annex 3. Statistical Analysis (One-Way ANOVA) | 159 |

List of Tables

| | | |
|-----------|--|-----|
| Table 3.1 | Type I and Type II Reactions in Photodynamic Therapy [83] | 32 |
| Table 3.2 | Formulas of Reactive Oxygen Species (ROS) [104] | 47 |
| Table 3.3 | Nanogel Types and Example Materials. | 55 |
| Table 3.4 | Methods for Nanogel Synthesis [122] | 57 |
| Table 4.1 | Evaluation of Nanogel Copolymer Materials | 72 |
| Table 4.2 | Evaluation of Nanogel Synthesis Methods | 74 |
| Table 4.3 | Surface Functionalization and Concentration of SiQDs | 83 |
| Table 4.4 | Summary of the Number of Samples Used in Fluorescence Analysis | 92 |
| Table 4.5 | Samples for NMR Analysis | 96 |
| Table 5.1 | Nanogel Characterization Parameters | 109 |
| Table 5.2 | Comparison of Fluorescence Intensities for Acid-SiQDs | 114 |
| Table 5.3 | Fluorescence Intensities at Peak Wavelength | 116 |
| Table 5.4 | Comparison of Fluorescence Intensities for Acid-PEO-SiQDs | 117 |
| Table 5.5 | Fluorescence Intensities at Peak Wavelength | 120 |
| Table 5.6 | Comparison of Encapsulation Efficiencies for Acid-SiQDs and Acid-PEO-SiQDs | 121 |
| Table 5.7 | Comparison of Effective Diameter and Polydispersity Index of Nanogel at Different Temperatures | 124 |
| Table 5.8 | Comparison of DLS Results for Acid-SiQDs-loaded Nanogel at 25°C and 37°C | 130 |

| | |
|---|-----|
| Table 6.1 Cell Viability (%) for NG-SiQDs and NG-Acid-PEO-SiQDs under Different Concentrations | 159 |
|---|-----|

List of Figures

| | | |
|-------------|---|----|
| Figure 2.1 | QD–polypeptide nanogel [73] | 26 |
| Figure 3.1 | Comparison between normal cells and cancerous cells [76] | 28 |
| Figure 3.2 | Intravenous chemotherapy [77] | 29 |
| Figure 3.3 | External beam radiation therapy and internal radiation therapy [79] | 30 |
| Figure 3.4 | Mechanism of action of photodynamic therapy (PDT) [83] | 32 |
| Figure 3.5 | Type I and Type II of photodynamic reaction [84] | 33 |
| Figure 3.6 | Chemical structure of Chlorin e6 [87] | 34 |
| Figure 3.7 | Chemical structure of Porphyrin [89] | 34 |
| Figure 3.8 | Chemical structure of Carbon Dots [92] | 35 |
| Figure 3.9 | Therapeutic Application of PDT [93] | 36 |
| Figure 3.10 | Passive targeting of cancer cell [34] | 37 |
| Figure 3.11 | Active targeting of cancer cell [34] | 38 |
| Figure 3.12 | The activation is triggered by the pH response of the tumor microenvironment: (A)Preparation of Ce6- and Gd3+-loaded pH-responsive nanoparticles S-NP. (B) Tumor acidity-responsive S-NP for fluorescence/MR imaging-guided PDT. [94] | 39 |
| Figure 3.13 | Application of a laser to generate necrosis [95] | 40 |
| Figure 3.14 | Delivery systems in clinical PDT for cancerous tumor eradication [97] | 42 |
| Figure 3.15 | Infrared radiation can be subdivided further into three categories: Near infrared, Mid infrared and Far infrared [100] | 44 |
| Figure 3.16 | Reactive oxygen species (ROS) generation [103] | 45 |

| | |
|---|----|
| Figure 3.17 Reactions of chemical species in (ROS) [104] | 46 |
| Figure 3.18 Silicon Quantum Dots [108] | 48 |
| Figure 3.19 Photoluminescence spectrum of silicon quantum dots (SiQDs) showing characteristic peaks for the silicon core, SiO_2 shell, and chitosan layer [111] | 49 |
| Figure 3.20 Delivery systems in clinical PDT for cancerous tumor eradication [109] | 50 |
| Figure 3.21 Functionalization strategies of quantum dot cores [114] | 52 |
| Figure 3.22 Enhancing the generation of reactive oxygen species [117] | 54 |
| Figure 3.23 Nanogel in drug delivery [120] | 55 |
| Figure 3.24 Different biomedical applications based on methods for the synthesis of nanogels [122] | 56 |
| Figure 3.25 Different stimuli-responsive nanogels [23] | 59 |
| Figure 3.26 Reversible addition-fragmentation chain transfer (RAFT) polymerization [129] | 60 |
| Figure 3.27 Functional groups in monomers and polymers [135] | 62 |
| Figure 3.28 Chemical structure of DEGMA [53] | 63 |
| Figure 3.29 Chemical structure of MPC [138] | 64 |
| Figure 3.30 Formation pathways of macromolecular, micromolecular, and nanogels from polymer chains under different reaction conditions [122] | 65 |
| Figure 3.31 Structure of the P(NIPAM-TBMA) copolymer nanogel [141] | 65 |
| Figure 3.32 The MTT compound is reduced by mitochondrial reductase enzymes in viable cells to form formazan, a colored compound. [144] | 66 |
| Figure 3.33 Microplate assay illustrating the increasing number of cells per well (left to right) and the replicates (top to bottom). The gradient of color intensity represents the varying cell densities across the wells. [144] | 67 |
| Figure 4.1 First option of materials for a copolymer nanogel [83] | 69 |
| Figure 4.2 Second option of materials for a copolymer nanogel [83] | 70 |

| | | |
|-------------|--|-----|
| Figure 4.3 | Workflow for the experimental procedure | 77 |
| Figure 4.4 | Synthesis of the nanogel. (A) Weighing the polymerized and ready MPC-macroCTA. (B) Weighing the ACVA reagent. (C) Placing the weighed MPC-macroCTA and ACVA into a test tube. (D) Weighing mBAM. (E) Placing mBAM into an Eppendorf tube. (F) Dissolving mBAM in DMF. (G) Combining all previously weighed components, adding mBAM dissolved in DMF, water, 2-propanol, and DEGMA. (H) Purging process with gaseous nitrogen. (I) Start of the polymerization. | 82 |
| Figure 4.5 | Two types of SiQDs | 84 |
| Figure 4.6 | Dialysis for SiQDs | 85 |
| Figure 4.7 | Encapsulation Workflow for Acid-SiQDs | 86 |
| Figure 4.8 | Encapsulation Workflow for Acid-PEO-SiQDs | 87 |
| Figure 4.9 | Encapsulation Efficiency Workflow for Acid-SiQDs | 89 |
| Figure 4.10 | Encapsulation Efficiency Workflow for Acid-PEO-SiQDs | 90 |
| Figure 4.11 | Measure of Efficiency for Acid-SiQDs | 92 |
| Figure 4.12 | Measure of Efficiency for Acid-PEO-SiQDs | 93 |
| Figure 4.13 | Protocol for DLS | 94 |
| Figure 4.14 | Nanogel sample loaded into a small inert container specifically designed for thermogravimetric analysis | 95 |
| Figure 4.15 | Analysis of cell viability using trypan blue solution | 99 |
| Figure 4.16 | Assessment of cytotoxicity for both treatments | 100 |
| Figure 4.17 | Cylindrical red light-emitting device for photodynamic therapy . . | 102 |
| Figure 4.18 | Area of illumination per activation and the sequential trajectory of the laser across the 96-well plate | 103 |
| Figure 4.19 | Application of a laser to start the ROS production | 103 |
| Figure 4.20 | Application of MTT reagent | 104 |
| Figure 4.21 | Assessment of photodynamic therapy for both treatments | 105 |
| Figure 5.1 | Synthesized MPC-macro CTA | 109 |

| | | |
|-------------|---|-----|
| Figure 5.2 | Synthesized Copolymer Nanogel | 110 |
| Figure 5.3 | Encapsulation of Acid-SiQDs in the Nanogel | 112 |
| Figure 5.4 | Encapsulation of Acid-PEO-SiQDs in the Nanogel | 113 |
| Figure 5.5 | Evaluation of Encapsulation Efficiency for Acid-SiQDs | 114 |
| Figure 5.6 | Fluorescence spectrum of NG-Acid-SiQDs and Acid-SiQDs at 40 °C | 115 |
| Figure 5.7 | Evaluation of Encapsulation Efficiency for Acid-PEO-SiQDs | 118 |
| Figure 5.8 | Fluorescence spectrum of NG-Acid-PEO-SiQDs and Acid-PEO- SiQDs at 40 °C | 119 |
| Figure 5.9 | Dynamic Light Scattering (DLS) results for the synthesized copoly- mer nanogel at 25°C | 122 |
| Figure 5.10 | Dynamic Light Scattering (DLS) analysis of the nanogel at 37°C | 123 |
| Figure 5.11 | Nanogel sample dissolved in PBS after DLS analysis at 25°C and 37°C | 125 |
| Figure 5.12 | (a) DLS analysis data of Acid-SiQDs-loaded nanogel at 25°C | 127 |
| Figure 5.13 | DLS analysis data of Acid-SiQDs-loaded nanogel at 37°C | 128 |
| Figure 5.14 | Thermogravimetric Analysis (TGA) curves for the nanogel alone and the nanogel encapsulating Acid-SiQDs | 132 |
| Figure 5.15 | ¹ H NMR spectrum of the synthesized nanogel (NG) showing dis- tinct peaks corresponding to various proton environments in the polymer matrix | 134 |
| Figure 5.16 | ¹ H NMR spectrum of Acid-SiQDs showing distinct peaks corre- sponding to various proton environments | 136 |
| Figure 5.17 | ¹ H NMR spectrum of the nanogel encapsulating Acid-functionalized SiQDs showing distinct peaks corresponding to various proton environments | 138 |
| Figure 5.18 | Cell viability of HDFa cells after 24 hours of treatment with various concentrations of NG-Acid-SiQDs and NG-Acid-PEO-SiQDs | 140 |
| Figure 5.19 | MTT Assay Results for HeLa Cells | 141 |

Figure 6.1 Differential Scanning Calorimetry (DSC) curves for the nanogel and Acid-SiQDs-loaded nanogel, showing heat flow against temperature. The blue line represents the nanogel without Acid-SiQDs, while the red line represents the nanogel with encapsulated Acid-SiQDs. 157

List of Abbreviations

In this thesis, several abbreviations are used to facilitate the reading and comprehension of the text. These abbreviations include:

- **NG:** Nanogel.
- **DEGMA:** Di(ethylene glycol) Methyl Ether Methacrylate.
- **MPC:** 2-Methacryloyloxyethyl phosphorylcholine.
- **RAFT:** Reversible Addition-Fragmentation Chain Transfer.
- **SiQDs:** Silicon Quantum Dots.
- **Acid-SiQDs:** Functionalized Acid Silicon Quantum Dots.
- **Acid-PEO-SiQDs:** Polyethylene Oxide Functionalized Acid Silicon Quantum Dots.
- **NG-Acid-SiQDs:** Nanogel Encapsulating Acid Functionalized Silicon Quantum Dots.
- **NG-Acid-PEO-SiQDs:** Nanogel Encapsulating Polyethylene Oxide Functionalized Acid Silicon Quantum Dots.
- **PDT:** Photodynamic Therapy.
- **NIR:** Near-Infrared Radiation.
- **ROS:** Reactive Oxygen Species.

RESUMEN

SÍNTESIS Y CARACTERIZACIÓN DE UN NANOGEL QUE ENCAPSULA PUNTOS CUÁNTICOS DE SILICIO (SIQDS) PARA MEJORAR LA TERAPIA FOTODINÁMICA DIRIGIDA EN CÉLULAS CANCEROSAS HELA

La prevalencia del cáncer sigue siendo un problema de salud significativo a nivel mundial. Los tratamientos actuales, como la quimioterapia y la radiación, a menudo resultan en efectos secundarios severos debido a su naturaleza no selectiva. Como alternativa, la terapia fotodinámica (PDT) dirigida ha emergido como una solución prometedora debido a su especificidad y toxicidad sistémica reducida. Sin embargo, desafíos como la solubilidad y estabilidad en medios biológicos deben abordarse para mejorar la eficacia clínica. Esta tesis tiene como objetivo desarrollar y evaluar un sistema de nanogel novedoso para encapsular dos tipos de puntos cuánticos de silicio (SiQDs): SiQDs ácidos y SiQDs ácidos-PEO, y evaluar su eficacia en la PDT contra células HeLa. Los nanogeles se sintetizaron utilizando una matriz copolimérica de metacrilato de éter metílico de di-etilenglicol (DEGMA) y 2-metacriloxietil fosforilcolina (MPC) mediante polimerización por transferencia de cadena reversible por adición-fragmentación (RAFT). Se evaluó la viabilidad celular de estos nanogeles con SiQDs en fibroblastos dérmicos humanos adultos (HDFa) utilizando el ensayo MTT (3-(4, 5-dimetiltiazol-2-il)-2, 5-difeniltetrazolio bromuro). Además, se probó la efectividad de la PDT contra células HeLa bajo radiación infrarroja cercana. Los nanogeles con SiQDs demostraron una viabilidad celular superior al 80% en varias concentraciones cuando se probaron en cultivos de fibroblastos. Los SiQDs encapsulados, especialmente los de superficie ácida-PEO (SiQDs OX), mostraron un potencial efecto fotodinámico para inducir apoptosis en células HeLa. El comportamiento termorresponsivo de los nanogeles, gracias a DEGMA, fue fundamental para mejorar su estabilidad a la temperatura fisiológica de 37°C.

Palabras clave:

Nanogel, Puntos Cuánticos de Silicio, Polimerización RAFT, Terapia Fotodinámica

ABSTRACT

The prevalence of cancer remains a major health issue globally. Current treatments, such as chemotherapy and radiation, often result in severe side effects due to their non-selective nature. As an alternative, targeted photodynamic therapy (PDT) has emerged as a promising solution due to its specificity and reduced systemic toxicity. However, challenges such as solubility and stability in biological media need to be addressed to enhance efficacy. This research aims to develop and assess a novel nanogel system for encapsulating two types of SiQDs—Acid-SiQDs and Acid-PEO-SiQDs—and to evaluate their efficacy in targeted photodynamic therapy against HeLa cells. The nanogels were synthesized using a copolymer matrix of Di(ethylene glycol) methyl ether methacrylate (DEGMA) and 2-Methacryloyloxyethyl phosphorylcholine (MPC) via reversible addition-fragmentation chain transfer (RAFT) polymerization. The biocompatibility of these nanogels was assessed in Human Dermal Fibroblasts, adult (HDFa) cells using the MTT (3-(4, 5-dimethylthiazolyl-2)-2, 5-diphenyltetrazolium bromide) assay to evaluate cell viability post-exposure. Additionally, the effectiveness of the PDT was tested against HeLa cells under controlled near-infrared radiation to initiate the photodynamic effect. The synthesized nanogels demonstrated high biocompatibility, maintaining cell viability above 80% at various concentrations when tested in fibroblast cultures. In photodynamic therapy applications, the encapsulated SiQDs, especially the Acid-PEO-SiQDs (SiQDs OX), showed significant potential in inducing cytotoxicity in HeLa cells, confirming the targeted action of the therapy. The thermoresponsive behavior of the nanogels, driven by DEGMA, played a significant role in enhancing their stability at physiological temperature (37°C).

Keywords:

Nanogel, Silicon Quantum Dots, RAFT Polymerization, Photodynamic Therapy, MTT Assay

CHAPTER I

INTRODUCTION

Nanotechnology is a comprehensive domain that encompasses the study and manipulation of materials at the nanometric scale, specifically at the atomic and molecular levels [1]. Within this field, silicon quantum dots (SiQDs) have emerged as a promising material due to their unique optical and optoelectronic properties [2]. SiQDs are crystalline silicon nanoparticles [3], typically sized between 1 to 10, that exhibit the ability to emit light in the orange-red range with high efficiency, making them highly effective for a wide range of uses, including biomedical imaging, biosensing, drug delivery and cancer therapy [4], [5].

Cancer, a complex disease characterized by uncontrolled cell growth, remains among the primary causes of mortality globally, underscoring the urgent need for more effective and precise treatment strategies [6]. In 2020, GLOBOCAN estimated 69,869 new cancer cases in the general population of Peru, resulting in a crude incidence rate of 211.8 per 100,000 inhabitants [7]. This high incidence makes cancer the second most common cause of mortality in the country. According to the Regional Institute of Neoplastic Diseases (INEN), the most frequent types of cancer in Peru were breast cancer (16% of cases), cervical cancer (15% of cases), stomach cancer (10% of cases), skin cancer (9% of cases), and prostate cancer (7% of cases) [8], [9].

Traditional cancer treatments, such as chemotherapy, radiation therapy, and surgery, while effective to varying degrees, often come with debilitating side effects and limitations [10]. Chemotherapy, for instance, targets rapidly dividing cells but also affects healthy

cells, leading to severe adverse reactions [11]. Radiation therapy, while precise, can damage surrounding tissues. Surgical interventions, though effective in removing localized tumors, may not always be feasible, especially in cases of metastatic cancer [12].

In light of these challenges, there is a growing interest in alternative non-invasive therapies that can target cancer cells more precisely and with fewer side effects, enhancing both diagnostic and therapeutic outcomes [13]. One such promising approach is Photodynamic Therapy (PDT), which combines light, photosensitizers, and oxygen to treat cancer [14]. PDT has proven effective in eliminating cancer cells by generating reactive oxygen species (ROS) that cause cellular damage [15]. Utilizing protoporphyrin, a conventional photosensitizer, in combination with laser irradiation, it was possible to promote cell death in chemoresistant cells. This synergy achieved greater efficacy in inducing cell death, with a notable decrease in viability detected in 67.83% of the chemoresistant cells [16]. Commonly used photosensitizers in PDT include Chlorin e6 (Ce6) [17], porphyrins [18], and more recently, carbon dots [19]. However, these traditional photosensitizers face several challenges. Porphyrins, while widely used, have poor water solubility, limiting their bioavailability and tumor-targeting capabilities. They tend to aggregate in aqueous environments, reducing their ability to generate ROS. Furthermore, their absorption spectrum is typically in the visible light range, which has limited tissue penetration compared to near-infrared (NIR) light, and they can cause skin photosensitivity, leading to unwanted side effects [18]. Similarly, Ce6 lacks inherent tumor-targeting capabilities, leading to non-specific biodistribution and potential off-target effects [17]. Additionally, carbon dots face concerns about potential toxicity [19].

Given these challenges, silicon quantum dots (SiQDs) are being explored as a promising alternative photosensitizer [20]. SiQDs offer several advantages, including efficient light emission with a tunable wavelength range from visible to near-infrared [21]. They are also biocompatible and non-toxic, and can be specifically designed to target

subcellular organelles like lysosomes [22]. This targeting capability enhances their therapeutic efficacy while minimizing off-target effects.

An essential factor in maximizing the performance of SiQDs is surface functionalization, which critically determines their stability, solubility, dispersibility, and compatibility with diverse materials and environments [23]. Studies have shown that undecenoic acid-functionalized and COOH-functionalized SiQDs exhibit high-performance fluorescent properties [24], making them suitable for various biomedical applications [25]. Specific molecular attachments enhance the therapeutic efficacy of SiQDs by being specific to internal or external targets within tissues or cells [21], [26]. This selectivity also allows them to function as drug carriers that can discriminate among particular targets, thereby reducing possible side effects. These attributes underscore their immense potential across a broad spectrum of applications, particularly as photosensitizers in PDT, by increasing the cellular uptake of SiQDs and Photoluminescence Quantum Yield (PLQY) [27]. It is expected to improve the production of ROS upon light irradiation, inducing oxidative stress and apoptosis in cancer cells. To further enhance and understand these properties, this study will compare Acid-SiQDs functionalized with the addition of polyethylene oxide (PEO), a hydrophilic polymer, to evaluate its potential to improve the stability and dispersibility of SiQDs in water and biological fluids [28], facilitating better cellular uptake and charge transfer interactions for the production of ROS.

However, these photosensitizers need to be delivered using various carriers, and SiQDs, in particular, require encapsulation in appropriate materials to enhance their stability and bioavailability for practical use [29]. Furthermore, encapsulation improves the dispersion and solubility of SiQDs in various solvents, facilitating their handling and processing, which is crucial for applications requiring precise and consistent delivery [30]. For biomedical applications, such as controlled therapeutic delivery, encapsulating SiQDs in suitable carrier systems like hybrid nanoparticles that combine SiQDs with mesoporous materials enhances their biocompatibility and increases their loading capacity, making

them more effective for targeted treatments [31]. These systems mitigate adverse interactions with healthy cells by controlling release kinetics and optimizing receptor-ligand interactions. Additionally, the potential to modify SiQDs chemically, coupled with their small size and high surface-to-volume ratio, supports their integration into hybrid delivery systems for precise and controlled therapeutic delivery, providing new avenues for targeted approaches in cancer and other diseases [32].

Therefore, a critical demand exists for innovative therapies capable of precisely targeting cancer cells while sparing healthy tissues from damage [33]. Recent advancements in nanotechnology have resulted in the emergence of various nanocarriers, including liposomes, polymeric nanoparticles, and metallic nanoparticles [34]. These carriers can be engineered to possess specific properties, such as targeting ligands, that enhance their ability to interact with cancer cells. Additionally, nanoparticles can be designed to release therapeutic agents in response to specific stimuli, further enhancing their therapeutic potential [29].

Nanogels distinguish themselves as exceptional nanocarriers within drug delivery systems, combining unique physical properties with high biocompatibility [35]. These networks, primarily composed of crosslinked polymers, excel in encapsulating a diverse array of therapeutic agents, effectively protecting them from degradation and ensuring their targeted delivery to specific tissues or cells [36]. Their high water content and porous nature not only facilitate the loading of both hydrophilic and hydrophobic substances, enhancing their versatility, but also enable responsiveness to environmental stimuli like temperature, pH, and enzymatic activities [37]. Such dynamic responses allow for the controlled and sustained release of therapeutic payloads directly at the designated sites, optimizing efficacy and reducing systemic side effects [38].

The temperature-sensitive behavior of nanogels is a critical feature that enhances

their potential for targeted therapy [39]. Thermosensitive polymers like Di(ethylene glycol) methyl ether methacrylate (DEGMA) confer a property known as the Lower Critical Solution Temperature (LCST), which enables nanogels to respond dynamically to the thermal microenvironments of the body [40]. Below the LCST, nanogels remain hydrophilic, securely retaining their therapeutic cargo. However, in environments where the temperature surpasses this threshold—such as in tumor tissues characterized by slightly elevated temperatures due to increased metabolic activity—they undergo a phase transition, becoming hydrophobic and releasing their encapsulated agents [41], [42].

While both tumor and inflamed tissues can exhibit temperature elevations, the tumor microenvironment (TME) is distinct in its thermal profile and physiological features, such as sustained angiogenesis, hypoxia, and chronic inflammation, which differentiate it from general inflamed tissues [43], [44]. Thermoresponsive nanogels leverage these unique characteristics and the Enhanced Permeability and Retention (EPR) effect, which allows them to accumulate preferentially in tumors due to the abnormal vasculature and permeability [45]. Furthermore, their design can incorporate controlled release mechanisms that fine-tune the response to specific thermal and biochemical stimuli, minimizing off-target effects and accumulation in inflamed but non-tumoral sites [46]. By exploiting these differential responses, thermoresponsive nanogels achieve greater specificity in targeting tumor tissues, addressing concerns about their potential lack of selectivity. This mechanism ensures a precise therapeutic effect, releasing high concentrations of active agents exactly where needed while preserving healthy tissues and reducing side effects [40], [47].

This breakthrough in nanogel technology sets the stage for the potential integration of Photodynamic Therapy (PDT) through agents like silicon quantum dots (SiQDs) used as photosensitizers, which can be activated by specific wavelengths of light to produce therapeutic effects [19], [22]. By encapsulating SiQDs within nanogels, it is anticipated that their delivery and activation can be precisely controlled [48]. This approach aims to

ensure that these potent photosensitizers are released and activated exactly where needed. Upon activation by targeted light exposure, the SiQDs are expected to generate reactive oxygen species (ROS), which are molecules that trigger oxidative stress and can potentially promote the apoptosis of cancerous cells [20]. The ability of nanogels to localize and control the release of SiQDs could maximize the therapeutic efficacy of PDT while minimizing collateral damage to surrounding healthy tissues. This innovative technology holds the potential to transform cancer therapy through targeted and efficient delivery of therapeutic agents, thereby improving patient care and minimizing systemic toxicities [49].

This study focuses on the synthesis and characterization of a nanogel encapsulating SiQDs for enhanced targeted photodynamic therapy in HeLa cancer cells. This model was chosen because HeLa cells are a widely acknowledged model for cervical cancer research, offering a reliable and well-characterized system for evaluating the efficacy of new therapies. While this research specifically targets cervical cancer, the techniques and principles developed could potentially be applied to other types of cancer, offering a broader impact in the field of oncology. By integrating the cutting-edge photodynamic properties of SiQDs with the dynamic and responsive delivery system provided by nanogels, this study seeks to analyze the photodynamic effect of two types of SiQDs—Acid-SiQDs and Acid-PEO-SiQDs—activated when they are exposed to near-infrared (NIR) light and their resulting cytotoxicity induced in HeLa cells.

1.1 Problem formulation

Is a nanogel copolymer composed of Di(ethylene glycol) methyl ether methacrylate (DEGMA) and 2-(Methacryloyloxy)ethyl phosphorylcholine (MPC) effective for encapsulating and delivering silicon quantum dots (SiQDs) for targeted photodynamic therapy against HeLa cells in an *in vitro* setting?

Can the integration of nanogels and silicon quantum dots enhance the stability, solubility, targeting capabilities, and photodynamic properties of SiQDs to selectively induce cytotoxicity in cancer cells when activated by near-infrared light?

Do the functionalization strategies of Acid-SiQDs and Acid-PEO-SiQDs improve their solubility and uptake by cancer cells, thereby enhancing their therapeutic efficacy in photodynamic therapy?

1.2 Research objectives

General objective:

Synthesize and characterize a nanogel encapsulating silicon quantum dots (SiQDs) to enhance targeted photodynamic therapy in HeLa cancer cells.

Specific objectives:

1. Synthesize a copolymer nanogel using Di(ethylene glycol) methyl ether methacrylate (DEGMA) and 2-(Methacryloyloxy)ethyl phosphorylcholine (MPC) as monomers through Reversible Addition-Fragmentation chain Transfer (RAFT) polymerization.
2. Encapsulate two types of SiQDs, Acid Functionalized Silicon Nanocrystals (Acid-SiQDs) and Acid-Functionalized Poly(ethylene oxide)-Terminated SiQDs (Acid-PEO-SiQDs), within the synthesized copolymer nanogel.
3. Characterize the physical and chemical properties of the nanogel and SiQDs encapsulation to understand their distribution, encapsulation efficiency, and interaction.

4. Assess the *in vitro* cytotoxicity of the SiQDs-loaded nanogel with fibroblast cells through MTT (3-(4,5-Dimethylthiazol-2-yl)-2,5-Diphenyltetrazolium Bromide) assays by measuring cell viability.
5. Evaluate the *in vitro* efficacy of SiQDs-loaded nanogel in photodynamic therapy against HeLa cells using near-infrared red light and analyze cell viability using MTT tests to assess cytotoxic effects and therapeutic efficiency.

1.3 Hypothesis

The nanogel encapsulating silicon quantum dots (SiQDs), specifically those modified with polyethylene oxide (PEO), when activated by near-infrared (NIR) laser light, will demonstrate a heightened cytotoxic effect on HeLa cells due to increased solubility, photoluminescence quantum yield (PLQY), and cellular uptake. SiQDs with high PLQY values are expected to produce more reactive oxygen species (ROS), making them more effective as photosensitizing agents in photodynamic therapy (PDT). The presence of PEO is anticipated to enhance the endocytic uptake of SiQDs into cancer cells, facilitating a higher intracellular accumulation and thereby leading to more effective photodynamic action. This increased cellular uptake and higher PLQY should generate an elevated level of ROS, intensifying apoptosis within the cancerous cells.

The comparison between Acid-SiQDs and Acid-PEO-SiQDs is motivated by the hypothesis that PEO functionalization substantially augments the therapeutic efficacy of SiQDs by ensuring more robust intracellular delivery and interaction with cancer cells, as well as improving their optical properties. These enhancements are expected to generate increased levels of ROS, further intensifying apoptosis within the cancerous cells. SiQDs with acid functionalization and PEO molecules on their surface are anticipated to produce charge transfer interactions, becoming excited and reacting with oxygen to generate ROS. Acid functionalization provides a baseline for high-performance fluorescent properties

and compatibility, while the addition of PEO is expected to further improve stability, solubility, and ROS production, thus enhancing the overall effectiveness of SiQDs in PDT applications.

1.4 Justification

Photodynamic therapy (PDT) using silicon quantum dots (SiQDs) encapsulated in nanogels represents a pioneering approach in the treatment of cancer. This method aims to overcome the limitations of traditional cancer treatments, which often suffer from non-specific targeting, significant side effects, and reduced efficacy in tumor eradication. By integrating SiQDs into nanogel carriers, this approach seeks to enhance the precision of tumor targeting and the controlled release of therapeutic agents, thereby maximizing therapeutic efficacy while minimizing systemic toxicity.

The research focuses on determining the relative importance and synergistic effects of both the SiQDs and the nanogel. The synergy between the SiQDs and the nanogel is anticipated to enhance overall therapeutic efficacy by combining the photodynamic capabilities of the SiQDs with the controlled delivery and release properties of the nanogel. Specifically, the nanogel is expected to improve the stability, solubility, and bioavailability of the SiQDs, while the SiQDs generate the necessary reactive oxygen species (ROS) upon activation by NIR light. This combined approach aims to maximize the selective targeting and destruction of cancer cells while minimizing damage to healthy tissues, thereby improving the overall outcomes of photodynamic therapy.

Moreover, the project explores two types of SiQDs—Acid-SiQDs and Acid-PEO-SiQDs—each chosen for their unique optical properties and compatibility with the biological environment. By enhancing the stability and biocompatibility of these quantum dots within the nanogel matrix, the research aims to provide a robust solution that supports both active targeting and effective photodynamic action required for successful therapy. The

expected outcomes of this research include not only understanding the photodynamic therapeutic results but also expanding our knowledge of nanogel-based drug delivery systems in medical biotechnology. These advancements hold the potential to set new benchmarks for the treatment of various malignancies where targeted photodynamic therapy can be applied, extending the impact beyond cervical cancer.

This study also contributes to the ongoing efforts to develop smaller, optically superior, and biocompatible photosensitizers. By leveraging the unique properties of SiQDs, this research aims to advance the field of nanomedicine. The proposed nanogel, a polymeric carrier, not only enhances the delivery and efficacy of SiQDs but also offers thermoresponsive properties crucial for physiological conditions such as the human body temperature of 37°C. This thermoresponsive behavior ensures that the nanogel can respond dynamically to the slight variations in temperature within different body tissues, optimizing the release of therapeutic agents precisely at the target site.

Additionally, this research underscores the potential of nanogel-based systems to enhance the delivery and efficacy of therapeutic agents. By defining this potential, similar delivery systems for other nanoparticles and therapeutic compounds can be developed. Beyond photodynamic therapy, these systems could also be used in diagnostics and monitoring due to the bioimaging properties of SiQDs. Demonstrating this approach could pave the way for new treatments and diagnostic tools, leveraging nanomaterials to improve patient care and outcomes.

1.5 Scope and limitations

The present thesis was developed at the University of Alberta in Edmonton under the supervision of Dr. Ravin Narain. This research focuses on developing and characterizing a nanogel system for encapsulating two types of silicon quantum dots (SiQDs)—Acid-SiQDs and Acid-PEO-SiQDs—and assessing their efficacy and biocompatibility for targeted photodynamic therapy in HeLa cells. The study evaluates the photodynamic effects of these encapsulated SiQDs when activated by near-infrared light, analyzing their potential to induce cytotoxicity exclusively through *in vitro* experiments. The scope of this research is to provide a thorough understanding of the interactions and effectiveness of the SiQD-loaded nanogels within a controlled laboratory environment, laying the groundwork for future clinical applications.

The synthesis of the SiQDs themselves is undertaken by Applied Quantum Materials Inc., located in Edmonton, Canada, and not within the project's direct experimental activities. Additionally, this phase of the research does not extend to *in vivo* trials or progress into preclinical trial phases, as the current focus is on laboratory-based cell culture experiments.

The nanogel synthesis and subsequent experiments are conducted within the Chemical and Materials Engineering building facilities. Characterization of the nanogel is carried out using equipment available in the Natural Resources Engineering Facility (NREF) and supplemented by instruments from Applied Quantum Materials Inc. All cell culture and transfection experiments to evaluate cytotoxicity and cell viability are strictly performed *in vitro* in the laboratories of the Chemical and Materials Engineering building.

This study is limited to working with monoculture cell lines, specifically HeLa cells, to evaluate the potential of photodynamic therapy (PDT) using the two types of silicon quantum dots (SiQDs) encapsulated in the nanogel. However, HeLa cells are widely recognized as a robust model for PDT research due to their rapid proliferation, resilience

under laboratory conditions, and well-documented characteristics [50], [51]. These attributes facilitate reproducible results and consistent evaluation of PDT efficacy. Furthermore, their demonstrated sensitivity to a variety of photosensitizers and light treatments in multiple studies underscores their reliability as a proxy for investigating phototoxic effects. While the results may not fully represent the complex interactions in a multicellular tumor environment, HeLa cells share fundamental biological traits with other epithelial-derived cancer cell lines, reinforcing the broader applicability of these findings to other cancer models.

Similarly, for assessing biocompatibility and cytotoxicity, only Human Dermal Fibroblast adult (HDFa) cells were used as a model. HDFa cells, being primary, non-cancerous cells, provide a more realistic evaluation of toxicity in healthy tissues. Their heightened sensitivity to toxic effects compared to cancer cells allows for a conservative assessment of the biocompatibility of the SiQD-loaded nanogels. However, these findings are restricted to *in vitro* conditions and do not capture the complexity of interactions within a tumor microenvironment. A more comprehensive approach could involve transitioning to three-dimensional (3D) culture models that incorporate both tumor cells and stromal cells, such as cancer-associated fibroblasts. These 3D systems would better represent the tumor microenvironment, offering a more accurate prediction of therapeutic efficacy and safety *in vivo*.

Despite these limitations, the findings from the *in vitro* experiments provide valuable insights into the functionalization and photodynamic capabilities of the SiQD-loaded nanogels. By demonstrating their potential therapeutic efficacy in a controlled environment, this study establishes a solid foundation for further exploration of their performance in more complex systems. Testing these nanogels in *in vitro* conditions is a critical step toward validating their targeted delivery and phototoxic effects, enabling future investigations into multicellular systems such as tumor spheroids, advanced 3D culture models or *in vivo* studies.

1.6 Bases of the Bioengineering curriculum

This project integrates three foundational pillars of bioengineering: the chemistry of life, human physiology, and biophysics, demonstrating their interconnectedness in developing an innovative therapeutic solution.

Chemistry of Life

The synthesis and characterization of a nanogel for encapsulating silicon quantum dots (SiQDs) illustrate a profound application of chemical principles tailored to biological contexts. The reversible addition-fragmentation chain transfer (RAFT) polymerization process [52] used to create the nanogel matrix based on two molecules that govern cellular functions and interactions—namely, Di(ethylene glycol) methyl ether methacrylate (DEGMA) and 2-(Methacryloyloxy)ethyl phosphorylcholine (MPC), exemplify how synthetic chemistry can be harnessed to address specific biological challenges.

These substances play critical roles in the synthesis of the nanogel, chosen for their unique chemical properties. MPC, a key monomer of the nanogel, exhibits hydrophilic properties that enhance the solubility of the nanogel in biological fluids [53], thereby increasing the bioavailability of the encapsulated SiQDs. This hydrophilicity is crucial for the interaction of the nanogel with cellular environments, facilitating the transport of SiQDs to the target cells without inducing undesirable systemic effects. Additionally, the inclusion of DEGMA contributes to the thermoresponsive behavior of the nanogel [54], allowing for controlled release of the SiQDs in response to slight changes in temperature that may occur in different parts of the human body or upon triggered therapeutic intervention. On the other hand, MPC is a zwitterionic monomer selected for its structural similarity to components of the cellular membrane, specifically phospholipids, which enhances its integration into biological systems [55]. The incorporation of MPC into the nanogel matrix improves its biocompatibility and minimizes immune rejection, crucial for applications involving direct interaction with human cells.

The strategic synthesis of the nanogel via RAFT polymerization ensures precise control over the molecular weight and distribution of the copolymer, critical for achieving the desired mechanical properties and degradation rates [52], [56]. This level of molecular control is essential in tailoring the release profiles of SiQDs, optimizing the therapeutic outcomes of the photodynamic therapy.

Characterization techniques such as Dynamic Light Scattering (DLS), Thermogravimetric Analysis (TGA), and Nuclear Magnetic Resonance (NMR) spectroscopy were employed to analyze the nanogel's properties. DLS was used to determine the size distribution and stability of the nanogel particles, revealing the thermoresponsive behavior by showing size changes at different temperatures. TGA provided insights into the thermal stability and composition of the nanogel, ensuring it maintains its integrity under physiological conditions. NMR spectroscopy confirmed the successful incorporation of DEGMA and MPC into the nanogel structure, verifying the chemical composition and functional groups essential for its biocompatibility and performance.

Human Physiology

The choice of HeLa cells as a model system aligns with the project's focus on human physiology, particularly in the context of improving treatment strategies for cancer. The design of the nanogel encapsulating silicon quantum dots (SiQDs) is heavily influenced by a detailed understanding of cellular mechanisms and interactions within the human body, ensuring that the therapy is both effective and minimally invasive. By targeting cancerous HeLa cells, the nanogel system is engineered to enhance the uptake of SiQDs by these cells through endocytosis, a natural physiological process. By mimicking aspects of the cellular environment, particularly through the use of MPC, the nanogel promotes greater compatibility and integration within cellular systems. This targeted approach ensures that the SiQDs are delivered directly to the cancer cells, increasing the efficiency of the photodynamic therapy and reducing collateral damage to surrounding healthy tissues.

The therapeutic mechanism of the encapsulated SiQDs under near-infrared (NIR) radiation is specifically chosen to exploit the physiological response to light-based treatments. NIR light can penetrate deeper into tissues compared to visible light, allowing for effective activation of the SiQDs at the target site. Once activated, the SiQDs produce reactive oxygen species (ROS) that induce cell death in cancerous cells [19]. This process leverages the physiological vulnerabilities of cancer cells, such as their higher metabolic rate and increased demand for oxygen, making them more susceptible to ROS-induced damage than normal cells.

Recognizing the physiological implications of introducing foreign materials into the body, this project prioritizes the biocompatibility of the nanogels. The materials used in the nanogel formulation are selected for their proven safety profiles and ability to integrate without disrupting normal cell functions or provoking an immune response. By conducting thorough biocompatibility assessments, such as cell viability assays with HDFa (Normal Human Dermal Fibroblasts) cells, the project ensures that the nanogel-SiQD system is tolerated by the body and does not induce adverse physiological reactions.

Additionally, the project's consideration of the body's natural defense mechanisms against oxidative stress is crucial. The generation of ROS within cancer cells must be carefully controlled to avoid excessive damage to healthy tissues. The nanogel's design, incorporating MPC, helps to minimize potential adverse effects by ensuring that the photosensitizers are activated only within the target cells. This selective activation is vital for maintaining the balance between effective cancer cell destruction and the preservation of surrounding healthy tissue integrity [57].

Furthermore, the controlled release of SiQDs facilitated by the thermoresponsive nature of the nanogel is designed to align with the physiological conditions within the body. The ability of the nanogel to respond to slight temperature variations ensures that the SiQDs are released in a controlled manner, maximizing their therapeutic impact while minimizing potential side effects. This approach underscores the importance of aligning

the nanogel's functional properties with the dynamic and complex environment of human physiology [58].

Biophysics

The project's engagement with biophysics is linked to the manipulation and understanding of the optical properties of silicon quantum dots (SiQDs), which are central to the efficacy of photodynamic therapy (PDT). The encapsulated Acid-SiQDs and Acid-PEO-SiQDs are chosen not only for their biocompatibility but also for their unique photophysical behaviors, which are critical for achieving the desired therapeutic outcomes.

Silicon quantum dots are renowned for their robust photostability, high quantum yield, and tunable emission wavelengths, which make them ideal candidates for photodynamic applications. The two types of SiQDs used in this project—Acid-SiQDs and Acid-PEO-SiQDs—have been specifically chosen to leverage these properties. Acid-SiQDs exhibit strong absorption in the ultraviolet region, which, when coupled with their ability to emit at various wavelengths, can be finely tuned to match the absorption characteristics of pathological tissues. On the other hand, Acid-PEO-SiQDs are modified with polyethylene oxide to enhance their dispersibility and stability in biological fluids, ensuring that their optical properties are maintained within the physiological environment.

Fluorescence spectroscopy is employed to verify the encapsulation and photophysical properties of the SiQDs within the nanogel. The fluorescence spectrum provides critical data confirming that the SiQDs retain their characteristic emission properties after encapsulation [59]. The specific emission peaks observed in the spectrum correspond to the known fluorescence signatures of the Acid-SiQDs and Acid-PEO-SiQDs, confirming their presence and stability within the nanogel matrix.

When exposed to NIR light, the SiQDs absorb light energy and produce reactive oxygen species. This conversion process is highly dependent on the biophysical properties of the SiQDs, including their size, surface chemistry, and the matrix in which they are

embedded. The Acid-PEO-SiQDs, in particular, are designed to enhance light absorption efficiency and energy transfer processes, maximizing the photodynamic effects within the target cells [60].

CHAPTER II

CRITICAL REVIEW OF THE LITERATURE

In the dynamic field of medical nanotechnology, the strategic development of silicon quantum dots (SiQDs) stands out as a transformative approach to cancer therapy. By navigating through the latest advancements and dissecting the scientific discourse surrounding these novel nanocomposites, this chapter seeks to highlight the critical innovations of nanogel systems and the corresponding challenges that they bring to critically evaluate the integration of SiQDs as a promising alternative to conventional photosensitizers used in photodynamic therapy (PDT).

The study by Samia *et al.* [19] explores the potential of semiconductor quantum dots (QDs) in PDT by demonstrating their ability to generate reactive oxygen species (ROS). In PDT, a photosensitizing agent is activated by light to produce singlet oxygen (1O_2), which induces cytotoxic reactions in cancer cells. Traditionally, photosensitizers like phthalocyanines (Pc's) are used, but their poor water solubility and tendency to aggregate limit their effectiveness. The study highlights the use of CdSe QDs conjugated to a silicon Pc photosensitizer (Pc4), enabling excitation through fluorescence resonance energy transfer (FRET). This allows activation of CdSe QDs-Pc4 at wavelengths not absorbed by Pc4 alone, demonstrating a 77% FRET efficiency. Additionally, CdSe QDs independently generated 1O_2 with a moderate quantum yield of about 5%, attributed to the triplet state interaction with molecular oxygen. These findings suggest that QDs could serve dual roles in PDT by sensitizing both the PDT agent and molecular oxygen, potentially leading to more effective cancer treatments. The study also highlights ongoing efforts to enhance (1O_2) generation using less toxic QDs and improved surface-coating techniques.

In the context of using less toxic photosensitizers for PDT, silicon nanocrystals (SiNCs) have shown significant potential due to their biocompatibility. The study conducted by Beri *et al.* [61] synthesized conjugates of SiNCs and organic photosensitizers through a microwave-assisted hydrosilylation reaction. These conjugates demonstrated 1O_2 generation with a moderate quantum yield of up to 27% in cyclohexane. Ultra-small SiNCs (4.6–5.2 nm) absorbed UV and blue radiation, transferring the absorbed energy to the triplet state of the attached dyes, which increased the population of triplet states and enhanced 1O_2 generation. Functionalization with perylene derivatives improved energy transfer, as evidenced by singlet oxygen phosphorescence at 1270 nm. The quantum yields of (1O_2) generation decreased slightly to 20% under 317.5 nm laser excitation, showcasing the wavelength-dependent nature of the process [61]. This study underscored the advantages of Si-based systems, including improved biocompatibility and reduced systemic toxicity compared to CdSe QDs.

Additionally, silicon nanocrystals (nc-Si) exhibit significant potential as photosensitizers and sonosensitizers for biomedical applications, particularly in cancer therapy. In the study conducted by Osminkina *et al.* [62], nc-Si with sizes ranging from 2 to 5 nm, prepared from porous silicon (PSi), were shown to act as efficient photosensitizers for 1O_2 generation. This was demonstrated through the direct detection of luminescence at 1270 nm (0.98 eV). This generation of 1O_2 is due to the efficient energy transfer from the photo-excited SiNCs to the triplet state of oxygen molecules, facilitated by the Dexter mechanism. *In vitro* experiments demonstrated that photo-excited nc-Si significantly suppressed the proliferation of cancer cells. These properties, combined with the biocompatibility and biodegradability of SiNCs, pave the way for innovative applications in cancer treatment [62].

The three studies collectively demonstrate the evolving potential of quantum dots in PDT, with key differences in 1O_2 generation efficiency and material properties. Samia *et al.* [19] reported moderate efficiency (5%) using CdSe QDs, whereas Beri *et al.* [61]

significantly improved this to 27% through SiNC-dye conjugates. Osminkina *et al.* [62] showcased the photo-therapeutic potential of porous SiNCs, emphasizing their biocompatibility and significant suppression of cancer cell proliferation. These findings highlight the transition from CdSe to Si-based systems as a critical advancement in addressing wavelength specificity, energy transfer mechanisms, and material functionalization challenges.

Expanding on these developments, the study by Wang *et al.* [63] presents an innovative and biocompatible nanosystem, bovine serum albumin (BSA)-Ce6-SiQDs-MnO₂ (BCSM NPs), designed for enhanced photodynamic therapy (PDT) and dual-mode imaging. This nanocomplex addresses several limitations in conventional PDT, such as hypoxia in solid tumors and the hydrophobicity of photosensitizers. The BCSM NPs leverage the photostability and biocompatibility of silicon quantum dots (SiQDs) to effectively carry photosensitizers into tumor cells, significantly enhancing the formation of cytotoxic ¹O₂ through a pH and H₂O₂ responsive mechanism catalyzed by MnO₂. The BCSM NPs also serve as a dual-functional probe for fluorescence and magnetic resonance imaging (MRI), enabling real-time tracking and precise localization of the treatment. The study found that BCSM NPs could modulate the tumor microenvironment, improving oxygenation and increasing the production of ROS. This capability was confirmed through various imaging techniques, including fluorescence and MRI, which showed high accumulation and activity of the nanoparticles at the tumor site.

Further enhancing the application of SiQDs in cancer therapy and focusing on its synthesis method, the study by Özbilgin *et al.* [64] introduced carboxy-terminated silicon quantum dots (SiQDs) designed for use in fluorescence-guided photothermal nanotherapy. These SiQDs exhibit high water solubility due to substantial molecular coverage of surface monolayers, strong light emission with high photoluminescence quantum yields (PLQYs), prolonged photoluminescence stability for cell monitoring, low toxicity

to cells, and significant photothermal response. The water-soluble SiQDs were synthesized through the thermal hydrosilylation of 10-undecenoic acid on hydrogen-terminated surfaces, achieved via the thermal disproportionation of triethoxysilane hydrolyzed at pH 3 followed by hydrofluoric acid etching. The resultant 10-undecanoic acid-functionalized SiQDs (UA-SiQDs) showed prolonged stability in hydrophilic solvents, including ethanol and water (pH 7). UA-SiQDs exhibited low short-term toxicity, maintaining full cell viability up to 400 $\mu\text{g/mL}$, and a 50% cell viability after 14 days at a concentration of 50 $\mu\text{g/mL}$. The study underscores the potential of SiQDs in theranostics due to their excellent optical properties, photostability, and nontoxicity.

The concentration and localization of the photosensitizer affect how much light is absorbed and, consequently, the light dose required for effective treatment. Uniform distribution ensures consistent treatment efficacy, while uneven distribution may result in areas receiving insufficient light dose, reducing the overall therapeutic effectiveness. Optimizing photosensitizer distribution involves selecting appropriate delivery methods and ensuring adequate uptake by target tissues.

Nanogels have the ability to encapsulate, protect, and release therapeutic molecules and drugs in specific environments [65] [66]. The complexity and characteristics of each nanogel are directly related to its synthesis methodology and the molecules it aims to deliver, leading to ongoing research and development of new structures to address different therapeutic challenges [67]. Nanogels must not only encapsulate the molecules but also ensure their release at the right place and time for effective therapeutic response [42].

Reinforcing the idea that nanogels are efficient transporters because they can respond to stimuli, the study by Ganguly *et al.* [68] developed temperature-responsive microgels with a high content of zwitterionic poly(phosphorylcholine) (PMPC) using a macromonomer approach. The PMPC-based macromonomers were synthesized through a three-step process: RAFT polymerization to create PMPC homopolymers, end-group removal to generate reactive thiol groups, and introduction of polymerizable double bonds

at the chain ends. These macromonomers were then used in different molar ratios to synthesize microgels via precipitation polymerization using N-vinylcaprolactam (NVCL) as the main co-monomer. The extent of zwitterionic incorporation was found to depend on both the molar mass of the macromonomers and their molar fraction in the feed, affecting properties such as hydrodynamic radii and volume phase transition temperature (VPTT). These microgels demonstrated significant protein-repelling behavior, making them suitable for applications in protective coatings with anti-fouling properties.

This concept of stimuli-responsive nanogels is further exemplified in various biomedical applications. For instance, nanogels are versatile nano-delivery systems used for the controlled release of insulin in diabetes treatment [69]. Moreover, their ability to overcome the blood-brain barrier enables targeted drug delivery to the brain for treating neurodegenerative diseases, as well as neuroprotective agents [70]. In the realm of cancer therapies, nanogels facilitate the specific administration of notable anti-cancer agents such as doxorubicin, epirubicin, and paclitaxel, and the delivery of nucleotides that inhibit tumor growth [71] [38].

Recent developments have focused on hybrid nanogels that combine the advantages of inorganic materials and DNA polymers for enhanced PDT. For instance, a programmable hybrid DNA nanogel (H-DNA nanogel) has been developed for enhanced photodynamic therapy of hypoxic glioma [72]. This H-DNA nanogel is constituted with a virus-like mesoporous silica nanoparticle (VMSN) as the core, providing an appropriate nano-interface, and a self-assembly programmable DNA hydrogel layer based on rolling circle amplification (RCA) as the shell. Two kinds of G-quadruplex structures inserted with hemin and zinc phthalocyanine (ZnPc) photosensitizers are introduced into the H-DNA nanogel by base pairing. The G-quadruplex/hemin module works as a catalase to catalyze the conversion of accumulated H_2O_2 in cancer cells to O_2 , addressing the hypoxic tumor microenvironment. On the other hand, the G-quadruplex/ZnPc module increases

the yield of (1O_2) under laser irradiation, enhancing the PDT effect by inducing more intensive cell apoptosis.

Building upon the versatility of nanogels for encapsulation and responsive release, the study by Jie Yang *et al.* [73] presents an innovative use of QD–polypeptide hybrid nanogels for cancer therapy. These nanogels are engineered by metal-affinity driven self-assembly between artificial polypeptides and CdSe–ZnS core–shell quantum dots, resulting in a tunable sandwich-like microstructure. The study highlights the nanogels’ ability to simultaneously load and release hydrophobic and hydrophilic drugs in response to temperature, pH, and competing agents. The research demonstrates that these QD–polypeptide nanogels, particularly those with an arginine-glycine-aspartic acid (RGD) motif, can selectively target and be internalized by HeLa cells, enhancing therapeutic delivery while minimizing cytotoxicity to normal cells. This study underscores the potential of QD–polypeptide nanogels as a multifunctional platform for precise cancer diagnosis, imaging, and therapy.

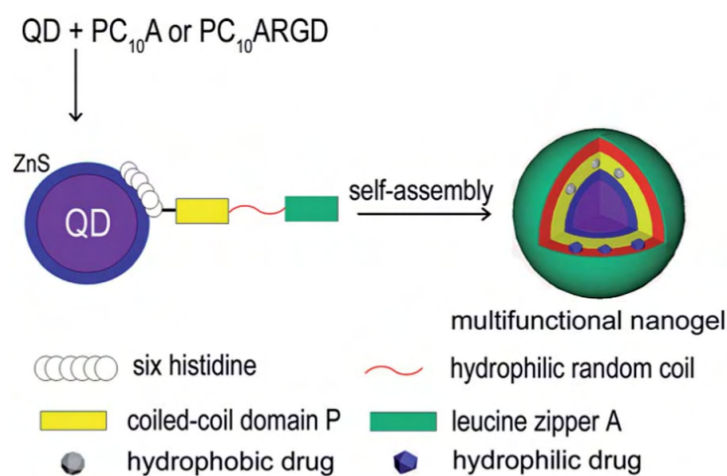


FIGURE 2.1: QD–polypeptide nanogel [73]

The innovative design of these nanogels allows for the simultaneous loading and controlled release of both hydrophobic and hydrophilic drugs, tailored by environmental stimuli such as temperature and pH. Importantly, the incorporation of the RGD motif facilitates targeted delivery to cancer cells, as evidenced by the selective uptake in HeLa

cells and reduced cytotoxicity to normal cells. This research not only demonstrates the multifunctional capabilities of QD–polypeptide nanogels but also opens new avenues for their application in cancer diagnosis, imaging, and therapy, offering a promising strategy to enhance the efficacy and specificity of cancer treatments [73].

Finally, the integration of silicon quantum dots (SiQDs) into nanogel systems demonstrates a significant advancement in the field of cancer therapy. The ability to generate reactive oxygen species, the versatility in drug delivery, and the dual functionality for imaging and therapy highlight the transformative potential of these nanocomposites. The comprehensive evaluation of various studies underscores the critical role of SiQDs and nanogels in overcoming the limitations of conventional PDT and enhancing the efficacy of cancer treatments. This chapter has illuminated the progressive trajectory of SiQDs in medical nanotechnology, emphasizing their promising future in the fight against cancer.

CHAPTER III

THEORETICAL FRAMEWORK

3.1 Cancer

Cancer is a disease characterized by alterations in the cell cycle that lead to the uncontrolled proliferation of cells. These altered cells can accumulate and form masses or tumors. While the human body has mechanisms to automatically correct these anomalies, it sometimes fails, allowing cancerous cells to grow without restraint [74]. Therefore, it is essential to recognize that not all cancers are the same, and cancer in specific organs can be classified based on its nature, whether benign or aggressive [75].

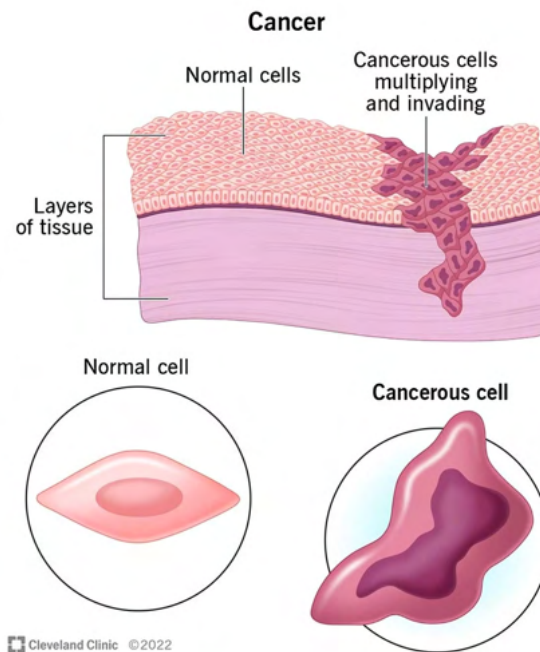


FIGURE 3.1: Comparison between normal cells and cancerous cells [76]

3.2 Conventional Treatments for Cancer

3.2.1 Chemotherapy

Chemotherapy is a medical treatment that uses drugs to fight cancer by slowing its growth or killing cancer cells. It can be administered in various ways, including orally or intravenously, as shown in Figure 3.2 [77]. It is a primary option for many types of cancer, potentially delaying its progression, shrinking tumors, and preventing its spread. Besides being a curative treatment, it can also be palliative, alleviating symptoms and enhancing the quality of life. However, it has side effects like nausea, fatigue, or hair loss. The choice and duration of the treatment depend on the type and stage of cancer and the overall health of the patient [78].

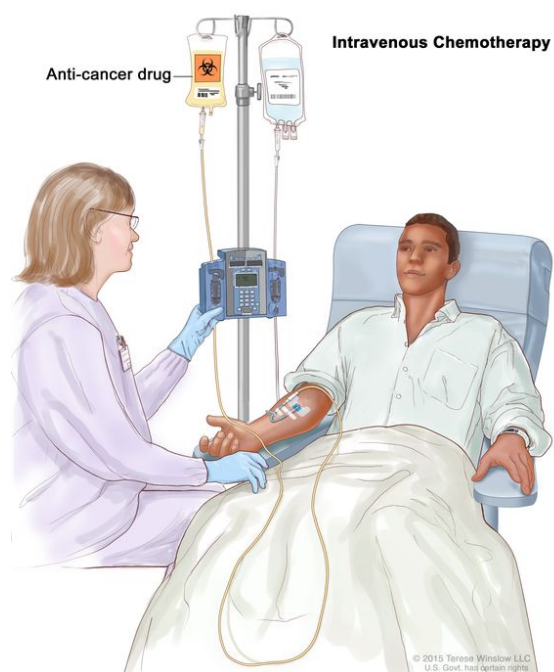


FIGURE 3.2: Intravenous chemotherapy [77]

3.2.2 Radiotherapy

Radiation therapy is a cancer treatment that employs high doses of radiation to destroy cancer cells and reduce tumor size. It can be administered in two ways: externally, using a specialized machine to deliver radiation from outside the body, and internally, known as brachytherapy, which involves placing a radioactive source inside or near the tumor [79]. This is a primary treatment option for various cancer types and can also be used to shrink tumors before surgery, eradicate residual cancer cells after surgery, or alleviate cancer-related symptoms to enhance the quality of life. It may lead to side effects such as fatigue, nausea, vomiting, diarrhea, hair loss, and eating difficulties [80].

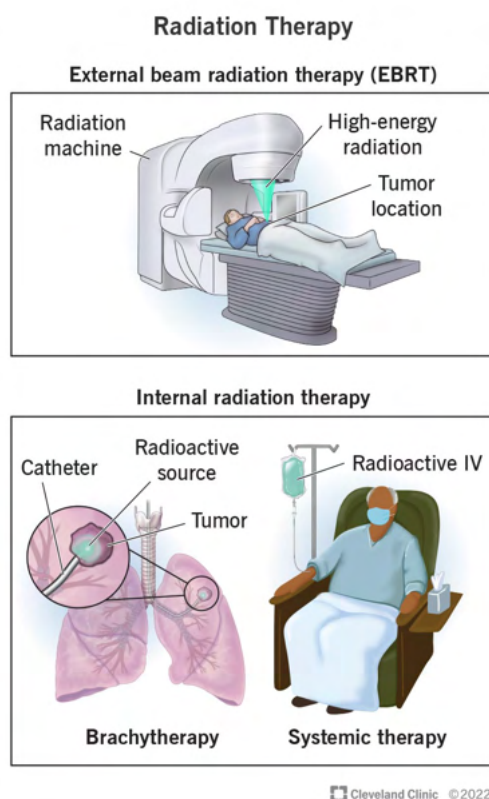


FIGURE 3.3: External beam radiation therapy and internal radiation therapy [79]

3.2.3 Surgery

Surgical treatment can be employed as a neoadjuvant therapy to reduce the size of the tumor before other treatments, or as an adjuvant therapy after other interventions to remove any remaining cancer cells. Surgery is particularly effective in cases where the cancer is localized to a specific area and has not spread to other parts of the body [81].

The decision to proceed with surgery depends on several critical factors, including the location and stage of the cancer, as well as the overall health of the patient. Standard procedures include removing the entire tumor along with a margin of surrounding healthy tissue and often involve excising nearby lymph nodes to assess cancer spread. However, complications such as bleeding, infections, or damage to nearby organs are possible [82]. In some cases, there is also an increased risk of developing a second primary cancer.

3.3 Photodynamic Therapy (PDT)

Photodynamic therapy (PDT) is a therapeutic approach that combines a photosensitizing drug activated by light with a specific wavelength to generate reactive oxygen species, effectively eradicating cancerous and other abnormal cells.

3.3.1 Principles of Photodynamic Therapy

The main elements of photodynamic therapy (PDT) include a photosensitizer, which is a light-sensitive compound that selectively accumulates in abnormal cells; light of a specific wavelength to activate the photosensitizer; and molecular oxygen, which is essential for the photodynamic reaction to take place [18]. When exposed to light of a suitable wavelength, the photosensitizer enters an excited state and transfers energy to surrounding oxygen molecules. This process produces highly reactive oxygen species

(ROS), including singlet oxygen and free radicals, which can harm cellular components and induce cell death, mainly in the illuminated area.

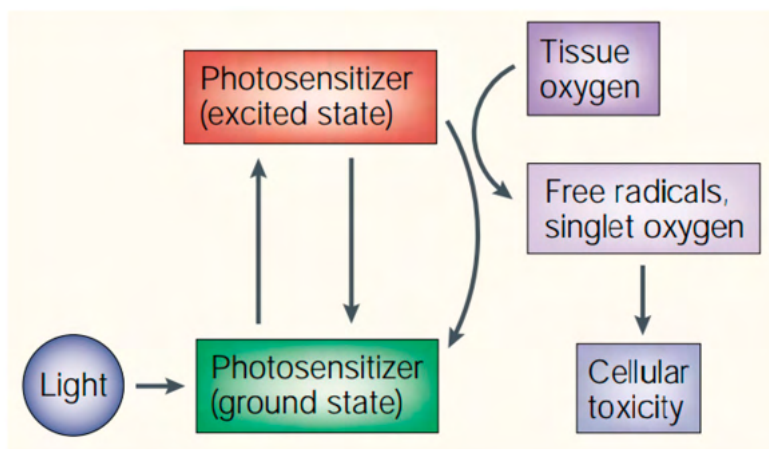


FIGURE 3.4: Mechanism of action of photodynamic therapy (PDT) [83]

3.3.2 Mechanism of Action

The photodynamic reaction can occur through two main pathways.

| Reaction Type | Process | Products |
|----------------|----------------------------|--------------------------------|
| Type I | Electron/Hydrogen transfer | Free radicals and radical ions |
| Type II | Energy transfer to oxygen | Singlet oxygen (1O_2) |

TABLE 3.1: Type I and Type II Reactions in Photodynamic Therapy [83]

In a Type I reaction, free radicals and radical ions are generated through the transfer of electrons or hydrogen between photosensitizers and substrate molecules. On the other hand, the Type II mechanism, which is predominant in photodynamic therapy (PDT), results in the production of highly cytotoxic singlet oxygen species via an energy transfer process from the photosensitizer to molecular oxygen [83], [84].

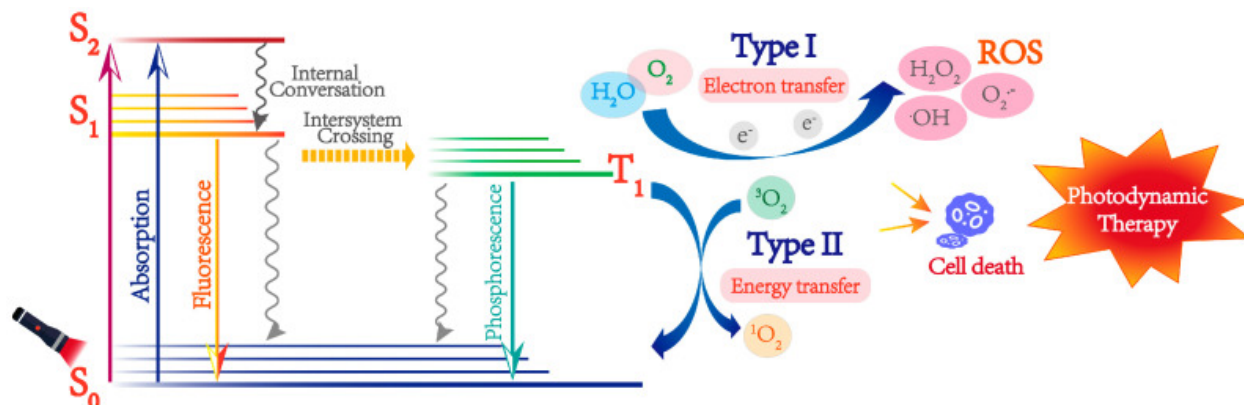


FIGURE 3.5: Type I and Type II of photodynamic reaction [84]

The Jablonski diagram on the left side of the figure illustrates the electronic states of a photosensitizer (PS) molecule. Upon absorption of light (indicated by the red flash-light), the PS transitions from the ground state (S_0) to an excited singlet state (S_1). The PS can return to the ground state via fluorescence, emitting light as it relaxes [84].

3.3.3 Photosensitizers

Photosensitizers are engineered to specifically target and accumulate in abnormal cells, such as cancerous ones, while being efficiently removed from healthy tissues. Commonly used photosensitizers in PDT include Chlorin e6 (Ce6) [17], porphyrins [18], and carbon dots [19]. Each of these photosensitizers has unique properties that make them suitable for specific applications in PDT:

- **Chlorin e6 (Ce6):** Ce6 is widely used due to its high efficiency in generating reactive oxygen species (ROS) and its ability to be activated by light in the therapeutic window (600-850 nm), allowing deeper tissue penetration. However, Ce6 can aggregate in aqueous solutions, reducing its photodynamic efficiency and lacking inherent tumor-targeting capabilities [85], [86].

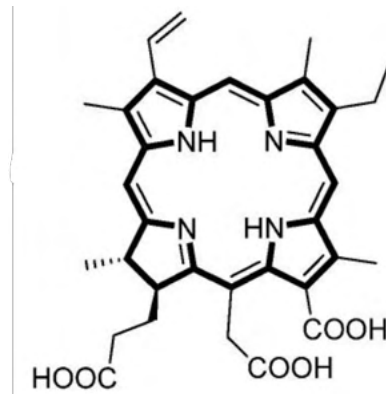


FIGURE 3.6: Chemical structure of Chlorin e6 [87]

- **Porphyrins:** Porphyrins are natural photosensitizers used in PDT for their high photodynamic activity. They can be activated by visible light, but their poor water solubility and tendency to aggregate in aqueous environments limit their bioavailability and effectiveness. Porphyrins can also cause skin photosensitivity, leading to unwanted side effects [88].

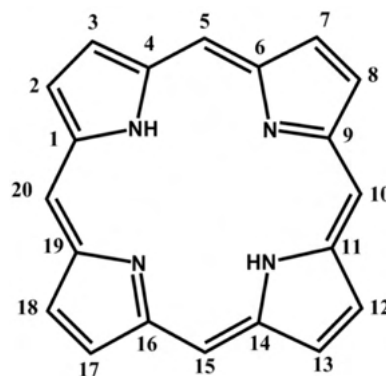


FIGURE 3.7: Chemical structure of Porphyrin [89]

- **Carbon Dots:** Carbon dots have emerged as a potential category of photosensitizers, attributed to their excellent photostability, biocompatibility, and tunable optical properties. They are capable of absorbing in the near-infrared (NIR) region, enabling deeper tissue penetration. However, their photophysical properties can vary

depending on their synthesis method and surface functionalization, and potential toxicity concerns need to be thoroughly investigated [90], [91].

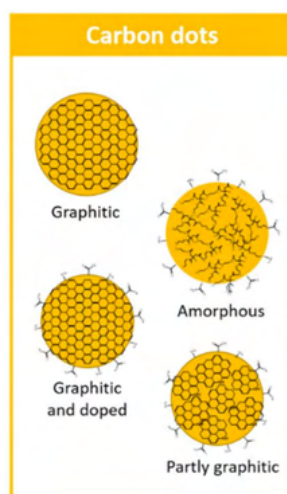


FIGURE 3.8: Chemical structure of Carbon Dots [92]

3.3.4 Administration of Photosensitizers (PSs)

The biodistribution and photochemical properties of photosensitizers (PSs) are essential factors in the effectiveness of PDT. Proper administration of PSs can significantly enhance their effectiveness in targeting tumor sites while minimizing effects on normal tissues.

3.3.4.1 Administration of PSs via Targeting

The biodistribution of photosensitizers *in vivo* poses a significant challenge for PDT. Once in the bloodstream, these drugs can redistribute throughout the body over time, potentially impacting the effectiveness of PDT. Ideally, PSs should accumulate predominantly at the targeted tumor site while minimizing their presence in healthy, non-targeted tissues [18].

Functional polymer nanocarriers improve the solubility of hydrophobic PSs and prevent their aggregation in the bloodstream. Additionally, drug delivery systems regulate the accumulation of hydrophobic drugs either through specific target recognition or via the enhanced permeability and retention (EPR) effect in solid tumors. As a result, nanocarriers are considered promising platforms for modulating the biodistribution of PSs.

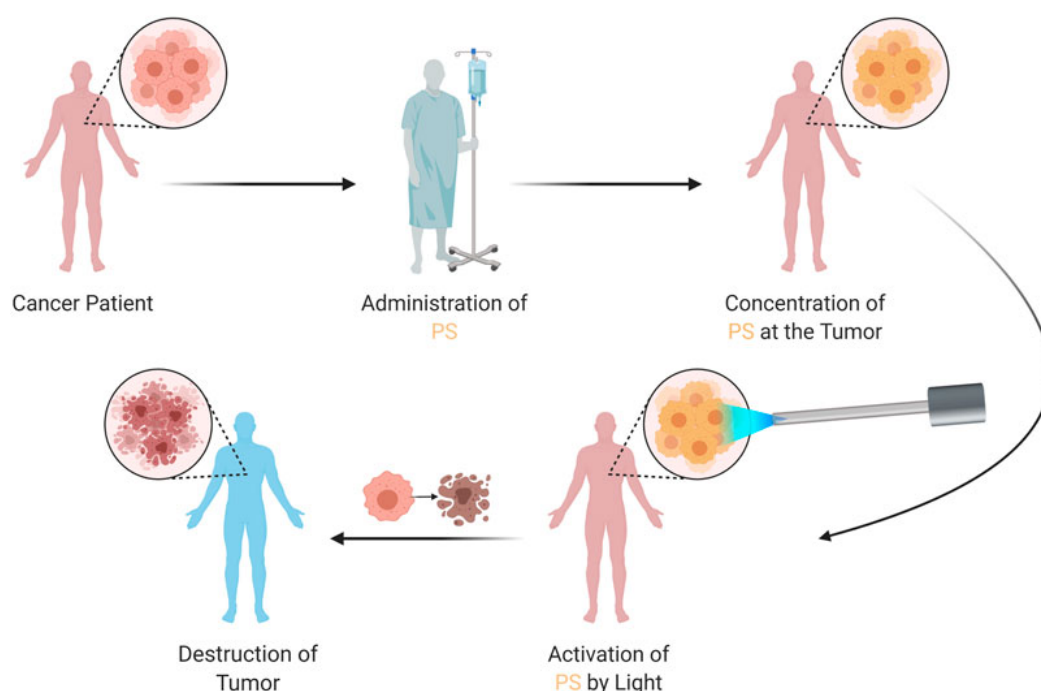


FIGURE 3.9: Therapeutic Application of PDT [93]

Typically, PSs remain inactive until they are exposed to specific wavelengths of light, and their photodynamic activity also requires the presence of oxygen. Upon activation by light, the PS produces reactive oxygen species (ROS), which are essential for the destruction of tumor cells [93].

3.3.4.2 Passive Targeting

Passive targeting is a widely employed approach to enhance the selective accumulation of therapeutic agents in target tissues. By optimizing their physicochemical properties, polymer nanocarriers can accumulate preferentially in tumor tissues via the EPR effect, facilitated by extended circulation time in the bloodstream. Numerous nanocarrier systems composed of biodegradable polymers have been applied in PDT. Incorporating hydrophobic PSs into nanoparticles can reveal higher $^1\text{O}_2$ quantum yield than their aggregates. These nanoparticles can selectively localize in tumor tissues and improve the light-dark toxicity ratio. Factors such as the geometrical shape and surface properties of nanocarriers significantly impact cellular internalization and targeting efficacy [83].

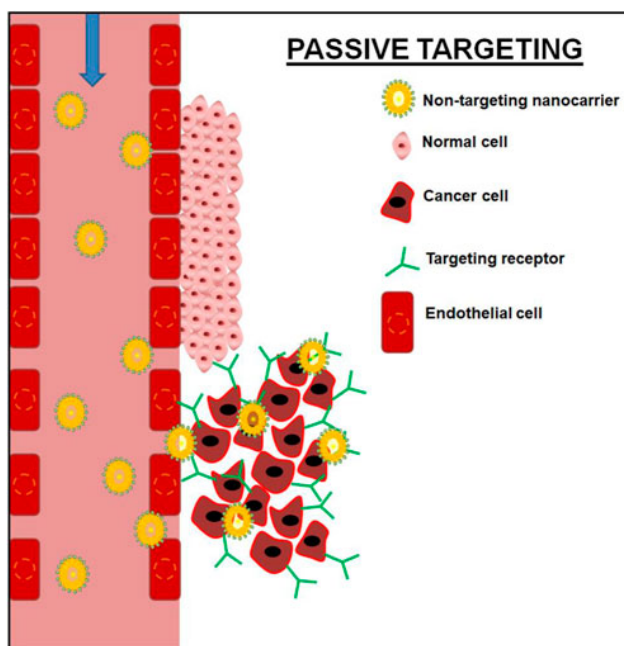


FIGURE 3.10: Passive targeting of cancer cell [34]

3.3.4.3 Active Targeting

Active targeting facilitates the delivery of PSs to cancer tissues through molecular recognition. Carriers with specific ligands can bind to receptors overexpressed at the target site, enabling the precise accumulation of nanoparticles in tumor tissues and enhancing the specificity of PDT. Targeting agents, such as peptides, aptamers, and proteins, have been employed to target tumor vasculature, tumor cells, and subcellular organelles. Active targeting strategies can significantly improve the selectivity and efficacy of PDT by ensuring that PSs are delivered specifically to cancer cells and their microenvironment [83].

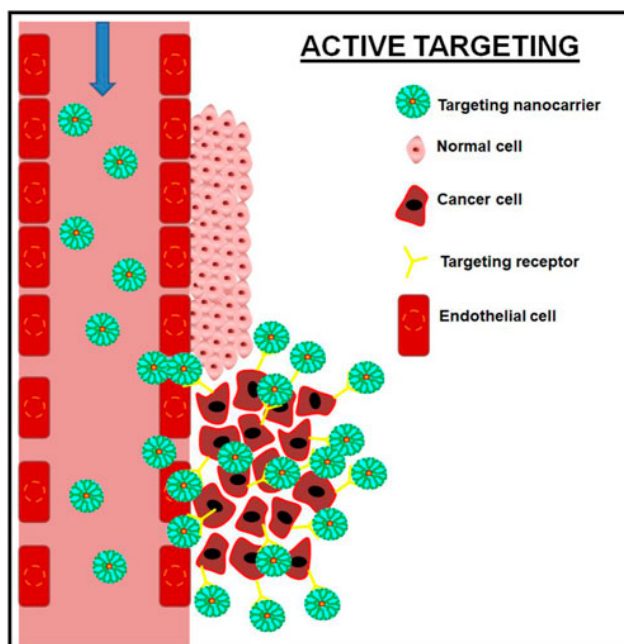


FIGURE 3.11: Active targeting of cancer cell [34]

3.4 Administration of PSs by Responses

While targeting strategies limit the localization of photosensitizers (PSs), controlling their activation is equally important. Polymer nanocarrier-based activatable PS formulations are designed to transition between inactive and active states. In their inactive state, PSs remain inert in the bloodstream and healthy tissues, exhibiting minimal phototoxicity even when exposed to light. Upon activation by specific stimuli at tumor sites, PSs regain their functionality and produce singlet oxygen to directly destroy cells during irradiation. Various methods, such as contact quenching, Förster resonance energy transfer (FRET), and stimuli-responsive nanocarriers, are employed to control PS activation and ensure effective PDT while minimizing side effects [83].

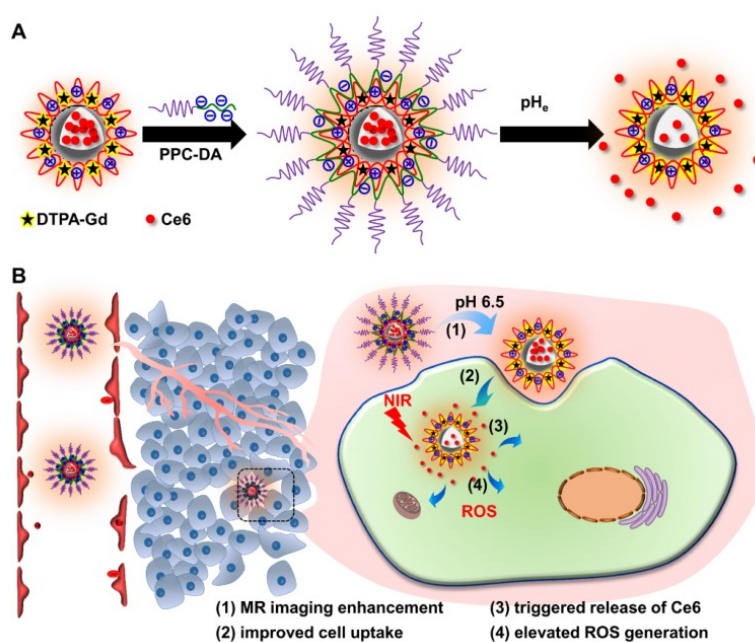


FIGURE 3.12: The activation is triggered by the pH response of the tumor microenvironment: (A) Preparation of Ce6- and Gd³⁺-loaded pH-responsive nanoparticles S-NP. (B) Tumor acidity-responsive S-NP for fluorescence/MR imaging-guided PDT. [94]

The figure 3.12 illustrates the design and mechanism of Ce6- and Gd³⁺-loaded

pHe-responsive nanoparticles (S-NP) for fluorescence and MR imaging-guided photodynamic therapy. The nanoparticles remain stable during circulation due to a PEG outer layer and release the photosensitizer Ce6 in response to the acidic tumor microenvironment [94]. This targeted release, triggered by the tumor's acidity, enhances MR signal intensity, improves cellular uptake, and generates ROS under NIR light, effectively inducing tumor cell death while minimizing systemic toxicity.

3.4.1 Light Delivery and Dosimetry

The effectiveness of PDT depends on the precise delivery of light that matches the absorption spectrum of the photosensitizer. Typically, the "therapeutic window" of 600-850 nm is used because it allows deeper penetration into tissues while minimizing damage to surrounding healthy cells [83]. Light delivery must be carefully managed to ensure that the appropriate dose reaches the target tissue without overexposing adjacent healthy areas. Key factors to consider in PDT dosimetry include light intensity, exposure time, and tissue oxygenation levels [95].

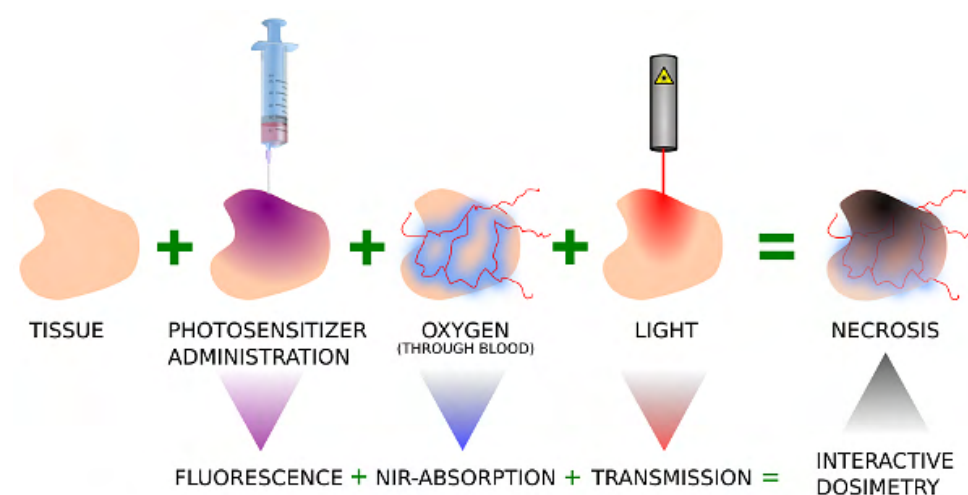


FIGURE 3.13: Application of a laser to generate necrosis [95]

3.4.1.1 Light Sources for PDT

The selection of the light source depends on factors such as the location of the target tissue, the specific photosensitizer used, and the required light dose.

- **Lasers** - These provide high-intensity, monochromatic light that can be precisely directed to target tissues using optical fibers. They are suitable for localized treatment [96].
- **Light-emitting diodes (LEDs)** - LEDs offer a cost-effective alternative to lasers. They allow for customization of the wavelength and beam profile, making them versatile for various applications [96].
- **Lamps** - These broadband light sources are useful for irradiating larger surface areas. They are typically used for superficial tumors or large treatment fields [96].

3.4.1.2 Light Delivery Techniques

The method of light delivery in PDT is influenced by the geometry of the target tissue:

- **Surface Irradiation** - Suitable for treating superficial tumors, where a direct beam of light is aimed at the treatment area [97].
- **Interstitial Irradiation** - Used for treating deeper or hard-to-reach tumors. Optical fibers are inserted directly into the tissue to deliver light internally [97], [98].
- **Intraluminal Irradiation** - Applied in the treatment of hollow organs, such as the bladder. Special light delivery probes are used to direct light into these cavities [97].

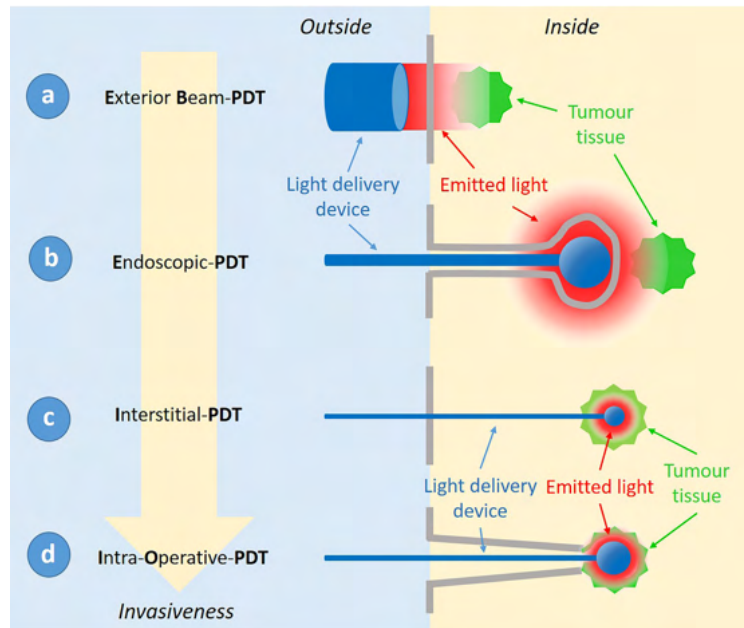


FIGURE 3.14: Delivery systems in clinical PDT for cancerous tumor eradication [97]

- (a) **Exterior Beam-PDT:** Exterior Beam-PDT is a non-invasive method that involves directing an external light beam towards the tumor tissue from outside the body. In this approach, a light delivery device emits light that penetrates the skin and reaches the tumor tissue. The photosensitizer present in the tumor absorbs this light, initiating the photodynamic effect. This method is suitable for treating superficial tumors or skin lesions where light penetration is sufficient to reach the target tissue.
- (b) **Endoscopic-PDT:** Endoscopic-PDT is a minimally invasive method that involves using an endoscope to deliver light directly to the tumor site inside the body. The endoscope, equipped with a light delivery device, is inserted into a body cavity or organ. The emitted light activates the photosensitizer in the tumor tissue. This method is commonly used for internal tumors in organs such as the esophagus, lungs, or bladder, where direct access to the tumor site is required.
- (c) **Interstitial-PDT:** Interstitial-PDT is an invasive method that involves inserting a light delivery device directly into the tumor tissue. The device, often a fiber optic

probe, is placed within the tumor, ensuring that the emitted light reaches the photosensitizer throughout the tumor mass. This method is effective for treating larger or deeper tumors that are not easily accessible through non-invasive methods.

- (d) **Intra-Operative PDT:** Intra-Operative PDT is used during surgical procedures to deliver light to the tumor tissue. During surgery, a light delivery device is applied directly to the tumor site, allowing for precise activation of the photosensitizer. This method is utilized for tumors that require surgical removal or for areas where direct access is achieved during surgery, ensuring thorough treatment [97].

3.4.1.3 Near-Infrared Radiation

Near-infrared (NIR) radiation is a segment of the electromagnetic spectrum with wavelengths extending from approximately 750 nm to 2500 nm, positioned just beyond the visible light range. It is characterized by its ability to penetrate deeper into materials compared to visible light, making it valuable for various diagnostic, industrial, and scientific applications. Though invisible to the human eye, NIR radiation can sometimes be perceived as a dull red glow [99].

NIR wavelengths specifically between 0.75 μm and 1.5 μm are detected by specialized photographic emulsions (up to 1 μm), photoconductor detectors, and photovoltaic devices. These detection methods are essential for capturing NIR radiation effectively, allowing for its application across different fields [100].

Instrumentation for near-infrared spectroscopy typically includes broadband light sources such as incandescent or halogen lamps, which provide the necessary illumination. Dispersive elements like prisms or diffraction gratings are employed to separate the NIR wavelengths for precise analysis. To capture the NIR signals, detectors sensitive to the NIR range, such as silicon-based charge-coupled devices (CCDs) or indium gallium arsenide (InGaAs) devices, are essential.

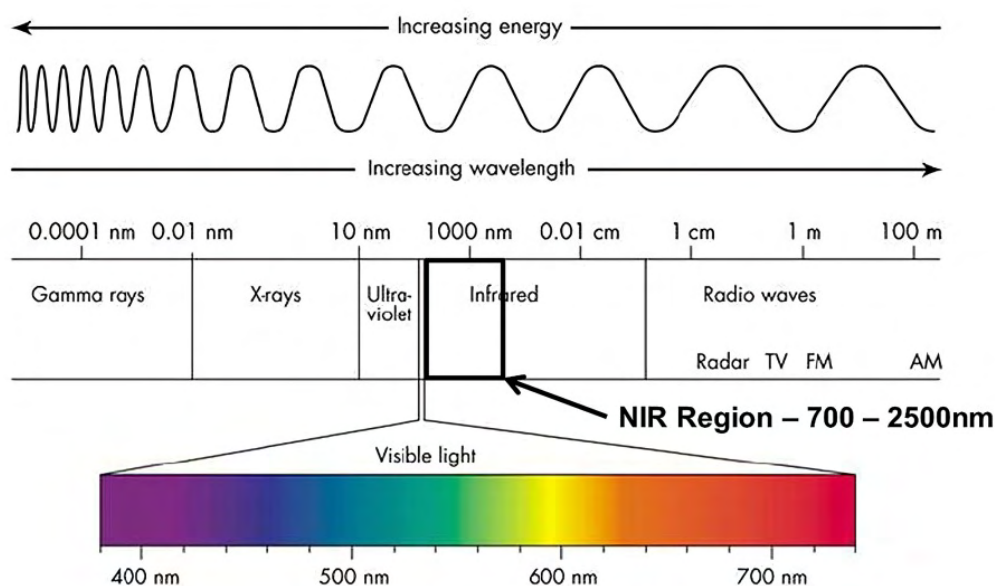


FIGURE 3.15: Infrared radiation can be subdivided further into three categories: Near infrared, Mid infrared and Far infrared [100]

3.4.2 Reactive Oxygen Species (ROS)

Reactive oxygen species (ROS) are highly reactive, oxygen-derived molecules that play critical roles in various biological processes. They are primarily generated as byproducts of cellular metabolism, particularly in the mitochondria during oxidative phosphorylation, and are involved in essential functions such as cell signaling, immune response, and the regulation of homeostasis. The maintenance of ROS levels within a narrow range, achieved through a delicate balance between their production and the activity of antioxidant defense systems, is crucial for ensuring cellular health and preventing oxidative damage [101].

Beyond their role as metabolic byproducts, ROS are key mediators of redox signaling, influencing cellular adaptation and survival. However, their dual nature as both signaling molecules and potential sources of oxidative stress highlights their complex role

in physiology and pathology. While moderate ROS levels are necessary for processes like immune defense and cellular proliferation, excessive ROS accumulation can overwhelm antioxidant mechanisms, leading to oxidative damage of lipids, proteins, and DNA. This imbalance is implicated in the pathogenesis of numerous diseases, including cancer, neurodegenerative disorders, and cardiovascular conditions, underscoring the importance of understanding ROS regulation for therapeutic interventions [102].

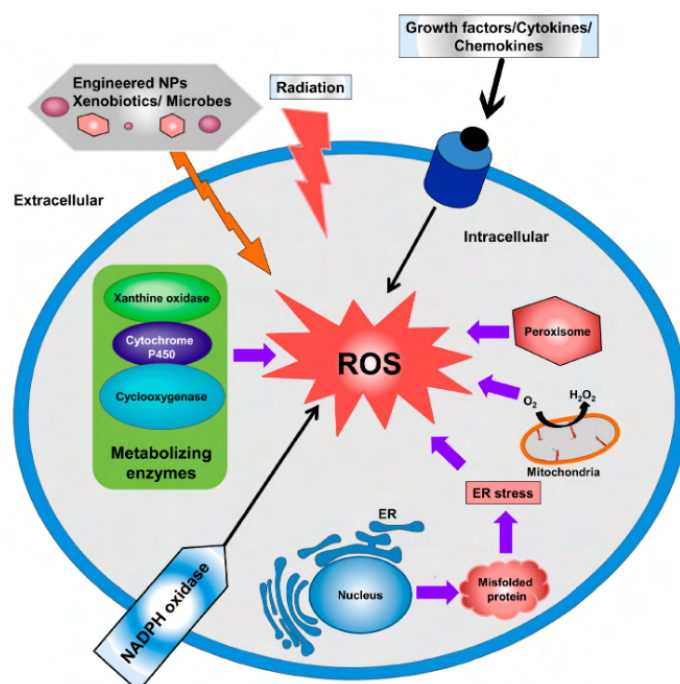


FIGURE 3.16: Reactive oxygen species (ROS) generation [103]

3.4.2.1 Types of Reactive Oxygen Species

Reactive Oxygen Species (ROS) encompass a diverse group of oxygen-containing molecules characterized by their high reactivity and potential to cause oxidative stress in biological systems. These molecules play dual roles in cellular processes, acting as both essential signaling mediators and potential threats to cellular integrity when present in excess.

The figure 3.17 presents the chemical reactions that lead to the formation of different members of ROS that were shown before.

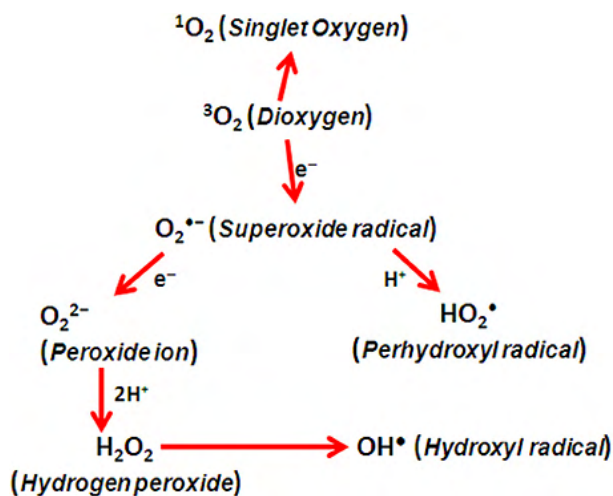


FIGURE 3.17: Reactions of chemical species in (ROS) [104]

- **Superoxide Radical ($\text{O}_2^{\bullet-}$):** Generated primarily in the mitochondria during the electron transport chain (ETC) through partial reduction of oxygen. It has a short half-life and moderate reactivity, often leading to the formation of more reactive species like hydrogen peroxide and hydroxyl radicals [105], [104].
- **Hydrogen Peroxide (H_2O_2):** Formed from the dismutation of superoxide radicals, either spontaneously or catalyzed by superoxide dismutase (SOD). It is moderately reactive, with a longer half-life than superoxide, and can diffuse across cell membranes. H_2O_2 can be converted into hydroxyl radicals via the Fenton reaction, contributing significantly to oxidative stress [104].
- **Hydroxyl Radical (OH^\bullet):** One of the most reactive and damaging ROS, produced through the Fenton reaction between hydrogen peroxide and transition metals like iron (Fe^{2+}). OH^\bullet can cause severe damage to lipids, proteins, and nucleic acids, leading to cellular dysfunction and death [104]. [106].

- **Singlet Oxygen (1O_2):** A highly reactive form of oxygen generated through energy transfer processes, such as those involving chlorophyll in photosynthesis or photodynamic therapy (PDT) in medical applications. Despite its short half-life, singlet oxygen can diffuse short distances and cause significant damage to cellular components, including lipids, proteins, and DNA [104], [107].

| ROS Type | Formula | Description |
|--------------------|---|---|
| Superoxide Radical | $O_2^- + Fe^{3+} \rightarrow ^1O_2 + Fe^{2+}$ $2O_2^- + 2H^+ \rightarrow O_2 + H_2O_2$ $Fe^{2+} + H_2O_2 + Fe^{3+} \rightarrow Fe^{3+} + OH^- + OH$ | Formed during the electron transport chain in mitochondria, can generate other ROS. |
| Singlet Oxygen | $Chl \rightarrow ^3Chl$ $^3Chl + ^3O_2 \rightarrow Chl + ^1O_2$ | Generated by energy transfer processes, especially in photosynthetic organisms or photodynamic therapy. |
| Hydrogen Peroxide | $2O_2^- + 2H^+ \rightarrow H_2O_2 + O_2$ $2O_2^- + 2H^+ \rightarrow H_2O_2 + O_2$ | Formed by dismutation of superoxide radicals, moderately reactive and can cross cell membranes. |
| Hydroxyl Radical | $H_2O_2 + O_2^- \rightarrow OH^- + O_2 + OH$ | The most reactive and toxic ROS, generated by the Fenton reaction. |

TABLE 3.2: Formulas of Reactive Oxygen Species (ROS) [104]

3.5 Silicon Quantum Dots (SiQDs)

Silicon quantum dots (SiQDs) are nanoscale particles of crystalline silicon that display distinctive optical and electronic properties attributed to quantum confinement effects. When the dimensions of silicon are reduced below the exciton Bohr radius, approximately 4.2 nm, these quantum confinement effects become significant, resulting in the material exhibiting behavior akin to a direct bandgap semiconductor [23].

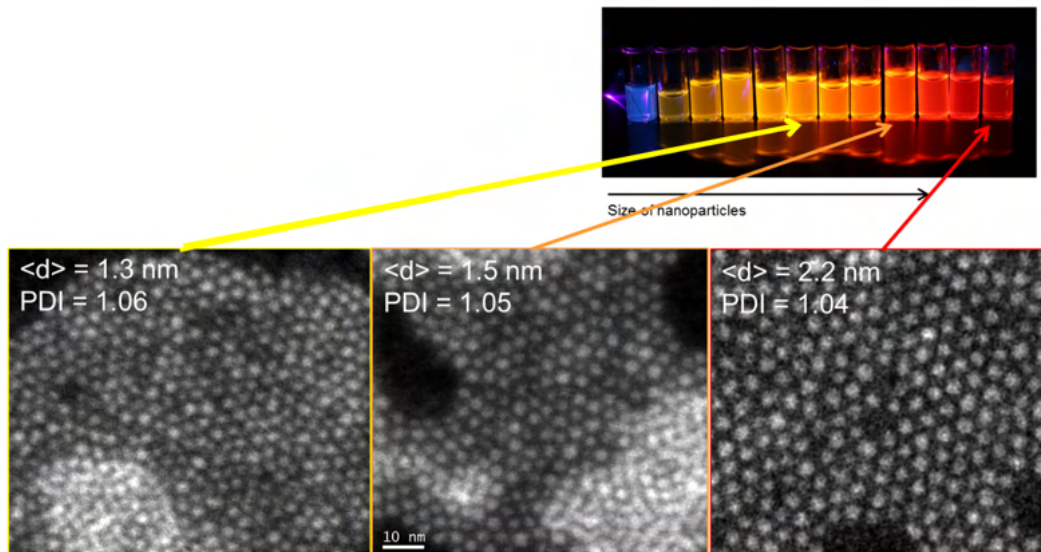


FIGURE 3.18: Silicon Quantum Dots [108]

3.5.1 Properties of Silicon Quantum Dots

3.5.1.1 Bright Light Emission

Silicon quantum dots (SiQDs) exhibit bright photoluminescence (PL) due to their direct bandgap nature at sizes below 5 nm. The quantum confinement effect in these small SiQDs allows for efficient light emission, with quantum yields up to 90% reported. The PL wavelength can be tuned across the visible spectrum by controlling the SiQD size, making them versatile for different optical applications [109].

3.5.1.2 Long-Term Stability in Photoluminescence (PL)

While SiQDs initially exhibit bright PL, maintaining this brightness over time can be challenging. The oxidation of the SiQD surface often leads to the formation of a SiO_2 shell, which can cause blue-shifting and quenching of the PL. Addressing this issue, research is actively exploring strategies like surface passivation to improve the long-term

stability of SiQDs' PL [110].

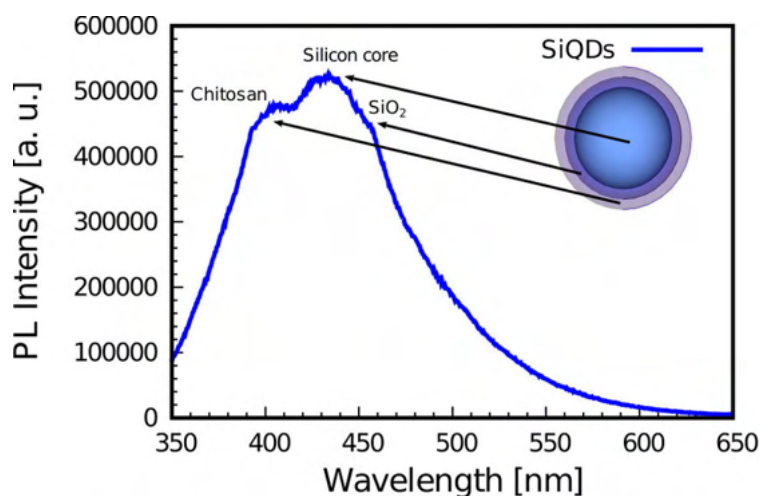


FIGURE 3.19: Photoluminescence spectrum of silicon quantum dots (SiQDs) showing characteristic peaks for the silicon core, SiO_2 shell, and chitosan layer [111]

Figure 3.19 presents the photoluminescence (PL) spectrum of SiQDs at room temperature, displaying three distinct emission peaks that correspond to different components of the nanoparticle. The second peak, observed at 434.5 nm (2.85 eV), originates from the silicon core and represents its intrinsic quantum confinement effect. The second peak, at 447.5 nm (2.77 eV), is attributed to the SiO_2 shell formed on the surface of the SiQDs due to oxidation. Lastly, the peak at 407.5 nm (3.04 eV) is caused by the chitosan (CS) polymer layer, which not only enhances the PL properties but also improves the biocompatibility of the SiQDs [111].

3.5.1.3 Less Toxicity to Cells

Compared to heavy metal-containing quantum dots like CdSe, SiQDs are considered less toxic. Their silicon-based composition contributes to greater biocompatibility, which is a critical factor for their use in biomedical applications. This reduced toxicity makes SiQDs more favorable for use in biological systems [112].

3.5.1.4 Theranostics

The unique optical properties and biocompatibility of SiQDs make them promising candidates for theranostic applications. These applications leverage SiQDs for both diagnostic imaging and therapeutic purposes. SiQDs have been explored for roles in drug delivery, regenerative medicine, and cancer treatment, highlighting their potential to serve as multifunctional tools in medical diagnostics and therapy [113].

3.5.2 SiQD Preparation

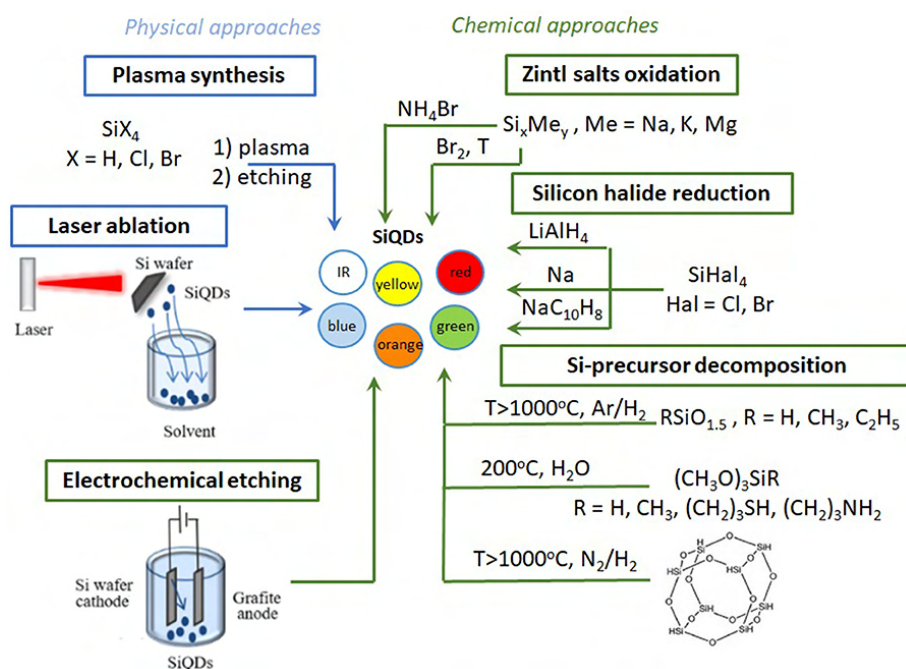


FIGURE 3.20: Delivery systems in clinical PDT for cancerous tumor eradication [109]

3.5.2.1 Physical Routes to Synthesizing SiQDs

- **Laser Generation:** Laser generation involves using a laser to ablate a silicon target in an inert gas atmosphere. The laser vaporizes the silicon, forming a plasma plume

that condenses into SiQDs. This method allows for good control over the size and crystallinity of the SiQDs [109].

- **Plasma Synthesis:** Plasma synthesis uses a plasma reactor to decompose silicon-containing precursor gases like silane (SiH_4) or silicon tetrachloride (SiCl_4). The high-energy plasma breaks down the precursors, allowing SiQDs to nucleate and grow. Plasma synthesis enables low-temperature growth and good control over the SiQD size and surface chemistry [109].

3.5.2.2 Chemical Routes to SiQDs

- **Electrochemical Etching:** Electrochemical etching starts with a silicon wafer as the anode in an electrochemical cell. The silicon is electrochemically dissolved and redeposits as SiQDs on the wafer surface. The size of the SiQDs can be controlled by the etching current density and time. Electrochemical etching is a simple, low-cost method [109].
- **Zintl Salt Oxidation:** Zintl salts are intermetallic compounds that can be oxidized to form SiQDs. For example, sodium silicide (Na_4Si_4) is reacted with silicon halides or bromine gas. This method produces SiQDs with photoluminescence quantum yields up to 60-75% [109].
- **Reduction of Silicon Halides:** Silicon halides like silicon tetrachloride (SiCl_4) can be reduced using reducing agents like sodium naphthalenide, sodium, lithium aluminum hydride, or tetraethylorthosilicate. The reduced silicon forms SiQDs that can be extracted and purified [109].
- **Decomposition of Si-Containing Precursors:** Thermal decomposition of silicon-containing precursors like silanes, siloxanes, or silsesquioxanes produces SiQDs. For example, hydrogen silsesquioxane (HSQ) can be annealed and etched to form SiQDs with near-infrared photoluminescence and high quantum yields [109].

- **Template Synthesis:** Template synthesis uses a porous material like anodic aluminum oxide or mesoporous silica as a template. Silicon is deposited into the pores, forming SiQDs with sizes defined by the pore dimensions. The template is then removed, leaving behind the SiQDs [109].

3.5.3 Functionalization of SiQDs

Functionalizing the surface of silicon quantum dots (SiQDs) is a critical approach for modifying their optical and electronic properties, enhancing their stability, and improving their biocompatibility for diverse applications. The characteristics of SiQDs, such as size, crystallinity, and surface chemistry, can be precisely controlled through the synthesis method.

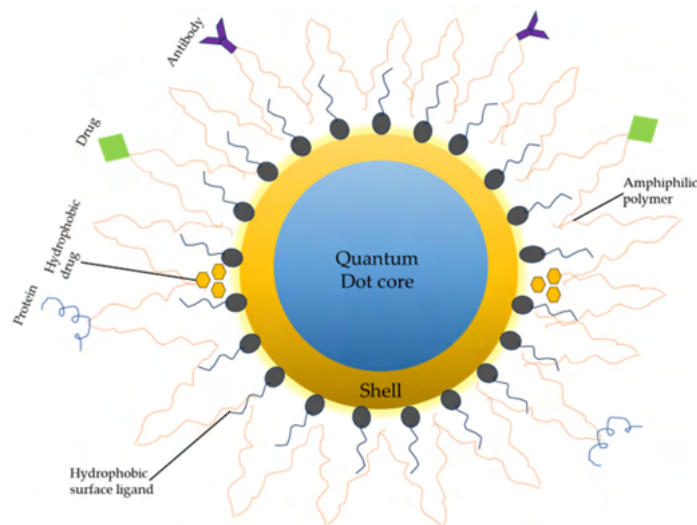


FIGURE 3.21: Functionalization strategies of quantum dot cores [114]

Surface functionalization entails the covalent bonding of diverse organic compounds, polymers, or biomolecules to the surface of SiQDs, leading to substantial modifications in their properties. Common strategies for functionalization include attaching aromatic fluorophores (such as phenanthrene, pyrene, and perylene), biomolecules (like

proteins and DNA), or other organic groups to the SiQD surface. This modification enhances photoluminescence, facilitates energy and electron transfer, and improves biocompatibility [27].

Functionalization also enables efficient FRET from the surface ligands to the SiQD core, allowing for the tuning of emission colors and improving quantum efficiency. Functionalized SiQDs are promising for bioimaging, drug delivery, photodynamic therapy, and other biomedical applications due to their enhanced water solubility, low toxicity, and targeting capabilities [115]. Despite these advantages, challenges remain in achieving long-term stability and high quantum yields in SiQD-based light-emitting diodes and other optoelectronic devices [109]. To overcome these limitations, researchers are investigating encapsulation techniques.

3.5.4 SiQDs as Photosensitizers for ROS Production

Silicon quantum dots (SiQDs) can function as photosensitizers to produce ROS, which are crucial for applications like photodynamic therapy (PDT).

3.5.4.1 Photosensitization Mechanism

When SiQDs absorb light, electrons within the quantum dots are excited from their ground state to higher energy levels, creating electron-hole pairs known as excitons. These excited electrons can transfer energy to ground-state oxygen molecules ($^3\text{O}_2$) through a process called intersystem crossing, converting the oxygen from its triplet ground state to an excited singlet state ($^1\text{O}_2$). Singlet oxygen is a highly reactive ROS capable of damaging cellular components such as proteins, lipids, and DNA. In this role, SiQDs act as photosensitizers by absorbing light and transferring energy to oxygen, generating cytotoxic ROS [116].

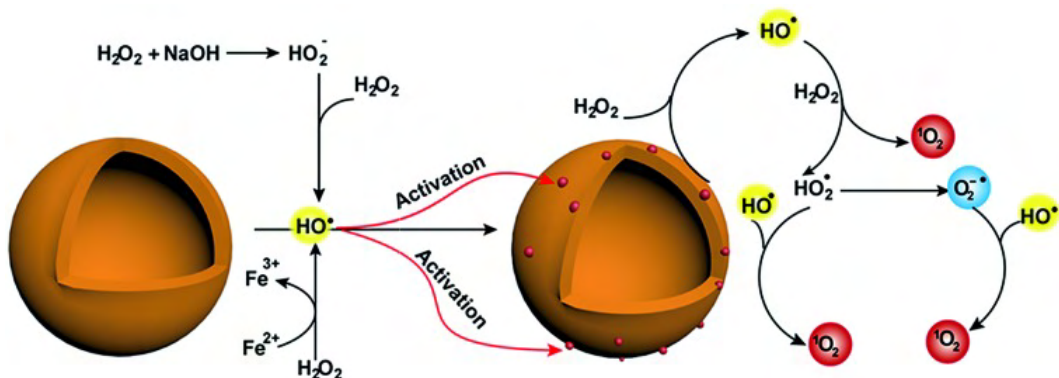


FIGURE 3.22: Enhancing the generation of reactive oxygen species [117]

3.5.4.2 Factors Affecting ROS Generation

The efficiency of ROS generation by SiQDs is influenced by several factors [118]:

- **Size and Surface Chemistry:** Smaller SiQDs with a high surface area can generate more ROS. Surface functionalization with photosensitizing dyes or biomolecules can further enhance ROS production.
- **Oxygen Availability:** Sufficient ground-state oxygen must be present for effective energy transfer. Hypoxic conditions can limit ROS generation.
- **Light Dose:** Higher light intensity and longer exposure times increase ROS levels, though excessive light can damage the SiQDs.
- **Cellular Environment:** The pH, redox state, and antioxidant levels in the cellular microenvironment affect the stability and ROS generation of SiQDs.

3.6 Nanogel

A nanogel is a submicron-scale hydrogel particle crosslinked with polymers. These intricate polymer networks offer a unique opportunity at the intersection of nanoparticles

and hydrogel synthesis in the field of drug delivery. Nanogels are three-dimensional hydrogel materials in the nanometer size range, composed of crosslinked polymer networks with a high drug-loading capacity. They are highly biocompatible and biodegradable, making them ideal for use as drug delivery vehicles. Essentially, nanogels are akin to hydrogels but on a scale of 20-200 nm [119].

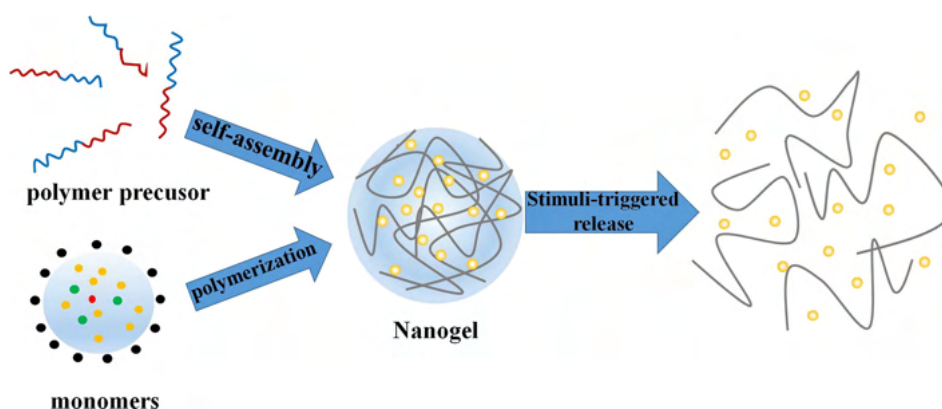


FIGURE 3.23: Nanogel in drug delivery [120]

3.6.1 Types of Nanogels

| Type | Description | Examples of materials |
|--------------------|--|--|
| Natural Nanogels | From natural polymers, biocompatible and biodegradable [119]. | Collagen, chitosan, gelatin, hyaluronic acid, etc. |
| Synthetic Nanogels | Made from synthetic polymers, highly controllable [119] [121]. | Poly(N-isopropylacrylamide), poly(ethylene glycol), poly(lactide-co-glycolide), etc. |
| Hybrid Nanogels | Blend of natural and synthetic polymers [65]. | Combination of natural and synthetic polymers . |
| Metallic Nanogels | Metallic nanoparticles coated with polymers. Unique optical and magnetic properties [121]. | Metallic nanoparticles coated with polymers . |

TABLE 3.3: Nanogel Types and Example Materials.

3.6.2 Synthesis of Nanogels

3.6.2.1 Physical Methods for Nanogel Formation

Physical methods produce more biocompatible nanogels through mechanisms such as electrostatic interactions, ionizing radiation, and hydrogen bonding, which do not involve covalent bonds and thus preserve biocompatibility [122].

3.6.2.2 Chemical Methods for Nanogel Formation

Chemical methods for nanogel formation utilize crosslinkers and covalent bond formation, resulting in nanogels with enhanced durability and stability [122].

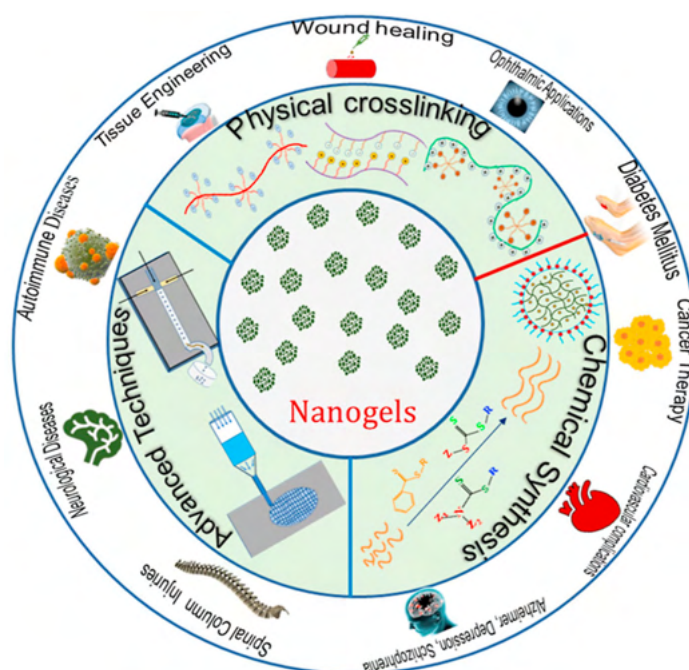


FIGURE 3.24: Different biomedical applications based on methods for the synthesis of nanogels [122]

| Method Type | Method | Description |
|--------------------|---------------------------------|---|
| Physical Methods | Self-Assembly | Formation of nanogels through the self-assembly of amphiphilic polymers in aqueous solutions driven by non-covalent interactions. |
| | Iontropic Gelation | Ionic crosslinking between oppositely charged polymers and ions to form nanogels. The properties can be tuned by adjusting polymer concentration, ionic strength, and pH. |
| | Thermal Gelation | Thermosensitive polymers undergo a sol-gel transition in response to temperature changes, forming a nanogel network above the LCST. |
| | Supramolecular Assembly | Self-assembly driven by host-guest interactions between macrocyclic compounds and guest molecules. |
| Chemical Methods | Precipitation Polymerization | Simultaneous polymerization and crosslinking in an aqueous solution to form insoluble nanogel particles. |
| | Inverse Emulsion Polymerization | Polymerization within the aqueous droplets of an oil-in-water emulsion to form nanogel particles. |
| | Microfluidic Synthesis | Utilization of microfluidic devices for precise control of fluid flows, emulsification, and in-situ polymerization. |
| | Click Chemistry | Bioorthogonal "click" reactions used to crosslink polymers and form nanogels, allowing incorporation of various functional groups. |

TABLE 3.4: Methods for Nanogel Synthesis [122]

3.6.3 Properties of Nanogels

3.6.3.1 Size and Morphology

Nanogels typically range in size from 10 to 200 nm, which allows them to effectively penetrate biological barriers and tissues. They can be engineered into various morphologies such as spherical, core-shell, or more complex structures, depending on the synthesis method and composition [123].

3.6.3.2 High Water Content

Nanogels are highly hydrophilic and can contain up to 99% water by weight, giving them a soft, gel-like consistency. This high water content enhances their biocompatibility and allows for efficient encapsulation and delivery of hydrophilic drugs and biomolecules [124].

3.6.3.3 Stimuli-Responsiveness

Nanogels can be designed to respond to various environmental stimuli such as pH, temperature, redox conditions, or the presence of specific enzymes or molecules. This stimuli-responsive behavior enables controlled and triggered release of the encapsulated cargo at the target site [125].

- **Thermosensitivity:**

Thermosensitivity refers to the ability of a material to respond to changes in temperature. The underlying mechanism is governed by molecular interactions, which can be hydrophobic or hydrophilic depending on the free energy change of the surrounding

solvent. A positive change in the free energy indicates hydrophobicity, while a negative change indicates hydrophilicity.

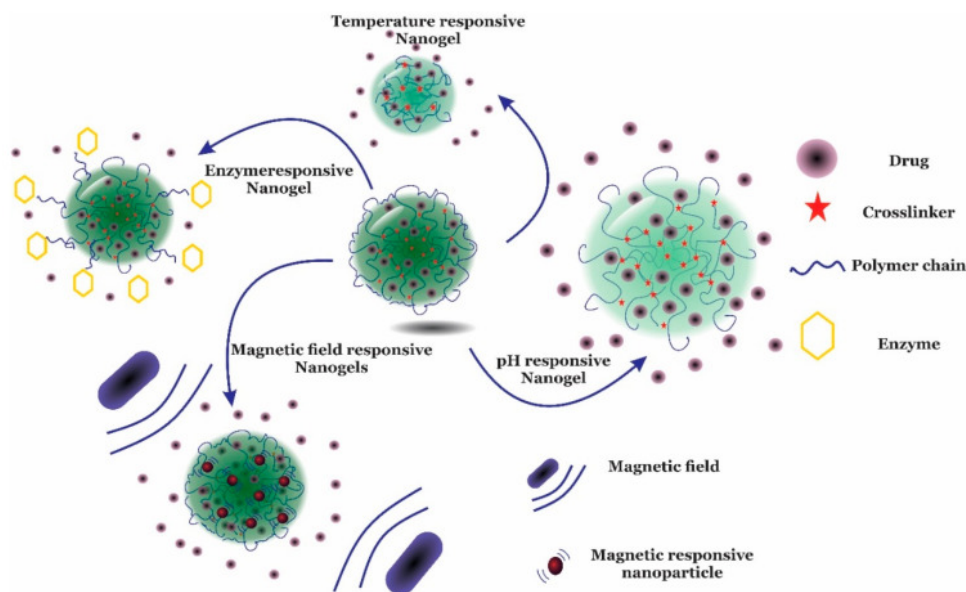


FIGURE 3.25: Different stimuli-responsive nanogels [23]

At temperatures below the Lower Critical Solution Temperature (LCST), water molecules align well around the hydrophilic parts of the material. However, as the temperature rises above the LCST, the surrounding groups become more hydrophobic, causing water molecules to detach and leading to phase separation between water and the polymers. As the temperature continues to increase, the alignment of water molecules collapses due to the presence of hydrophobic moieties, resulting in an increase in the system's entropy and the formation of a gel [126].

3.6.3.4 High Loading Capacity

The porous, hydrophilic network of nanogels can accommodate a wide range of guest molecules, including small drugs, proteins, nucleic acids, and even nanoparticles.

The high surface area-to-volume ratio of nanogels facilitates efficient loading and encapsulation of these therapeutic agents [127].

3.7 RAFT Polymerization Technique

RAFT (Reversible Addition-Fragmentation Chain Transfer) polymerization is a powerful controlled radical polymerization technique that allows for the synthesis of polymers with precise control over molecular weight, low polydispersity, and tailored end-group functionality. The key component in RAFT polymerization is the RAFT agent, a molecule containing a thiocarbonylthio group that acts as a mediator by forming a reversible bond with the growing polymer chain. This reversible bond enables a dynamic [128].

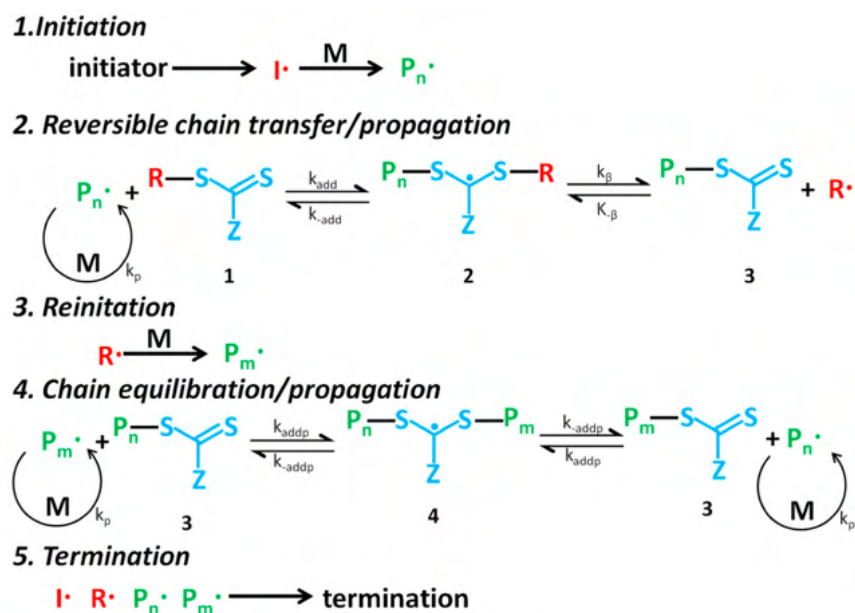


FIGURE 3.26: Reversible addition-fragmentation chain transfer (RAFT) polymerization [129]

3.7.1 Key Elements of RAFT Polymerization

3.7.1.1 Crosslinking Agent

A crosslinking agent is a molecule that forms chemical links between polymer chains to create a three-dimensional network structure. These agents contain two or more reactive ends that can attach to specific functional groups on polymers, such as primary amines or sulfhydryls[130].

These agents are crucial in enhancing rigidity, durability, and resistance to solvents in polymer structures. The degree of crosslinking can be measured by swelling tests in solvents, indicating the extent to which the polymer network has been formed [131].

3.7.1.2 Chain Transfer Agent

A chain transfer agent is a molecule used in free radical polymerization to control the molecular weight of the polymer produced. Chain transfer agents work by interrupting the growth of polymer chains, transferring the radical to themselves or another molecule. This process limits the maximum molecular weight attained and results in a narrower molecular weight distribution [132].

3.7.1.3 Free Radical Initiator

A free radical initiator is a molecule that decomposes to generate free radicals, initiating chain growth polymerization. These initiators contain weak bonds that can homolytically cleave to produce two free radicals. The rate of radical generation depends on the initiator concentration and the rate constant for decomposition [133].

The type of initiator used affects the polymerization rate, molecular weight, and degree of branching in the final polymer. The selection of an appropriate initiator is

crucial for controlling the kinetics and outcome of the polymerization process, ensuring the desired properties of the synthesized polymer [133].

3.7.2 Monomers

A monomer is a small molecule that can bond with other monomers to form larger molecules known as polymers. The term "monomer" is derived from the Greek words "mono," meaning "one," and "meros," meaning "part," signifying its role as a single part of a larger structure. Monomers serve as the fundamental building blocks of polymers, possessing two or more reactive sites that enable the formation of covalent bonds with other monomers [134].

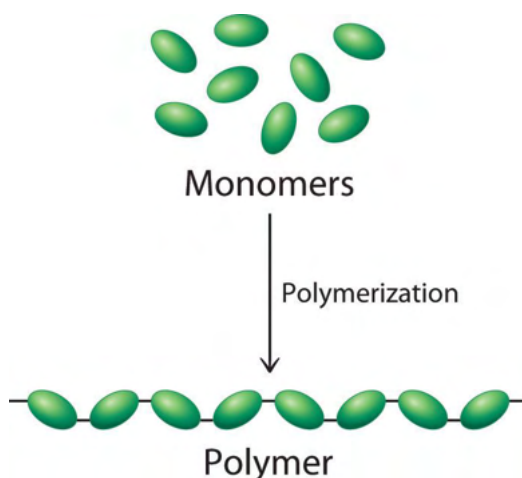


FIGURE 3.27: Functional groups in monomers and polymers [135]

Examples of monomers include amino acids, which compose proteins; nucleotides, which form DNA and RNA; and monosaccharides like glucose, which make up carbohydrates such as cellulose and starch. Isoprene is the monomer of natural rubber, while ethylene, vinyl chloride, and styrene are synthetic monomers used to produce plastics like polyethylene, PVC, and polystyrene [134].

3.7.2.1 Di(ethylene glycol) methyl ether methacrylate (DEGMA)

Di(ethylene glycol) methyl ether methacrylate (DEGMA) is a versatile monomer with the chemical formula $C_{12}H_{20}O_5$, characterized by its methacrylate ester structure that includes two ethylene glycol units and a methyl ether group. DEGMA is a liquid monomer with a molecular weight of 188.22 g/mol, a density of approximately 1.02 g/mL at 25°C, and a boiling point of 98°C at 3.5 mmHg. To maintain stability, it is often stabilized with inhibitors such as hydroquinone monomethyl ether or butylated hydroxytoluene [53].

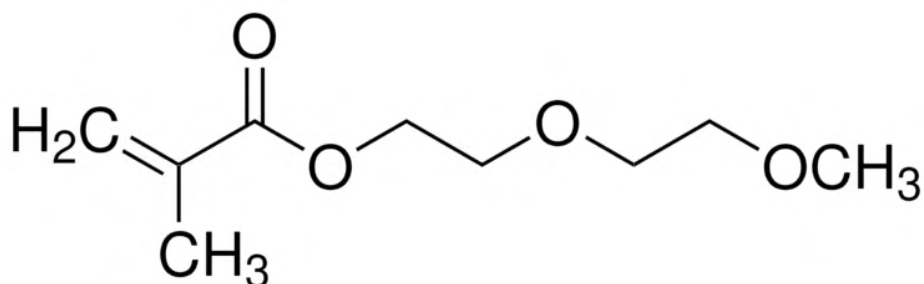


FIGURE 3.28: Chemical structure of DEGMA [53]

Through polymerization, DEGMA can form a wide range of polymers and copolymers, each with distinct properties. Polymers derived from DEGMA exhibit unique responses to temperature, pH, and salt concentrations, making them highly suitable for advanced applications like drug delivery systems, sensors, and smart materials [136].

3.7.2.2 2-(Methacryloyloxy)ethyl phosphorylcholine (MPC)

2-(Methacryloyloxy)ethyl phosphorylcholine (MPC) is a zwitterionic methacrylate monomer containing a phosphorylcholine group, known for its outstanding biocompatibility. With the chemical formula $C_{12}H_{21}NO_6P$ and a molecular weight of 311.30 g/mol, MPC is designed to undergo polymerization through its methacrylate group [137].

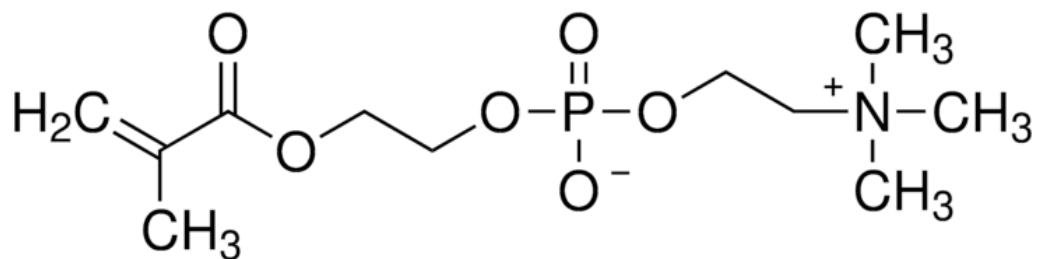


FIGURE 3.29: Chemical structure of MPC [138]

Polymers and copolymers incorporating MPC are highly valued for their excellent resistance to protein adsorption and cell adhesion, properties that make them ideal for biomedical applications. These MPC-based materials are commonly used in contact lenses, drug delivery systems, and tissue engineering scaffolds, owing to their ability to interact minimally with biological environments while providing the necessary functionality and performance [137], [139].

3.7.3 Polymer

A polymer is a large molecule composed of repeating subunits called monomers, linked together by covalent bonds. Polymers can be natural or synthetic, encompassing a wide range of properties and applications. Derived from the Greek words "polus" meaning "many" and "meros" meaning "parts," the term "polymer" aptly describes these macromolecules consisting of numerous monomers bonded in long chains or networks [140].

The formation of polymers occurs through polymerization, a process in which monomers are linked together into long chains via either step-growth or chain-growth mechanisms. Polymers possess unique properties such as toughness, elasticity, and the ability to form both amorphous and semicrystalline structures, with these characteristics depending on the type of monomers used and the nature of their bonding [135].

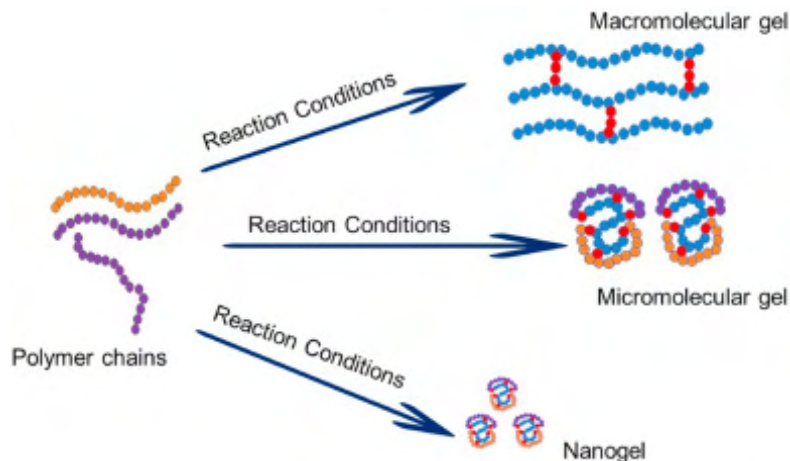


FIGURE 3.30: Formation pathways of macromolecular, micromolecular, and nanogels from polymer chains under different reaction conditions [122]

3.7.4 Copolymers

A copolymer is a polymer formed by chemically bonding two or more different monomer species in a repeating pattern along the polymer chain. Unlike homopolymers, which consist of only one type of monomer, copolymers incorporate multiple monomers, allowing for a diverse range of properties and applications.

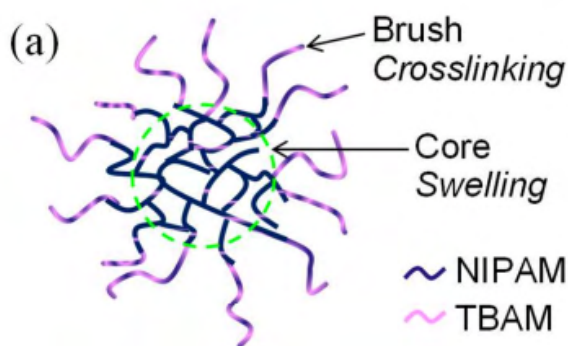


FIGURE 3.31: Structure of the P(NIPAM-TBMA) copolymer nanogel [141]

The arrangement and sequence of these monomers in the copolymer chain can be precisely controlled during the polymerization process, enabling the tailoring of the material's physical, chemical, and mechanical properties to suit specific needs. This versatility makes copolymers valuable in various industries, including pharmaceuticals, electronics, and materials science, where customized performance characteristics are often required [142].

3.8 Cellular Analysis

3.8.1 MTT Assay

The MTT assay is a widely used colorimetric test that measures cell metabolic activity as an indicator of cell viability and proliferation. This assay is based on the ability of metabolically active cells to reduce the yellow tetrazolium dye MTT (3-(4,5-dimethylthiazol-2-yl)-2,5-diphenyltetrazolium bromide) into purple formazan crystals [143].

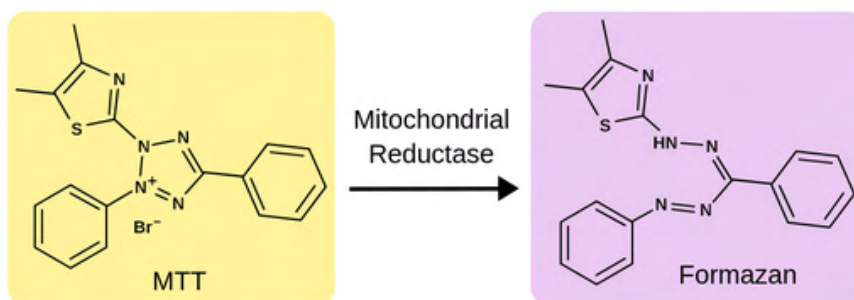


FIGURE 3.32: The MTT compound is reduced by mitochondrial reductase enzymes in viable cells to form formazan, a colored compound. [144]

The reduction process is facilitated by NAD(P)H-dependent cellular oxidoreductase enzymes, which are indicative of the number of viable cells present. As these enzymes reduce the MTT dye to insoluble formazan, the amount of formazan produced correlates with the level of metabolic activity in the cells. The formazan crystals are then

solubilized, typically using DMSO (Dimethyl Sulfoxide), and the resulting colored solution's absorbance is measured with a spectrophotometer [142].

The absorbance reading directly correlates with the number of viable, metabolically active cells; higher absorbance values indicate a greater number of healthy cells. The MTT assay is extensively employed to evaluate cell viability, proliferation, and cytotoxicity in response to various treatments, measure the metabolic activity of cells as an indicator of their health and function, and screen for potential cytotoxic agents, such as drugs or chemicals [143].

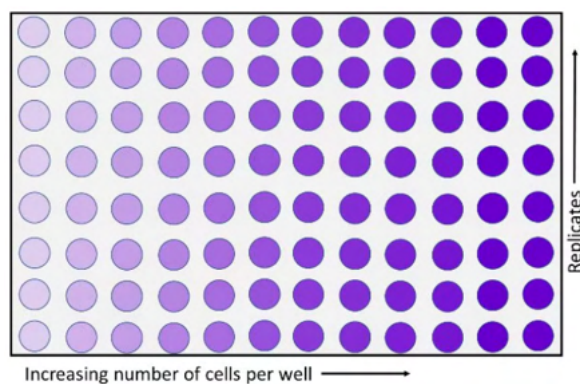


FIGURE 3.33: Microplate assay illustrating the increasing number of cells per well (left to right) and the replicates (top to bottom). The gradient of color intensity represents the varying cell densities across the wells. [144]

CHAPTER IV

METHODOLOGY

4.1 Development of Alternatives

Based on the literature review and theoretical framework, the following viable solution options were identified for the presented problem, focusing on the materials and methods for the synthesis of the nanogel that could potentially enhance the delivery and efficacy of silicon quantum dots (SiQDs) for photodynamic therapy (PDT). The performance of each alternative solution will be evaluated based on robust engineering judgments against engineering criteria and characteristics, providing a thorough basis before elaborating on the methodology utilized.

4.1.1 Nanogel Copolymer Materials

4.1.1.1 Polyethylene Glycol (PEG) and Trimethyl Chitosan (TMC)

PEG is a hydrophilic, biocompatible, and non-toxic polymer that significantly improves the solubility and stability of drugs. Its incorporation into a nanogel can enhance the overall delivery and effectiveness of the therapeutic agents it carries. TMC, on the other hand, is a cationic, biocompatible, and mucoadhesive polymer that can enhance cellular uptake and permeability of drugs. The combination of PEG and TMC in a nanogel provides a synergistic effect, resulting in improved biocompatibility, enhanced drug delivery, and superior physical properties compared to using either polymer alone. This combination leverages the hydrophilicity and stability of PEG with the permeability and

adhesive properties of TMC, making it a promising candidate for nanogel formulations aimed at efficient drug delivery systems.

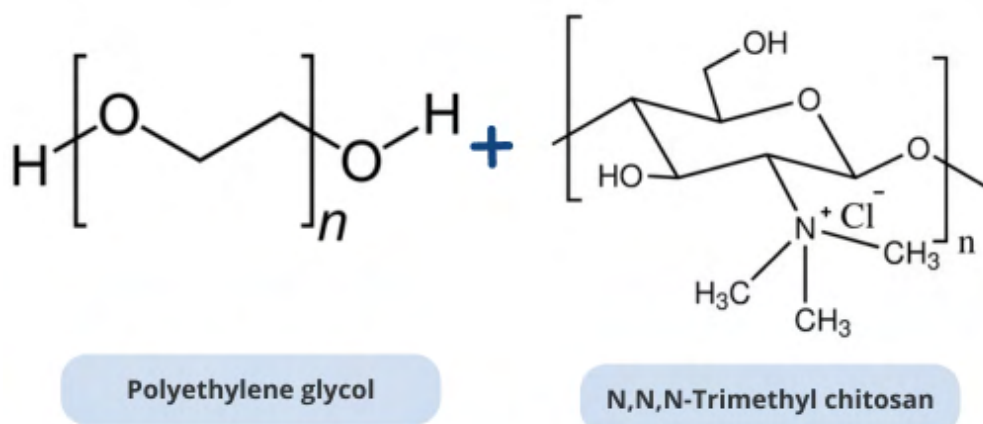


FIGURE 4.1: First option of materials for a copolymer nanogel [83]

4.1.1.2 DEGMA (Di(ethylene glycol) methyl ether methacrylate) and MPC (2-(Methacryloyloxy)ethyl phosphorylcholine)

DEGMA is a thermoresponsive polymer capable of undergoing reversible phase transitions in response to temperature changes, enabling controlled drug release based on thermal triggers. MPC is a zwitterionic polymer known for its excellent biocompatibility and resistance to protein adsorption, thereby reducing non-specific interactions. The combination of DEGMA and MPC in a nanogel results in a system that is both thermoresponsive and highly biocompatible. This dual functionality makes it suitable for various biomedical applications where precise control over drug release and minimal immune response are critical. The thermoresponsive nature of DEGMA allows for temperature-controlled drug delivery, while MPC's biocompatibility ensures safe and effective use *in vivo*.

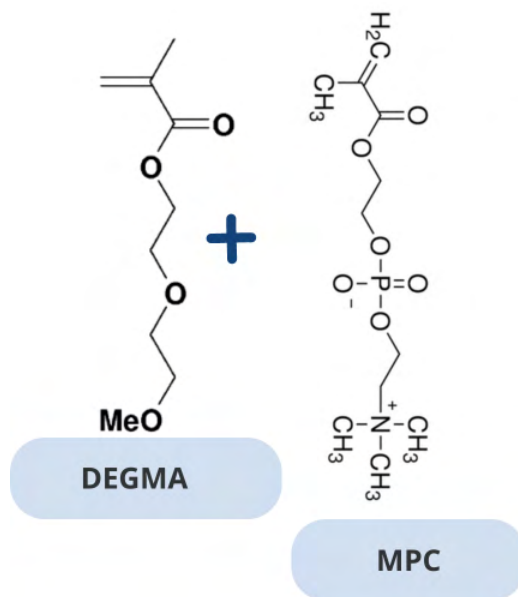


FIGURE 4.2: Second option of materials for a copolymer nanogel [83]

4.1.2 Nanogel Method of Synthesis

4.1.2.1 Atom Transfer Radical Polymerization (ATRP)

ATRP is a controlled/living radical polymerization technique that enables the synthesis of well-defined polymers with controlled molecular weight, composition, and architecture. This technique provides a high degree of control over the physical and chemical properties of the resulting nanogels, such as size, crosslinking density, and responsiveness. ATRP can be utilized to prepare nanogels with precise specifications, making it ideal for applications requiring specific and consistent performance characteristics. The ability to finely tune the polymerization process allows for the creation of nanogels tailored to meet the demands of various drug delivery and biomedical applications.

4.1.2.2 Reversible Addition-Fragmentation Chain Transfer (RAFT) Polymerization

RAFT polymerization is another controlled/living radical polymerization technique that offers excellent control over molecular weight, polydispersity, and chain-end functionality. This method can be employed to synthesize complex nanogel structures, such as core-shell architectures, with a high degree of control over their composition and responsiveness. RAFT polymerization is particularly advantageous for creating nanogels with intricate designs and specific functional attributes. The precise control provided by RAFT polymerization makes it suitable for developing advanced nanogel systems that require tailored functionalities for targeted drug delivery and other biomedical applications.

4.2 Evaluation of Alternative Solutions Based on Engineering Criteria and Characteristics

4.2.1 Nanogel Copolymer Materials Analysis

To create a comprehensive table to evaluate the alternatives for the nanogel copolymer materials using the provided information, the table will be structured to include criteria, scoring, and a summary. The table 4.1 will compare the two options: Polyethylene Glycol (PEG) and Trimethyl Chitosan (TMC) versus DEGMA (Di(ethylene glycol) methyl ether methacrylate) and MPC (2-(Methacryloyloxy)ethyl phosphorylcholine). Each solution is evaluated under a weighted point system ranging from 1 to 20, allowing for a detailed comparison based on various important factors such as biocompatibility, thermoresponsive properties, drug delivery efficiency, scalability, and cost.

The criterion of biocompatibility is the most important in the evaluation of materials for biomedical applications, as indicated by its highest weight of 30% in the table.

Biocompatibility ensures that the material will not induce an adverse reaction when introduced into the body, which is crucial for patient safety and the success of the medical treatment. Materials that are not biocompatible can cause inflammation, toxicity, or immune responses, potentially leading to severe complications and treatment failures. Thus, ensuring high biocompatibility is essential for the development of safe and effective medical devices, drug delivery systems, and other biomedical applications. This prioritization reflects the critical need to minimize any risk to patients and to comply with regulatory standards for medical materials.

| Criteria | PEG and TMC | DEGMA and MPC | Weight (%) |
|--------------------|---|---|------------|
| Biocompatibility | PEG: Hydrophilic, biocompatible, FDA approved TMC: Cationic, mucoadhesive, enhances uptake Score: 20 | DEGMA: Limited biocompatibility data MPC: Excellent biocompatibility, antifouling properties Score: 18 | 30 |
| Thermoresponsive | None Score: 0 | DEGMA: Thermoresponsive, LCST around 26°C Score: 20 | 20 |
| Drug Delivery | PEG: Improves solubility and stability TMC: Enhances uptake and permeability Score: 20 | DEGMA: Temperature-controlled release MPC: Reduces protein adsorption Score: 20 | 25 |
| Scalability | PEG: Widely used, scalable TMC: Moderately scalable Score: 18 | DEGMA: Scalable MPC: Limited scalability data Score: 15 | 15 |
| Cost | PEG: \$6 to \$1,300 per unit TMC: \$185 to \$425 per unit Score: 10 | DEGMA: \$30 to \$121 per unit MPC: \$171 Score: 16 | 10 |
| Total Score | 68 | 90 | 100 |

TABLE 4.1: Evaluation of Nanogel Copolymer Materials

The use and selection of 2-methacryloyloxyethyl phosphorylcholine (MPC) in the

synthesis of the nanogel is confirmed by its well-documented properties [145]. MPC is a zwitterionic monomer known for its high biocompatibility and antifouling properties. Its structure includes a phosphate group that provides a negative charge and a trimethylammonium group that provides a positive charge, resulting in an overall electrically neutral molecule. This zwitterionic nature minimizes toxicity and immune response, making MPC an excellent choice for biomedical applications. The potential of MPC in gene therapy is demonstrated through its ability to form stable and biocompatible polyplexes for efficient gene knockdown. These properties validate the selection of MPC in our nanogel synthesis for enhanced biocompatibility and functionality .

Furthermore, the justification for using a nanogel is supported by research exploring the synthesis and evaluation of temperature-responsive nanogels [146]. This study varies charges in their core and shell, demonstrating their hemocompatibility and potential for biomedical applications. The findings show that nanogels with neutral or zwitterionic surfaces, similar to our MPC-based nanogel, exhibit excellent blood compatibility, making them suitable for *in vivo* applications. The tunable physical and biological properties of nanogels, which can be optimized for specific therapeutic purposes, support the use of our synthesized nanogel incorporating MPC and DEGMA. This provides a biocompatible and thermoresponsive material for potential applications in drug delivery and photodynamic therapy

4.2.2 Analysis of Nanogel Synthesis Methods

In this table 4.2, the two primary synthesis methods for nanogels—Atom Transfer Radical Polymerization (ATRP) and Reversible Addition-Fragmentation Chain Transfer (RAFT) Polymerization—are assessed. The evaluation utilizes a weighted point system, ranging from 1 to 20, to determine the optimal synthesis technique.

| Criteria | ATRP | RAFT | Weight (%) |
|--------------------|--|--|------------|
| Polymer Definition | Controlled molecular weight and narrow polydispersity Tolerates a wide range of functional groups Score: 20 | Controlled molecular weight, low polydispersity Tolerant of a wide range of functional groups and reaction conditions Score: 18 | 25 |
| Functionalization | Bromine end groups enable further chain extension and functionalization Score: 20 | Residual RAFT end groups maintain reactivity and can be used for further functionalization Score: 18 | 20 |
| Catalyst/Initiator | Requires transition metal catalysts, potential toxicity concerns Score: 15 | Requires addition of a RAFT agent, can be expensive Score: 18 | 20 |
| Polymerization | Limited tolerance for aqueous media, acidic monomers Score: 14 | Applicable in aqueous media, tolerant of acidic monomers Score: 20 | 15 |
| Cost | Transition metal catalysts and ligands can be expensive Score: 12 | RAFT agent can be expensive Score: 14 | 20 |
| Total Score | 81 | 88 | 100 |

TABLE 4.2: Evaluation of Nanogel Synthesis Methods

Atom Transfer Radical Polymerization (ATRP) presents several disadvantages compared to Reversible Addition-Fragmentation Chain Transfer (RAFT) polymerization for the synthesis of nanogels. One significant drawback of ATRP is the requirement for a transition metal catalyst, such as copper, which can be challenging to remove completely from the final product. The presence of residual metal traces in the nanogels can pose problems, especially for biomedical applications, due to potential toxicity. Additionally, ATRP has limitations in aqueous media, as conventional ATRP struggles to perform efficiently in hydrophilic environments. The ligands used in ATRP can protonate in acidic conditions, negatively impacting the control of polymerization and limiting its applicability for synthesizing hydrophilic nanogels [147].

In contrast, RAFT polymerization offers several advantages that make it more suitable for synthesizing nanogels. RAFT is more versatile, allowing for polymerization in aqueous media with greater tolerance to oxygen. This flexibility makes RAFT more adaptable to various synthesis conditions and applications. Furthermore, RAFT polymerization facilitates easier removal and modification of terminal groups, overcoming one of the significant limitations of ATRP. These benefits make RAFT polymerization a more robust and adaptable method for producing nanogels, particularly for biomedical applications where biocompatibility and precise control over polymer properties are crucial [148].

4.3 Description of the Research Methodology

Building upon the previously mentioned details, the methodology of the present thesis focuses on developing a copolymer nanogel optimized for the encapsulation and evaluation of two types of silicon quantum dots (SiQDs) for potential use in photodynamic therapy targeting HeLa cancer cells.

The chapter is divided into five interconnected sections, each designed to address specific aspects of the nanogel development process and its evaluation. The first phase involves the synthesis of the copolymer nanogel, achieved through RAFT polymerization of DEGMA (Diethylene Glycol Methyl Ether Methacrylate) and MPC (2-Methacryloyloxyethyl Phosphorylcholine). This section details the preparation of the reaction mixture, polymerization conditions, and purification of the synthesized nanogel.

The second phase focuses on the encapsulation of two types of SiQDs: Acid Functionalized Silicon Nanocrystals (Acid-SiQDs) and Acid-Functionalized Poly(ethylene oxide)-Terminated Silicon Nanocrystals (Acid-PEO-SiQDs). It covers the preparation of SiQDs solutions, the encapsulation procedure within the nanogel, and the determination of loading efficiency using fluorescence analysis.

Next, comprehensive characterization of the nanogel and SiQDs encapsulation is carried out in the third phase, including an in-depth assessment of its morphology and physicochemical properties using techniques such as dynamic light scattering (DLS), thermogravimetric analysis (TGA), and nuclear magnetic resonance (NMR). These analyses are crucial for understanding the distribution, encapsulation efficiency, and interactions within the nanogel-SiQDs complex.

The fourth phase involves assessing the biocompatibility of the SiQDs-loaded nanogel with fibroblast cells. This phase includes preparing fibroblast cell cultures, conducting MTT assays to evaluate cytotoxicity, and analyzing cell viability to ensure the safety of the nanogel for biomedical applications.

Finally, the fifth phase focuses on evaluating the *in vitro* delivery and photodynamic therapy efficacy of the SiQDs-loaded nanogel against HeLa cells. This includes the preparation of nanogel-SiQDs complexes, the application of near-infrared (NIR) light to induce photodynamic effects, and MTT assays to measure changes in cell viability, assessing both cytotoxic effects and therapeutic efficiency.

It is important to compare the two types of silicon quantum dots to understand the interaction between the DEGMA and MPC monomers once the nanogel is successfully characterized. Additionally, this comparison is crucial for evaluating their encapsulation efficiency, stability within the nanogel, and overall performance to be uptaken by the cells to gain deeper insights.

The detailed sequence of experimental processes can be visualized in the workflow presented in Figure 4.3:

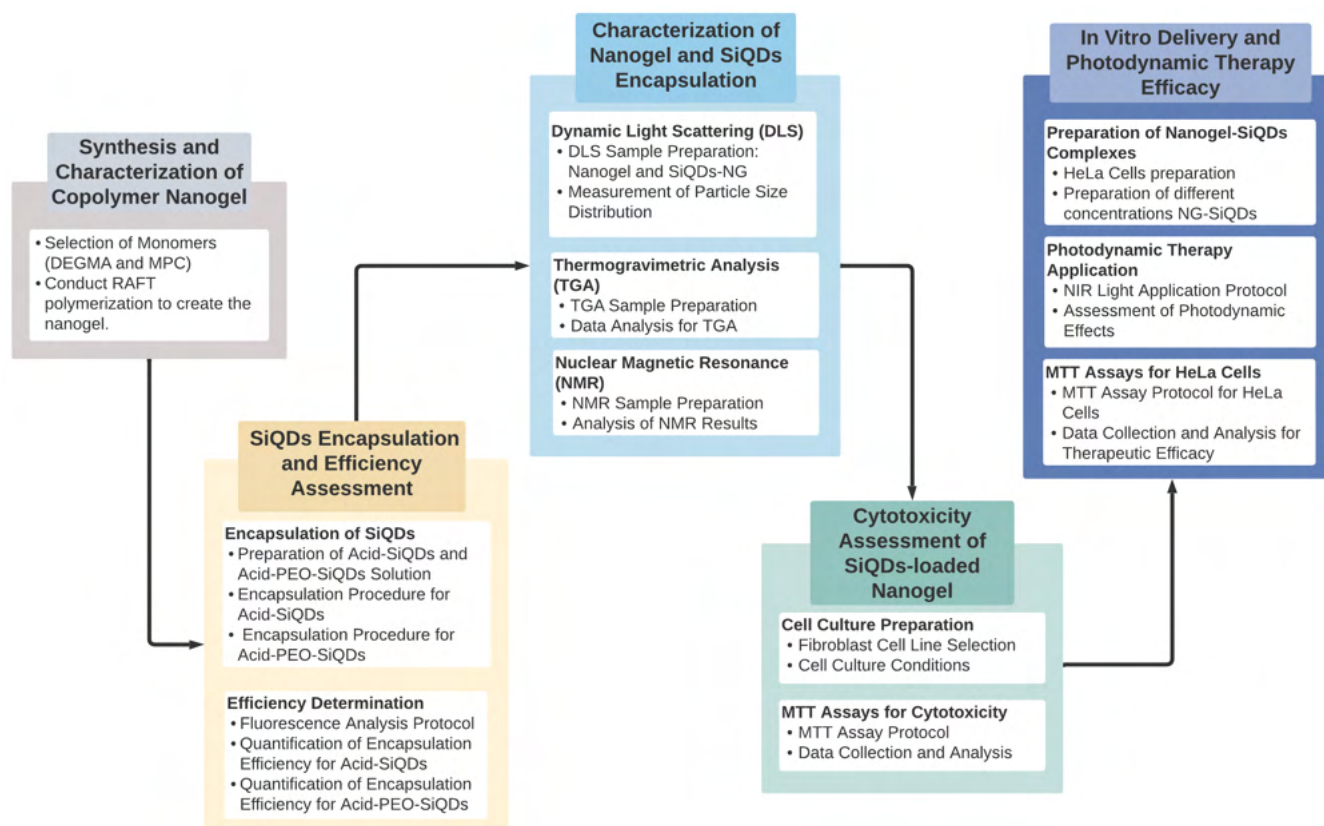


FIGURE 4.3: Workflow for the experimental procedure

4.4 Research Characterization

This research is driven by the goal of developing a practical and innovative solution in the realm of targeted cancer therapy. The focus is on the creation of a copolymer nanogel specifically designed for the encapsulation and evaluation of two types of silicon quantum dots (SiQDs) for potential use in photodynamic therapy targeting HeLa cancer cells. The objective is to produce a tangible and applicable product, demonstrating a clear intent to address a specific challenge in medical treatment, particularly in the context of cancer therapeutics. This approach positions the study within the applied research domain, as it seeks to deliver direct and practical contributions to the field of cancer treatment.

The methodology of this research predominantly takes a quantitative approach. This is evident in the extensive use of precise measurements, numerical data collection, and quantitative analysis techniques. Methods such as dynamic light scattering (DLS), thermogravimetric analysis (TGA), nuclear magnetic resonance (NMR), and MTT assays for cell viability assessment are inherently quantitative. These methods provide objective, numerical data that form the basis for the study's findings, aligning the research firmly within the quantitative research paradigm.

The research design is experimental as it involves a series of controlled laboratory experiments, including the synthesis of the nanogel, the encapsulation of SiQDs, and the subsequent evaluation of their effects on HeLa cells. This experimental setup allows for the observation and measurement of the cause-and-effect relationship between the nanogel-SiQDs complex and its impact on cell viability and photodynamic therapy efficacy. Such a design is quintessential to experimental research, where the manipulation of variables and observation of their effects in a controlled setting are central to the methodology.

This study can be aptly categorized as descriptive-propositive. Initially, it delves into describing the properties and interactions of the nanogel with the two types of SiQDs. Moreover, the research ambitiously proposes a novel application for this nanogel in the realm of cancer therapy. Moving beyond just descriptive observation, the research innovatively proposes and demonstrates the potential use of the nanogel as an effective delivery system for SiQDs in photodynamic therapy. This dual focus—encompassing both description and proposition—distinctly places the study in the descriptive-propositive category. The aim is twofold: to characterize a new scientific phenomenon and to propose its practical application, thereby bridging the gap between theory and practice *in vitro*.

Finally, this study is characterized as cross-sectional. It involves the collection of data at specific points in time, particularly following certain experimental procedures or upon the completion of defined stages within the cell culture experiments. This approach

stands in contrast to longitudinal studies, which are characterized by data collection over more extended periods. The cross-sectional nature of this study is particularly suited for observing and analyzing the immediate or short-term effects of the nanogel-SiQDs complex on HeLa cells.

4.5 Synthesis and Characterization of Copolymer Nanogel

4.5.1 Materials for the Nanogel Structure

The synthesis of the copolymer nanogel required several specific materials and reagents. The primary monomer used was 2-(Methacryloyloxy)ethyl phosphorylcholine (MPC). For the RAFT polymerization, 4-Cyano-4-(phenylcarbonothioylthio)pentanoic acid (CTP) served as the chain transfer agent. Polymerization was initiated using 4,4'-Azobis(4-cyanovaleric acid) (ACVA) as a free radical initiator. The crosslinking agent was N,N'-Methylenebis(acrylamide) (mBAm), while Di(ethylene glycol) methyl ether methacrylate (DEGMA) was added to provide hydrophilic properties. Dimethylformamide (DMF) was employed to dissolve mBAm, and tetrahydrofuran (THF) was used for precipitation steps. Throughout the process, deionized (DI) water was used to ensure purity and consistency.

4.5.2 RAFT Polymerization Process

4.5.2.1 Preparation of MPC-macroCTA

The preparation of MPC-macroCTA began with accurately weighing 1.5 grams of MPC, which served as the primary monomer for polymer block formation. Next, 36 milligrams of CTP (the chain transfer agent) and 0.09 milligrams of ACVA (the free radical initiator) were added to the mixture. To dissolve the monomers and initiator, 5.1

milliliters of methanol was introduced as a solvent. The reactive mixture was then purged with nitrogen for 15 to 30 minutes to eliminate oxygen, thereby preventing inhibition or premature termination of the polymerization reaction.

The polymerization reaction was conducted at a controlled temperature of 67-70°C for 20 hours, allowing MPC to polymerize in the presence of CTP and form the macroCTA with a controlled structure and molecular weight. Following polymerization, the product was precipitated in THF to purify the MPC-macroCTA, effectively separating it from any unreacted monomers and low molecular weight impurities. The polymer was dissolved again in methanol to ensure complete solubilization and separation of any remaining insoluble impurities. To further purify the polymer, the process of dissolving in methanol and precipitating in THF was repeated three times. The purified MPC-macroCTA was then retrieved and characterized using gel permeation chromatography (GPC) to determine its molecular weight and molecular weight distribution (Annex 1).

4.5.2.2 DEGMA Purification

The DEGMA monomer was purified using a column filtration method with alumina. A layer of cotton or glass wool was placed at the base of the column to prevent alumina from spilling, and alumina was added on top. The DEGMA was loaded onto the prepared column, where the alumina acted to purify it by selectively retaining impurities. The column was eluted with a suitable solvent, carrying the DEGMA through the column while separating the impurities. The DEGMA eluted from the column was collected, and the solvent was evaporated to obtain purified DEGMA.

4.5.2.3 Nanogel Synthesis

For the synthesis of the nanogel, precise amounts of the reactants were weighed: 50 milligrams of MPC macro CTA, 15 milligrams of mBAm, 64 milligrams of ACVA,

and 0.258 grams of purified DEGMA. The mBAm was transferred into an Eppendorf tube, while the MPC macro CTA and ACVA were placed together in a test tube. The mBAm was then dissolved in 0.364 milliliters of DMF.

- **Preparation of Reaction Mixture:** The reaction mixture was prepared in a test tube by combining the following components: 50 milligrams of MPC macro CTA, 64 milligrams of ACVA, 15 milligrams of mBAm (dissolved in 0.364 milliliters of DMF), 0.258 grams of purified DEGMA, 3 milliliters of deionized water, and 3.56 milliliters of 2-propanol. The mixture was sonicated to homogenize the solution and subsequently purged with nitrogen for 15 to 30 minutes to eliminate oxygen and prevent undesired free radical formation.
- **Polymerization Conditions and Reaction:** Following the nitrogen purge, the mixture was placed in an oil bath at 75°C with constant agitation to facilitate the polymerization reaction. The test tube was maintained under these conditions for 14 hours to ensure the proper formation of the polymer network. After polymerization, the product underwent dialysis for three days to remove residual solvents, unreacted monomers, and other low molecular weight impurities. The sample was transferred into a specialized dialysis membrane, sealed with two clips and two rubber bands for extra security, and placed in a bowl filled with deionized water on a magnetic stirrer. The water was changed twice daily.
- **Purification of Synthesized Nanogel:**

After three days of dialysis, the sample was removed from the membrane, transferred to a test tube, frozen with liquid nitrogen, and subjected to lyophilization (freeze-drying) to obtain a dry, purified polymer. The test tube was covered with aluminum foil with holes before being transferred to the lyophilizer. The lyophilization process removed all moisture by sublimation under reduced pressure, resulting in a dry powder form of the nanogel. This powder could then be stored or further processed as needed.

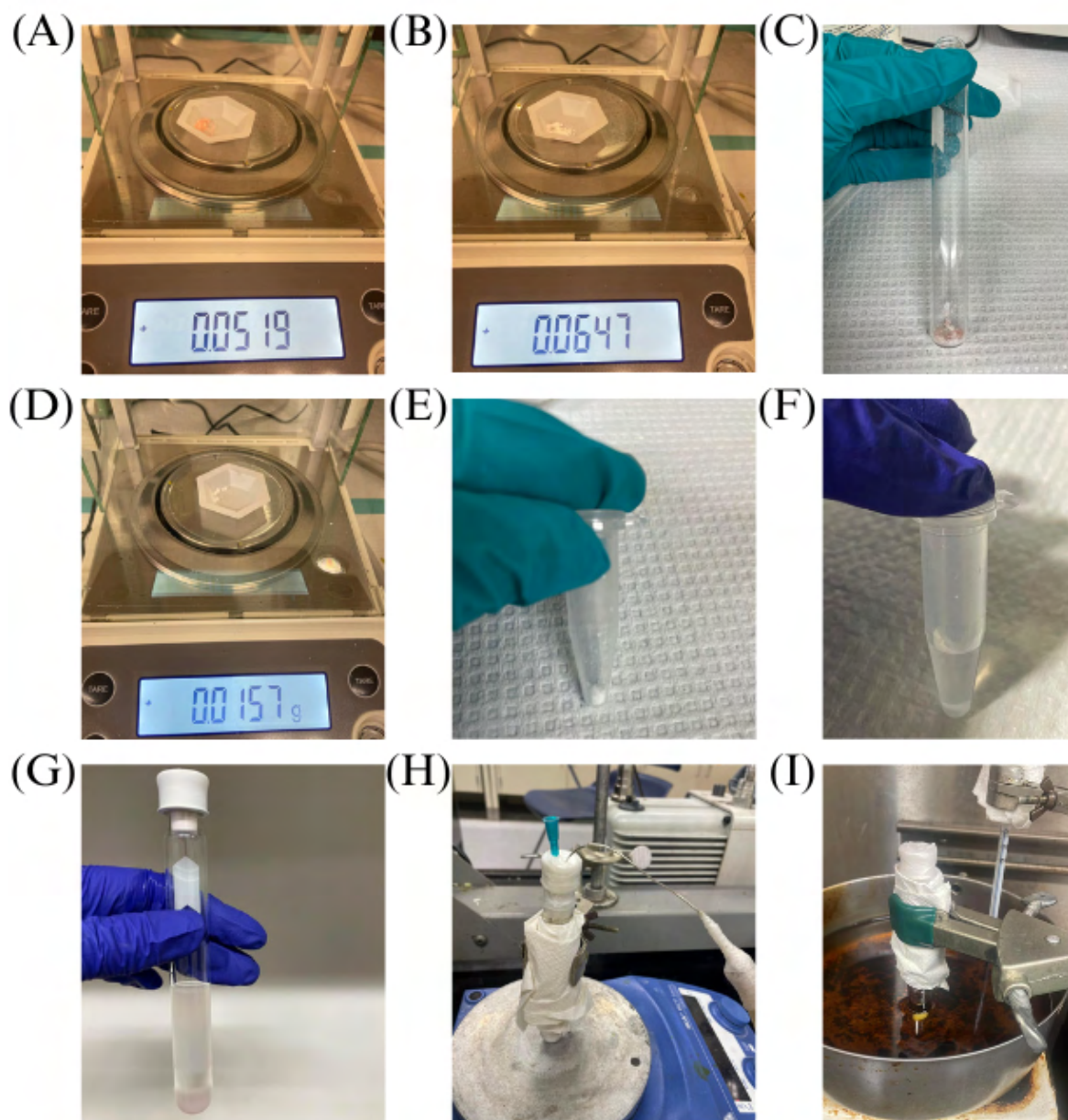


FIGURE 4.4: Synthesis of the nanogel. (A) Weighing the polymerized and ready MPC-macroCTA. (B) Weighing the ACVA reagent. (C) Placing the weighed MPC-macroCTA and ACVA into a test tube. (D) Weighing mBAM. (E) Placing mBAM into an Eppendorf tube. (F) Dissolving mBAM in DMF. (G) Combining all previously weighed components, adding mBAM dissolved in DMF, water, 2-propanol, and DEGMA. (H) Purging process with gaseous nitrogen. (I) Start of the polymerization.

The successful completion of the lyophilization process yielded the nanogel in

a dry powder form, demonstrating the efficacy of the RAFT methodology in polymer engineering. This nanogel possessed the specific properties and architecture as designed.

4.6 SiQDs Encapsulation and Efficiency Assessment

4.6.1 Encapsulation of SiQDs

The encapsulation process of silicon quantum dots (SiQDs) within the nanogel matrix will be based on electrostatic interactions. This method is chosen to ensure efficient encapsulation and stability of the SiQDs within the nanogel structure.

| Type of Quantum Dots | Functionalization | PLQYs | Concentration |
|--|---------------------------|--------------------|---------------|
| Acid Functionalized SiNCs by thermal (Acid-SiQDs) | Acid Functionalized | $29.19 \pm 2.66\%$ | 3 mg/ml |
| Acid-Functionalized Poly(ethylene oxide)-Terminated (Acid-PEO-SiQDs) | Acid-Poly(ethylene oxide) | $22.77 \pm 3.54\%$ | 15 mg/ml |

TABLE 4.3: Surface Functionalization and Concentration of SiQDs

4.6.1.1 Preparation of SiQDs Solution

Two types of SiQDs will be utilized, each synthesized by Applied Quantum Materials Inc. These SiQDs differ in their surface functionalization and initial concentrations, which will influence their encapsulation efficiency and stability within the nanogel.

- **Acid Functionalized SiNCs (Acid-SiQDs):** These SiQDs are functionalized with carboxylic acid groups, providing a negative surface charge. The initial concentration of Acid-SiQDs is 3 mg/ml according to the specifications provided by Applied Quantum Materials Inc.

- **Acid-Functionalized Poly(ethylene oxide)-Terminated SiQDs (Acid-PEO-SiQDs):**

These SiQDs are functionalized with poly(ethylene oxide) chains terminated with carboxylic acid groups. The initial concentration of Acid-PEO-SiQDs is 15 mg/ml based on the manufacturer's guidelines.

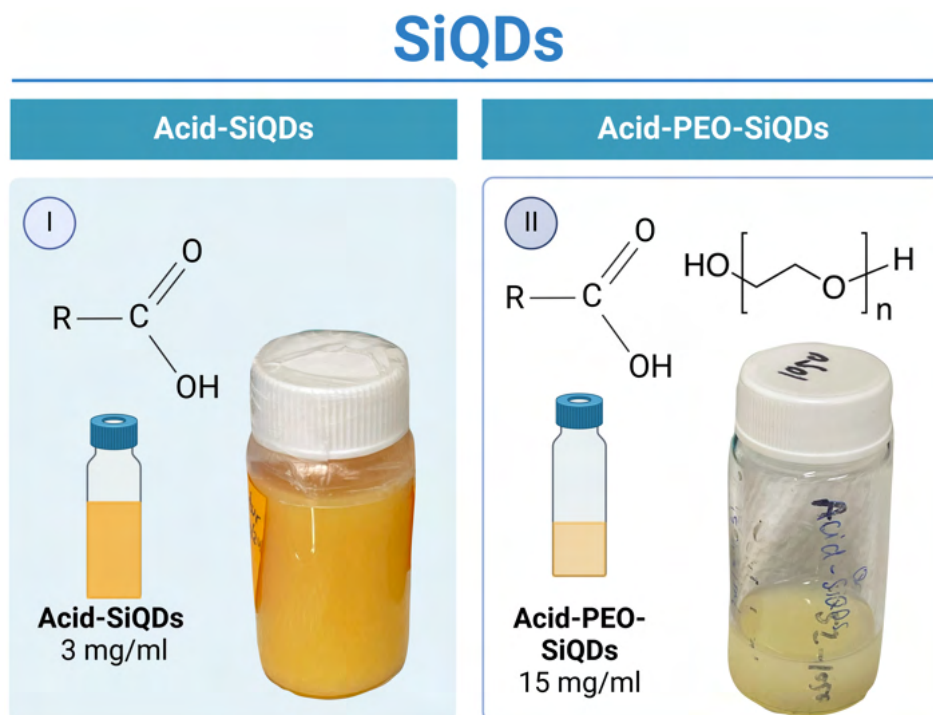


FIGURE 4.5: Two types of SiQDs

The methodology for performing dialysis involves transferring the entire content of the SiQDs solution into a porous dialysis membrane. The membrane is securely closed at both ends using clips to prevent any leakage. The sealed membrane is then placed into a bowl containing a mixture of 70% methanol and deionized (DI) water. The solution is allowed to dialyze in this solvent mixture, which is changed twice a day. This process is repeated for two days to ensure thorough purification. On the second day, only DI water is used for dialysis, which helps in removing any residual methanol from the SiQDs solution.

Pre-processing of SiQDs

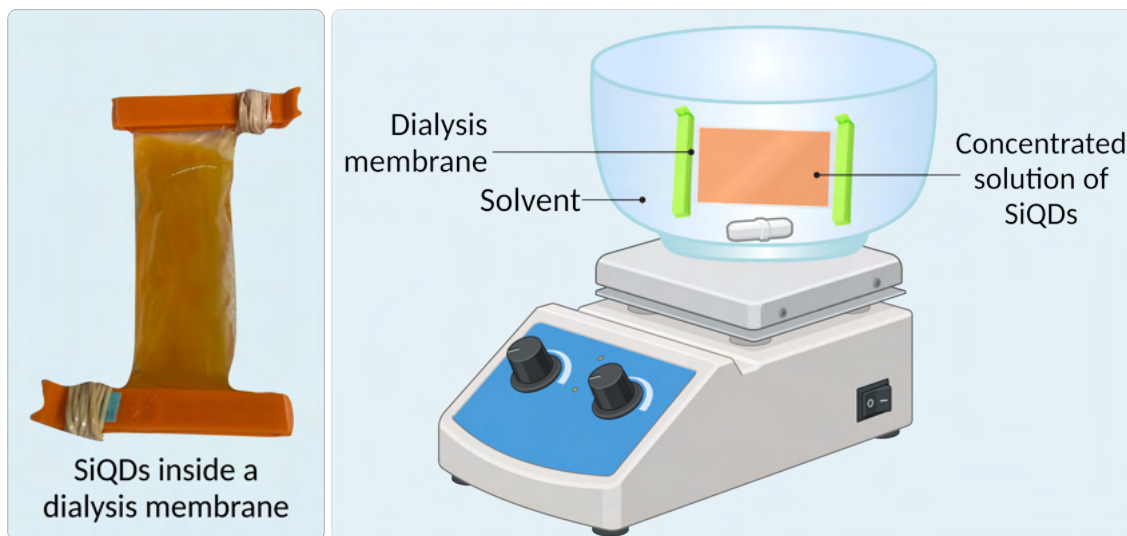


FIGURE 4.6: Dyalisis for SiQDs

4.6.1.2 Encapsulation Procedure for Acid-SiQDs

This protocol describes the adjusted steps for preparing a nanogel solution incorporating silicon quantum dots (SiQDs) with a revised concentration of 3 mg/ml. The adjustments ensure the correct amount of SiQDs is maintained in the final mixture.

To prepare the nanogel solution, first, a 5 mg/5 ml nanogel solution is prepared in phosphate-buffered saline (PBS). The solution is then stirred continuously until it dissolves completely, which takes approximately 2 hours. After ensuring complete dissolution, 1 ml of the SiQDs solution with a concentration of 3 mg/ml is added to the nanogel solution. This adjustment will result in a final volume of 6 ml in the mixture, containing a total of 3 mg of SiQDs, following the modified protocol.

To achieve the desired concentration in the final mixture, the following parameters are considered:

- $C_2 = 3 \text{ mg/ml}$ (desired concentration in the final mixture)

- $V_2 = 6$ ml (total volume after SiQDs solution addition)

By adding 1 ml of the SiQDs solution at a concentration of 3 mg/ml, the total volume becomes 6 ml with the desired concentration of SiQDs maintained.

Once the SiQDs have been added, the reaction is allowed to proceed at room temperature for 24 hours. After the reaction time, the mixture undergoes a freeze-drying process for 48 hours to ensure complete encapsulation and stability of the SiQDs within the nanogel matrix.

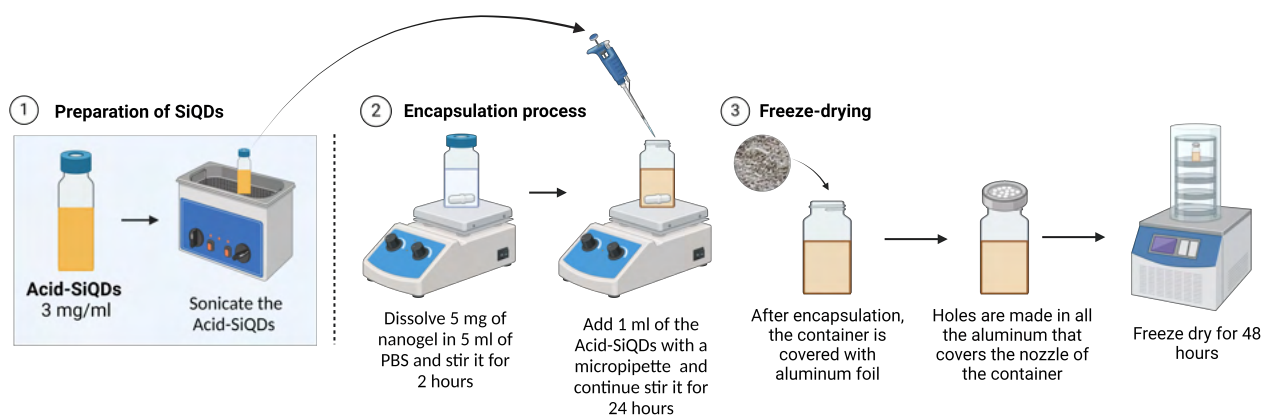


FIGURE 4.7: Encapsulation Workflow for Acid-SiQDs

4.6.1.3 Encapsulation Procedure for Acid-PEO-SiQDs

This protocol describes the adjusted steps for preparing a nanogel solution incorporating Acid-PEO-silicon quantum dots (Acid-PEO-SiQDs) with a revised concentration of 15 mg/ml. The adjustments ensure the correct amount of SiQDs is maintained in the final mixture.

First, a 5 mg/5 ml nanogel solution is prepared in phosphate-buffered saline (PBS). The solution is stirred continuously until it dissolves completely, which takes approximately 2 hours.

For the SiQDs solution addition, the updated concentration of 15 mg/ml is used to maintain a final SiQDs content of 3 mg in the mixture. The volume of SiQDs solution to be added is calculated using the dilution equation $C_1V_1 = C_2V_2$, where C_1 is the initial SiQDs concentration (15 mg/ml), V_1 is the volume of SiQDs solution to be added, C_2 is the desired concentration, and V_2 is the total volume after addition. Given that the desired total amount of SiQDs is 3 mg and the new concentration is 15 mg/ml, V_1 is calculated as:

$$V_1 = \frac{3 \text{ mg}}{15 \text{ mg/ml}} = 0.2 \text{ ml}$$

Therefore, 0.2 ml of the 15 mg/ml SiQDs solution is added to the nanogel solution.

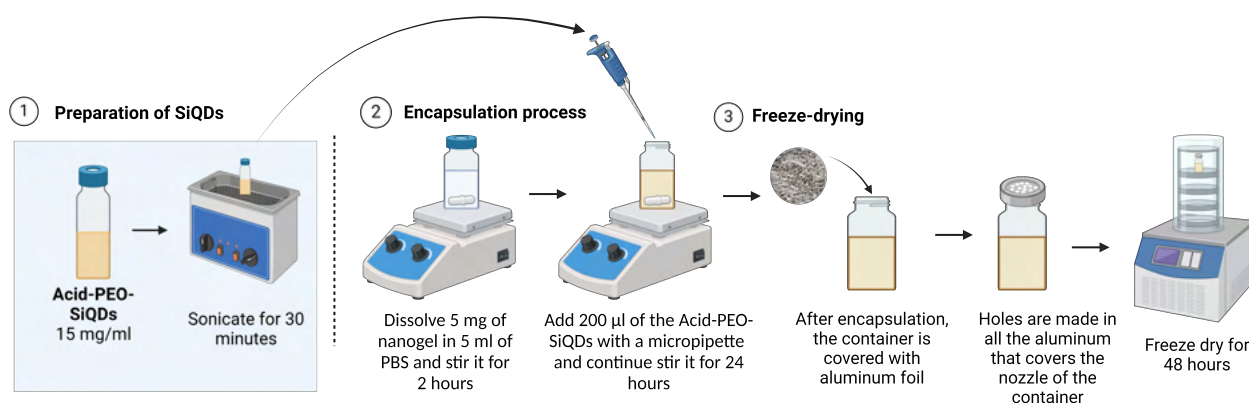


FIGURE 4.8: Encapsulation Workflow for Acid-PEO-SiQDs

The reaction is allowed to proceed at room temperature for 24 hours. After the reaction time, the mixture undergoes a freeze-drying process for 48 hours to ensure complete encapsulation and stability of the SiQDs within the nanogel matrix.

4.6.2 Loading Efficiency Determination

4.6.2.1 Encapsulation Efficiency for Acid-SiQDs

First, a 5 mg/5 ml nanogel solution is prepared in phosphate-buffered saline (PBS). The solution is then stirred continuously until it dissolves completely, which takes approximately 2 hours. After ensuring complete dissolution, 1 ml of the SiQDs solution with a concentration of 3 mg/ml is added to the nanogel solution. This adjustment will result in a final volume of 6 ml in the mixture, containing a total of 3 mg of SiQDs, following the modified protocol. To achieve the desired concentration in the final mixture, the following parameters are considered:

- $C_2 = 3 \text{ mg/ml}$ (desired concentration in the final mixture)
- $V_2 = 6 \text{ ml}$ (total volume after SiQDs solution addition)

By adding 1 ml of the SiQDs solution at a concentration of 3 mg/ml, the total volume becomes 6 ml with the desired concentration of SiQDs maintained.

The reaction is allowed to proceed at room temperature for 24 hours. After the reaction time, the solution is centrifuged at an appropriate speed for the particle size to separate encapsulated SiQDs from unencapsulated SiQDs. The supernatant is carefully removed without disturbing the pellet, as the pellet contains the unencapsulated SiQDs, which is the fraction of interest for further processing. If necessary, the pellet is gently resuspended in a suitable buffer. Finally, the prepared sample undergoes freeze-drying for 48 hours to obtain the final nanogel product encapsulating SiQDs.

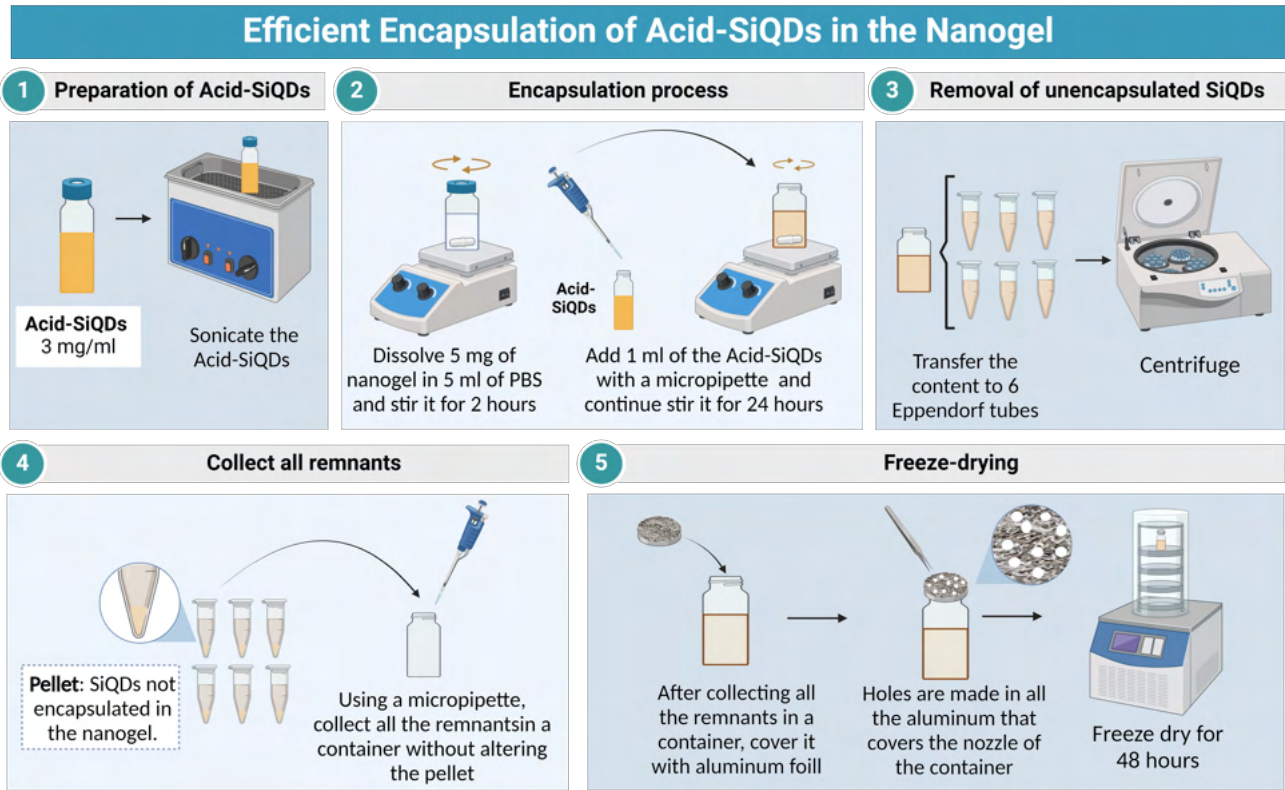


FIGURE 4.9: Encapsulation Efficiency Workflow for Acid-SiQDs

4.6.2.2 Encapsulation Efficiency for Acid-PEO-SiQDs

First, a 5 mg/5 ml nanogel solution is prepared in phosphate-buffered saline (PBS). The solution is then stirred continuously until it dissolves completely, which takes approximately 2 hours.

For the SiQDs solution addition, the updated concentration of 15 mg/ml is used to maintain a final SiQDs content of 3 mg in the mixture. The volume of SiQDs solution to be added is calculated using the dilution equation $C_1V_1 = C_2V_2$, where C_1 is the initial SiQDs concentration (15 mg/ml), V_1 is the volume of SiQDs solution to be added, C_2 is the desired concentration, and V_2 is the total volume after addition. Given that the desired total amount of SiQDs is 3 mg and the new concentration is 15 mg/ml, V_1 is calculated as:

$$V_1 = \frac{3 \text{ mg}}{15 \text{ mg/ml}} = 0.2 \text{ ml}$$

Therefore, 0.2 ml of the 15 mg/ml SiQDs solution is added to the nanogel solution.

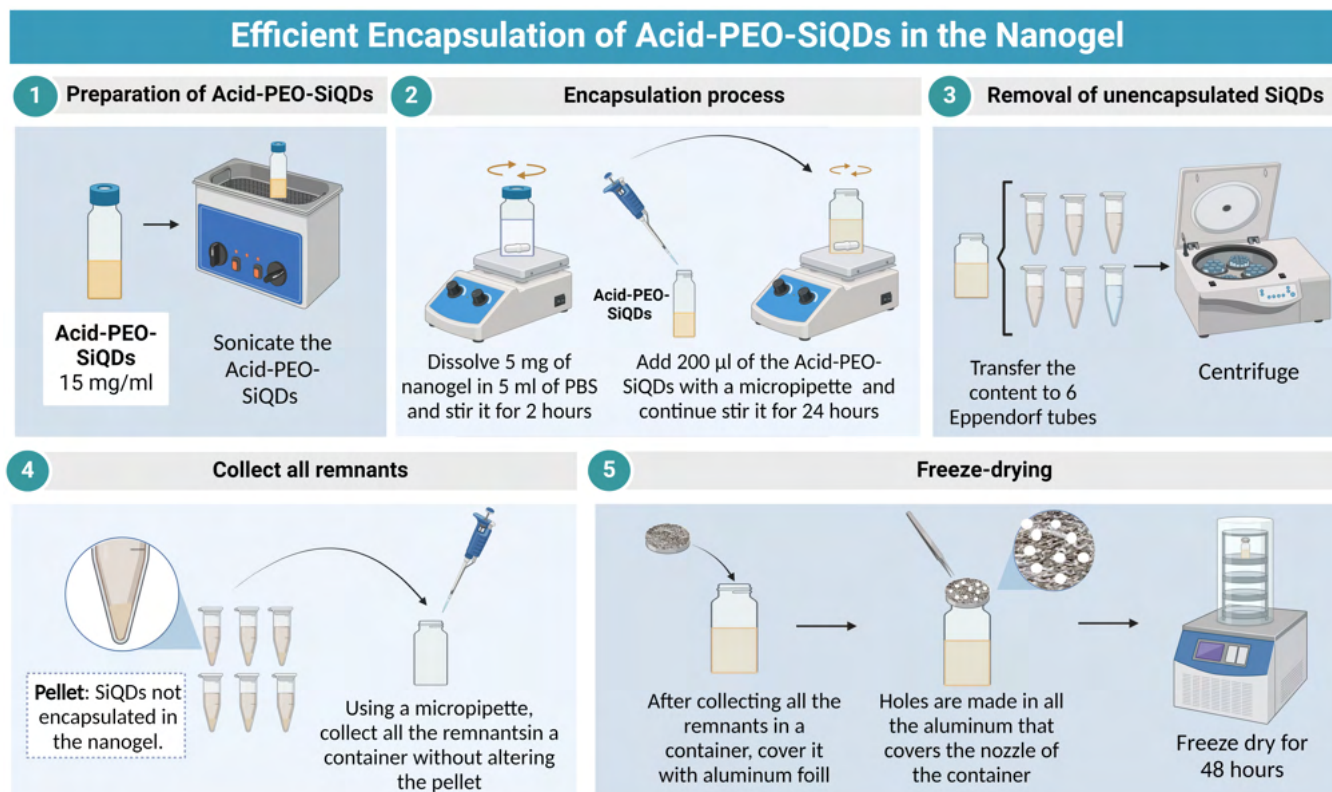


FIGURE 4.10: Encapsulation Efficiency Workflow for Acid-PEO-SiQDs

The reaction is allowed to proceed at room temperature for 24 hours. After the reaction time, the solution is centrifuged at an appropriate speed for the particle size to separate encapsulated SiQDs from unencapsulated SiQDs. The supernatant is carefully removed without disturbing the pellet, as the pellet contains the unencapsulated SiQDs, which is the fraction of interest for further processing. If necessary, the pellet is gently resuspended in a suitable buffer. Finally, the prepared sample undergoes freeze-drying for 48 hours to obtain the final nanogel product encapsulating SiQDs.

4.6.2.3 Fluorescence Analysis Protocol

The fluorescence analysis protocol aims to determine the encapsulation efficiency of the SiQDs within the nanogel. After centrifugation, but before lyophilization, samples are taken from each type of SiQDs (Acid-SiQDs and Acid-PEO-SiQDs) to measure their fluorescence intensity.

To begin, an Eppendorf tube is used to collect samples of the encapsulated SiQDs. Using a micropipette, 100 microliters of the sample containing Acid-SiQDs, which are expected to be encapsulated within the nanogel, are drawn and placed into a well plate. This process is repeated three times, filling three wells with 100 microliters each. The same procedure is followed for the Acid-PEO-SiQDs samples.

Next, the encapsulation efficiency is verified by comparing the fluorescence intensity peaks of the encapsulated SiQDs against a control sample, which consists of the unencapsulated SiQDs provided by the manufacturer. For the control, 100 microliters of the Acid-SiQDs with a concentration of 3 mg/ml are placed into three separate wells, replicating the triplicate process.

For the Acid-PEO-SiQDs, the sample is first dissolved in PBS to achieve the same concentration of 3 mg/ml. Then, 100 microliters of this solution are transferred into three separate wells, ensuring triplicate measurements. This allows for a direct comparison of the fluorescence intensities, facilitating the calculation of encapsulation efficiency.

The fluorescence measurements were processed with Skanlt Software 6.1 RE for Microplate Reader. The following parameters are set for the fluorescence analysis:

- Excitation wavelength (nm): 365
- Emission wavelength range (nm): 400 to 800, with a step size of 1 nm
- Measurement time (ms): 100

The encapsulation efficiency (%) is calculated using the formula:

$$\text{Encapsulation Efficiency (\%)} = \left(\frac{\text{Fluorescence Intensity of Encapsulated SiQDs}}{\text{Fluorescence Intensity of Control SiQDs}} \right) \times 100 \quad (\text{IV.1})$$

Table 4.4 summarizes the number of samples prepared in triplicate for fluorescence analysis, including both encapsulated and control SiQDs.

| Sample Type | Volume per Well (μl) | Number of Wells |
|-----------------------------|-----------------------------------|-----------------|
| Encapsulated Acid-SiQDs | 100 | 3 |
| Encapsulated Acid-PEO-SiQDs | 100 | 3 |
| Control Acid-SiQDs | 100 | 3 |
| Control Acid-PEO-SiQDs | 100 | 3 |

TABLE 4.4: Summary of the Number of Samples Used in Fluorescence Analysis

By following this detailed fluorescence analysis protocol, the encapsulation efficiency of the SiQDs within the nanogel can be accurately assessed, ensuring the reliability of the encapsulation process.

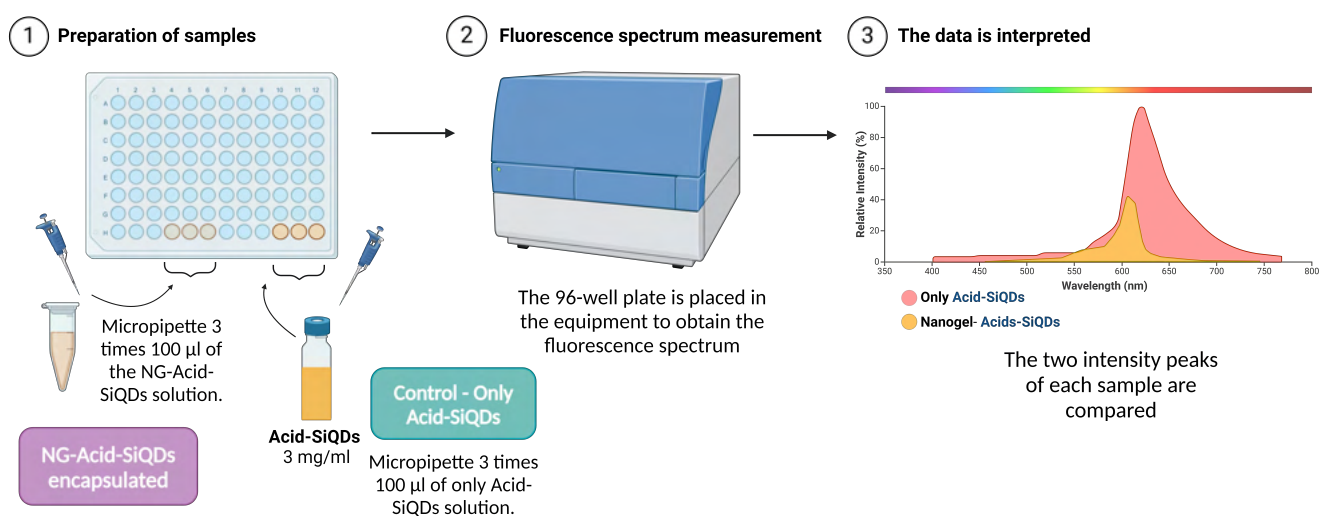


FIGURE 4.11: Measure of Efficiency for Acid-SiQDs

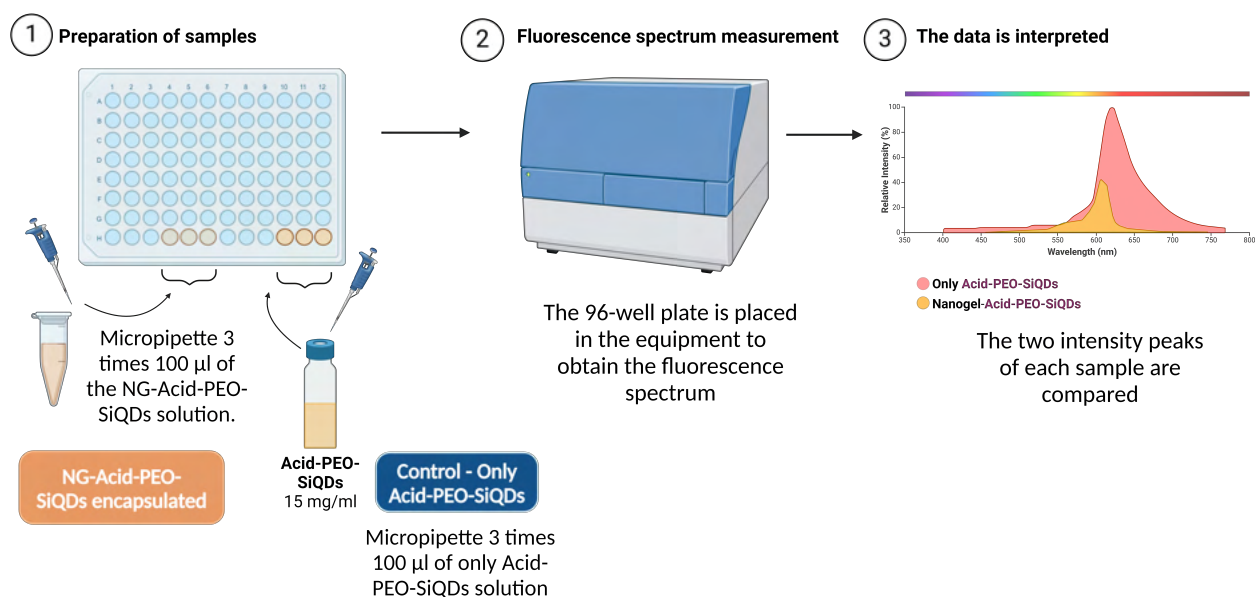


FIGURE 4.12: Measure of Efficiency for Acid-PEO-SiQDs

4.7 Characterization of Nanogel and SiQDs Encapsulation

4.7.1 Dynamic Light Scattering (DLS)

Particle size measurements were performed with Dynamic Light Scattering (DLS) analysis. Samples were prepared at a concentration of 1 mg/mL by precisely weighing 2 mg of the substance and dissolving it in 2 mL of Phosphate Buffered Saline (PBS). This concentration was chosen to optimize the accuracy of particle size measurements while preventing aggregation and ensuring compatibility with the physiological conditions of the analysis. The solution was sonicated until fully dissolved to ensure homogeneity, a critical factor for reliable DLS measurements. The same preparation method was applied to both types of SiQDs encapsulated in the nanogel, which had been lyophilized prior to the analysis.

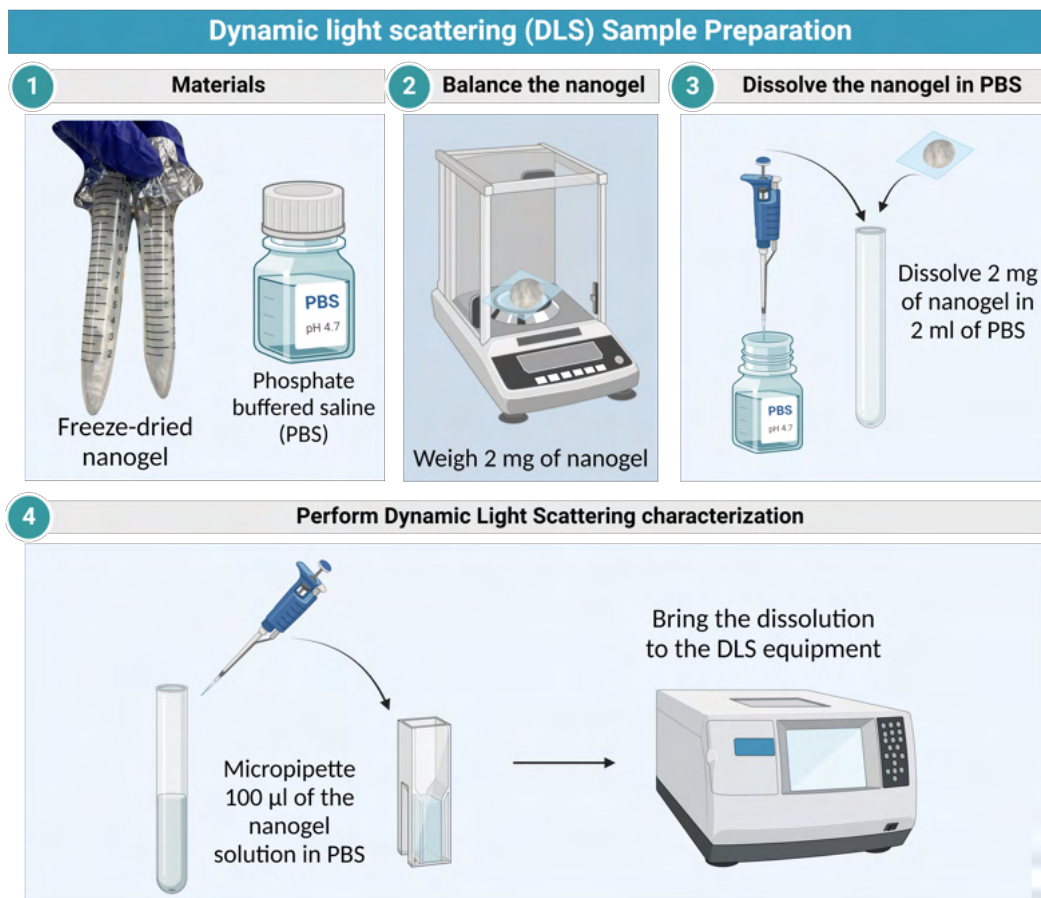


FIGURE 4.13: Protocol for DLS

4.7.2 Thermogravimetric Analysis (TGA)

Thermogravimetric Analysis (TGA) was conducted to evaluate the thermal stability and composition of the nanogel encapsulating silicon quantum dots (SiQDs). Approximately 5–10 mg of the sample was carefully weighed and placed in a platinum crucible under a nitrogen atmosphere to prevent oxidation during the analysis. The sample was subjected to a controlled temperature ramp from room temperature up to a maximum of 693.89°C at a heating rate of 10°C/min. The weight loss of the sample was recorded continuously as a function of temperature to identify the thermal degradation points, including the loss of water, decomposition of organic components, and the integrity of the

SiQDs within the nanogel matrix.

The analysis was performed using a TA Instruments Q600 TGA/DTA, a high-precision thermogravimetric and differential thermal analyzer. This equipment, refurbished and provided by RT Instruments Inc. (California, US), is widely recognized for its reliability and accuracy in thermal analysis. Its advanced features allowed for precise monitoring of the sample's thermal transitions, ensuring reproducible and reliable data.



FIGURE 4.14: Nanogel sample loaded into a small inert container specifically designed for thermogravimetric analysis

The same procedure was followed for both types of SiQDs encapsulated in the lyophilized nanogel, providing a comprehensive assessment of their thermal behavior within the nanogel system.

4.7.3 Nuclear Magnetic Resonance (NMR)

Nuclear Magnetic Resonance (NMR) spectroscopy was conducted to analyze the molecular structure, interactions, and composition of the samples. The primary objectives were to individually identify and confirm the presence of specific functional groups in the silicon quantum dots (SiQDs) and nanogel, verifying the acid functionalization of SiQDs

by comparing spectra before and after modification. NMR also investigated the interactions between Acid-SiQDs and the nanogel matrix, observing any changes in the chemical environment of atoms involved in the encapsulation process. Additionally, this technique provided critical insights into the purity and composition of the samples, detecting potential impurities or residual reactants from the synthesis process, and ensuring the quality and integrity of both the SiQDs and the nanogel.

| Sample | Description |
|---------------------------------|--|
| SiQDs | Silicon quantum dots without acid functionalization |
| Acid-SiQDs | Acid-functionalized silicon quantum dots |
| Nanogel-Encapsulated Acid-SiQDs | Nanogel encapsulating acid-functionalized silicon quantum dots |
| Only Nanogel | Pure nanogel without any SiQDs |

TABLE 4.5: Samples for NMR Analysis

4.7.3.1 NMR Sample Preparation

NMR sample preparation involved several steps to ensure high-quality spectra. Shigemi 5 mm Symmetrical NMR microtubes were used, accommodating a sample volume of 300 μL . The tubes were inspected to ensure they were free of defects such as scratches, cracks, or chips. They were cleaned with acetone and allowed to dry upside down in a fume hood overnight. Additionally, the outside of the tubes was cleaned with acetone before placing them in the NMR instrument. For the samples, an appropriate amount of material was used. Small organic molecules (< 1000 g/mol) were measured, with typical ^1H NMR requiring 5-25 mg of material and ^{13}C NMR requiring 50-100 mg. Samples were shaken well to ensure uniform concentration throughout the tube.

Deuterated chloroform (CDCl_3) was used as the solvent, providing a lock signal and avoiding interference with the ^1H or ^{13}C spectra. An internal standard, such as TMS, was added to provide a reference signal. The solvent was carefully chosen to avoid moisture absorption, which could introduce unwanted water signals. To prepare the samples, the analyte was dissolved in the appropriate deuterated solvent (CDCl_3). A small amount of internal standard was added, if required. The solution was then transferred to a clean, dry Shigemi 5 mm Symmetrical NMR microtube. The tube was filled with 300 μL to ensure homogeneous magnetic fields in the sample. The tube was sealed carefully to prevent surface damage or contamination. Finally, the tube was labeled clearly with a permanent marker, ensuring that the label would not interfere with insertion or spinning during the NMR analysis.

4.7.3.2 NMR Spectroscopy Procedure

The experimental procedure for NMR spectroscopy included several steps. The measurements were performed using a Bruker Avance NEO 400 NMR Spectrometer, featuring a 9.4 Tesla/400 MHz standard bore. First, log in to the NMR instrument computer system. Change the sample in the NMR probe. Lock and shim the magnet. Set up the experiment parameters and run the NMR experiment, using the 1D spectra already obtained to adjust experiment settings, paying special attention to important acquisition parameters such as Acquisition Time (AQ), Dwell Time, Digital Resolution, Number of Scans, TD1 (number of data points in the first time domain), SW1 (spectral width in the first dimension), TD2 (number of data points in the second time domain), and SW2 (spectral width in the second dimension). Process the obtained data and print the spectrum. Finally, exit and log out of the system.

4.8 Biocompatibility Assessment of SiQDs-loaded Nanogel

4.8.1 Cell Culture Preparation

For the biocompatibility assessment, the fibroblast cell line used was Human Dermal Fibroblasts, Adult (HDFa), which are primary cells isolated from adult human skin tissue. The cells were prepared in a 96-well plate. When the HDFa cells reached approximately 70% confluence, they were trypsinized to create a cell suspension for counting. The trypan blue cell counting protocol was employed to determine the number of viable cells. A 0.4% trypan blue solution in PBS was prepared and filtered. The cell sample was collected and centrifuged to pellet the cells, which were then resuspended in 1 mL PBS. Equal volumes of cell suspension and trypan blue solution were mixed and incubated for 3-5 minutes at room temperature. The mixture was loaded onto a hemocytometer, and both viable (clear cytoplasm) and non-viable (blue) cells were counted under a microscope. The percentage of viable cells was calculated using the formula:

$$\% \text{ Viable Cells} = \left(\frac{\text{Number of Viable Cells}}{\text{Total Cells}} \right) \times 100 \quad (\text{IV.2})$$

The number of viable cells per mL was determined by:

$$\text{Viable Cells/mL} = (\text{Average viable cells per square}) \times (\text{Dilution factor}) \times 10,000 \quad (\text{IV.3})$$

For the experiments, 200,000 cells were seeded per well.



(a) Pipetting trypan blue solution



(b) Placing under the microscope for analysis

FIGURE 4.15: Analysis of cell viability using trypan blue solution

4.8.2 MTT Assays for Cytotoxicity

4.8.2.1 MTT Assay Protocol for HDFa

The MTT (3-(4,5-dimethylthiazol-2-yl)-2,5-diphenyltetrazolium bromide) assay was conducted to assess the biocompatibility and cytotoxicity of the SiQDs-loaded nanogel. Initially, the cells (HDFa) were seeded in a 96-well plate and allowed to attach. Different concentrations of the nanogel encapsulating Acid-SiQDs and Acid-PEO-SiQDs were prepared in DMEM, specifically at 10, 25, 50, 100, 250, and 300 $\mu\text{g}/\text{mL}$. Control groups included wells with only cells and wells with only SiQDs.

The prepared concentrations were applied to the cells and incubated for 48 hours. Following this incubation, red light NIR was applied to activate the SiQDs. The MTT reagent was then added to each well and incubated for 2-4 hours, allowing the metabolically active cells to reduce the MTT to purple formazan crystals. These crystals were

dissolved, and the absorbance was measured at 570 nm using a Varioskan LUX Multi-mode Microplate Reader.

To ensure reliable results, the experiment was conducted in triplicate for each concentration and control. The cell viability was calculated relative to the untreated control cells. Materials were considered biocompatible if the cell viability exceeded 80% of the control. The results were compared across different dilutions of the extract to assess the overall biocompatibility and cytotoxicity of the SiQDs-loaded nanogel.

$$\text{Cell Viability (\%)} = \left(\frac{\text{Absorbance of treated cells}}{\text{Absorbance of control cells}} \right) \times 100 \quad (\text{IV.4})$$

To ensure reliable results, each treatment and control group was tested in 4 wells of the 96-well plate. This protocol enabled a comprehensive evaluation of the biocompatibility of the SiQDs-loaded nanogel by measuring the metabolic activity of the HDFa cells after exposure to the nanogel formulations.

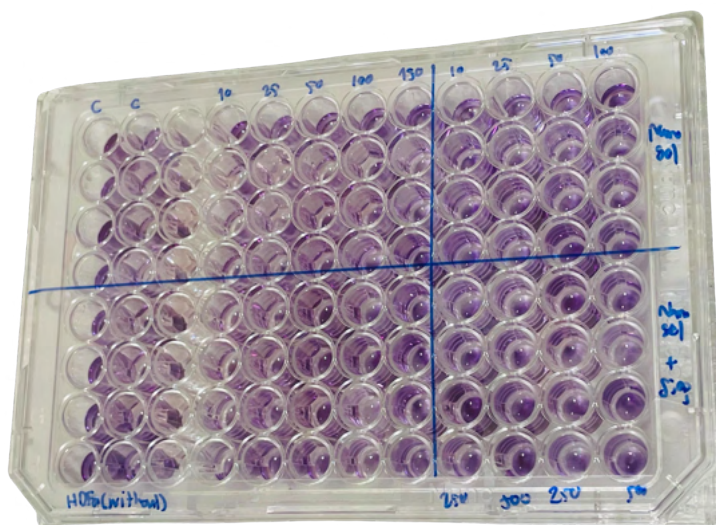


FIGURE 4.16: Assessment of cytotoxicity for both treatments

4.9 *In vitro* Delivery and Photodynamic Therapy Efficacy

4.9.1 Cell Culture Preparation

For the *in vitro* delivery and photodynamic therapy (PDT) efficacy studies, HeLa cells were used. The HeLa cells were seeded in a 96-well plate and allowed to attach and reach the appropriate confluence. Once the cells reached approximately 70% confluence, they were trypsinized to create a cell suspension for counting, similar to the method used for HDFa cells.

4.9.2 Preparation of Nanogel-SiQDs Concentration

The same nanogel-SiQDs concentrations as previously described (10, 25, 50, 100, 250, and 300 $\mu\text{g/mL}$) were prepared in DMEM. The nanogel encapsulating Acid-SiQDs and Acid-PEO-SiQDs were applied to the HeLa cells. Control groups included wells with only cells and wells with only SiQDs.

4.9.3 Photodynamic Therapy Application

After applying the nanogel-SiQDs solutions to the cells and incubating for 48 hours, the samples were prepared for photodynamic therapy application. The therapy aims to generate reactive oxygen species (ROS) through the interaction of SiQDs and NIR light, inducing oxidative stress and apoptosis in cancer cells. This step is crucial to evaluating the therapeutic potential of the nanogel formulations. Specific specifications of the laser include:

- Material: Stainless Steel
- Irradiance @ 1 inch: $>141 \text{ mW/cm}^2$, 3 inch: $> 30.1 \text{ mW/cm}^2$

- Illuminance: 180 lux at 15 cm
- Wavelength: 630:660:850 nm

The NIR light source used for photodynamic therapy (PDT) in this experiment was the iRed TORCH™, a product from iRED USA, as illustrated in Figure 4.17. This compact and efficient flashlight is part of the Bullet™ series, which is known for its precision and reliability.



FIGURE 4.17: Cylindrical red light-emitting device for photodynamic therapy

4.9.3.1 NIR Light Application Protocol

The NIR laser was applied sequentially across the 96-well plate to ensure even and consistent exposure for all wells. Due to the limited illumination area of the NIR laser, the plate was divided into 9 distinct zones, as illustrated in Figure 4.18. Each zone required a total exposure of 3 minutes to achieve uniform photodynamic activation of the silicon quantum dots (SiQDs) encapsulated in the nanogel formulations.

To activate the flashlight, a button was pressed, which was programmed to keep the light on for 1 minute. Since each zone required a total exposure of 3 minutes, it was necessary to press the button three additional times to complete the required duration for each area. The process followed a systematic approach, moving from one zone to the next in a top-to-bottom and left-to-right sequence, as shown in Figure 4.18. This ensured complete and consistent coverage of all wells.

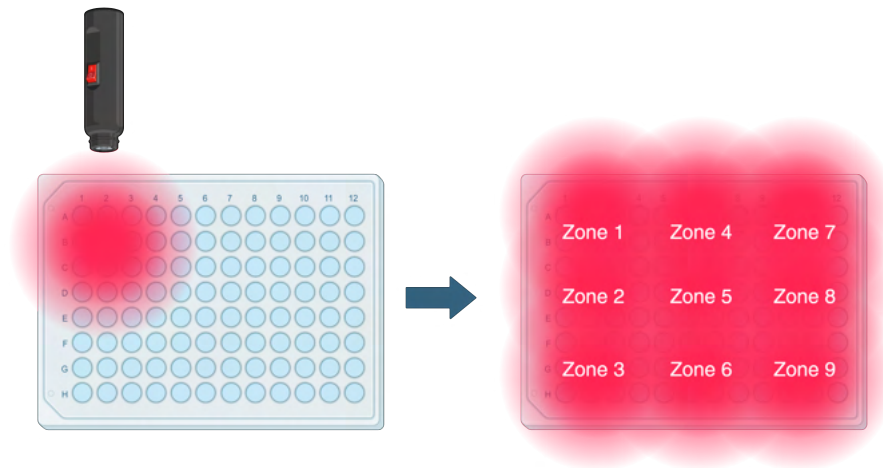


FIGURE 4.18: Area of illumination per activation and the sequential trajectory of the laser across the 96-well plate

To optimize the light delivery and enhance the precision of the procedure, a custom enclosure was constructed, as shown in Figure 4.19.

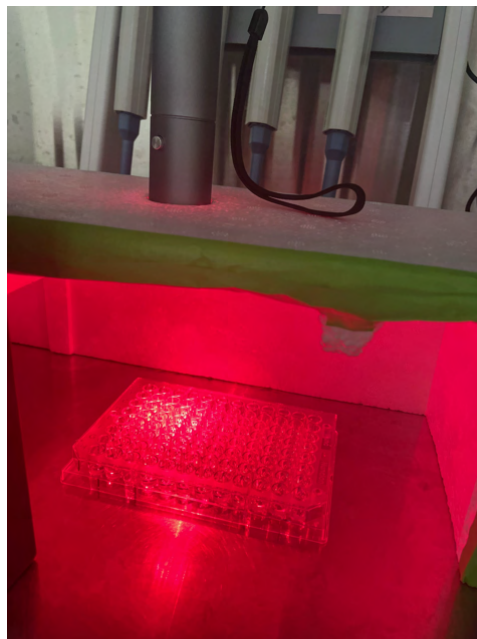


FIGURE 4.19: Application of a laser to start the ROS production

This box was designed to darken the surrounding environment and prevent external light interference, creating controlled conditions ideal for PDT experiments. The enclosure featured a circular opening specifically tailored to the diameter of the NIR flashlight (iRed TORCH™), allowing the device to be securely positioned and held during illumination. This setup not only improved the accuracy of light application but also facilitated ease of handling throughout the protocol.

4.9.4 MTT Assays for Photodynamic Efficacy

4.9.4.1 MTT Assay Protocol for HeLa Cells

The MTT assay was conducted to evaluate the therapeutic efficacy of the nanogel formulations loaded with SiQDs under photodynamic conditions. HeLa cells were seeded in a 96-well plate and treated with varying concentrations of Acid-SiQDs and Acid-PEO-SiQDs nanogels (10, 25, 50, 100, 250, and 300 $\mu\text{g}/\text{mL}$). The cells were incubated for 24 hours, and NIR light was applied to activate the SiQDs after incubation, following the time and pathway outlined in the protocol.

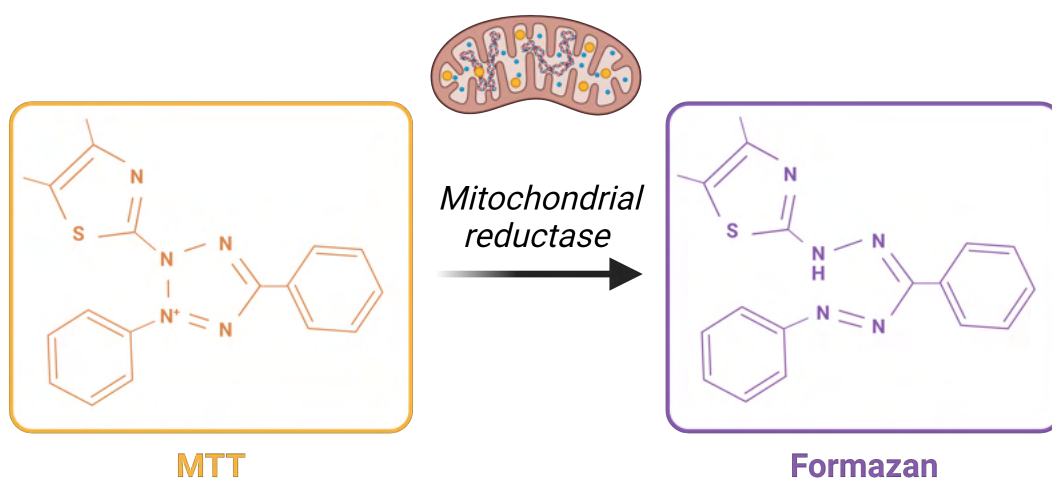


FIGURE 4.20: Application of MTT reagent

After light activation, the MTT reagent was added to each well and incubated for 2-4 hours, allowing metabolically active cells to reduce the MTT into purple formazan crystals. The crystals were then dissolved, and the absorbance was measured at 570 nm using a Varioskan LUX Multimode Microplate Reader.

4.9.4.2 Data Collection and Analysis for Therapeutic Efficacy

Cell viability was calculated relative to untreated controls, providing a basis for evaluating the cytotoxic and therapeutic potential of the nanogels in inducing cell death through photodynamic mechanisms.

The experiment was performed in at least three replicate wells of the 96-well plate for each concentration and control to ensure the reliability of the results. The cell viability was calculated relative to the untreated control cells using the formula:

$$\text{Cell Viability (\%)} = \left(\frac{\text{Absorbance of treated cells}}{\text{Absorbance of control cells}} \right) \times 100 \quad (\text{IV.5})$$

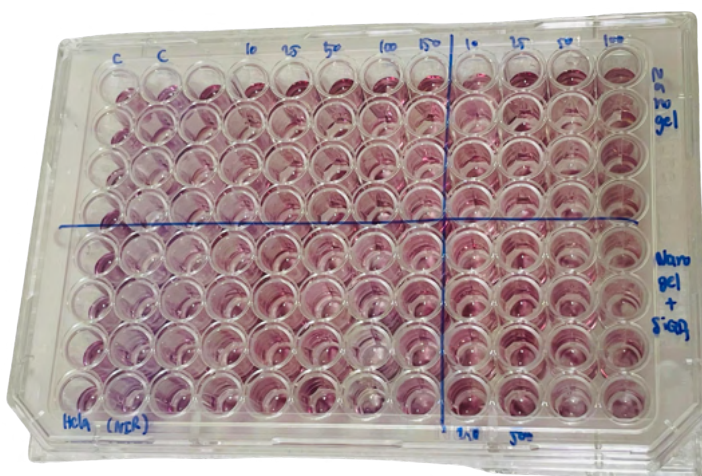


FIGURE 4.21: Assessment of photodynamic therapy for both treatments

This protocol allowed for the comprehensive evaluation of the therapeutic efficacy of the SiQDs-loaded nanogel by measuring the metabolic activity of the HeLa cells after photodynamic therapy and subsequent exposure to the nanogel formulations.

4.10 Ethical Considerations

For the development of a nanogel for targeted cancer therapy in HeLa cells, responsible reporting is paramount. It is essential to communicate the findings with an awareness of the study's limitations and potential risks. While the synthesis and application of nanogels represent a significant advancement in targeted cancer therapy, it's important to clearly outline the scope of the research. Acknowledge that the results obtained from cell line studies, like those involving HeLa cells, might not directly translate to *in vivo* scenarios due to the complex nature of human biology. Overstating the implications, such as suggesting immediate clinical applications without thorough *in vivo* testing and regulatory approval, could lead to misconceptions about the research's stage and potential. Therefore, any presentations or publications should aim for clarity and honesty, emphasizing that while the research is a promising step, it is one of many in the long journey towards practical, safe, and effective cancer treatments.

In addition, conducting research involving chemicals and biological materials, as in the case of HeLa cells, necessitates environmental considerations. Proper disposal methods for all materials used are critical, particularly for chemical reagents and biological waste. The disposal processes should comply with the University of Alberta and Canadian regulations to prevent environmental contamination. This includes segregating waste, using designated disposal containers, and possibly collaborating with specialized waste management services. Additionally, practices to minimize waste generation, such as precise measurements and recycling, contribute to sustainable scientific practices.

Furthermore, this research project, being conducted at the University of Alberta, actively explores potential intellectual property avenues. This includes evaluating patent prospects for the novel composition of the synthesized nanogel and its delivery system, which targets a specific biological marker in cancer treatment. The uniqueness of the nanogel composition and the targeted approach it embodies make it a candidate for intellectual property protection. Concurrently, there is a strong intent to publish the findings in a renowned journal specializing in polymers or biomaterials, ensuring that the research reaches a relevant audience and contributes to the scientific community.

Furthermore, the use of HeLa and HDFa cells in this study aligns with ethical research standards in Canada. According to the Canadian Panel on Research Ethics, research using exclusively identified human somatic cell lines that are publicly available, such as the HeLa cell line, is exempt from review by a Research Ethics Board (REB). Similarly, HDFa cells, as commercially available primary human fibroblasts, also meet the criteria for this exemption, provided they are publicly identified and accessible. This adherence to ethical guidelines underscores the integrity of this project.

In terms of ethical principles, the research adheres to a set of core values that guide every aspect from experimental design to publication. Respect for intellectual property, ensuring that all methodologies, reagents, and technologies derived from external sources are properly accredited, and any novel findings or innovations are handled in accordance with intellectual property laws. The principle of honesty, ensuring all results, whether expected or unexpected, are reported with accuracy and transparency, eschewing any data falsification or manipulation. The objectivity in this project will be maintained; all hypotheses and conclusions will be drawn based on empirical evidence to be gathered during the study, ensuring they are free from personal biases or assumptions.

CHAPTER V

RESULTS

This chapter details the main findings and results obtained throughout the research process in accordance with the fulfillment of the objectives. In this regard, each section of this chapter is related to a specific objective initially proposed. The results are organized into five main sections that reflect the study's objectives, from the synthesis of the copolymer nanogel, the encapsulation of the two types of silicon quantum dots and the application of various characterization techniques, to the evaluation of the biocompatibility and therapeutic efficacy of the nanogel-SiQDs system in photodynamic therapy. This structure allows for a clear and organized presentation of the obtained data and their corresponding analysis, facilitating the understanding of the progress achieved in each phase of the research.

5.1 Synthesis and Characterization of Nanogel

This section details the synthesis and characterization of the copolymer nanogel designed for the encapsulation and delivery of silicon quantum dots (SiQDs). The process begins with the polymerization of 2-(Methacryloyloxy)ethyl phosphorylcholine (MPC) to create the macro chain transfer agent (macroCTA), a crucial step that ensures controlled polymerization and precise molecular weight. The molecular weight of the MPC-macroCTA is determined using Gel Permeation Chromatography (GPC), providing a foundation for subsequent polymerization steps. This comprehensive characterization is essential to confirm the successful synthesis of the copolymer nanogel, which will be used later for SiQDs encapsulation and biomedical applications.

MPC-macro CTA

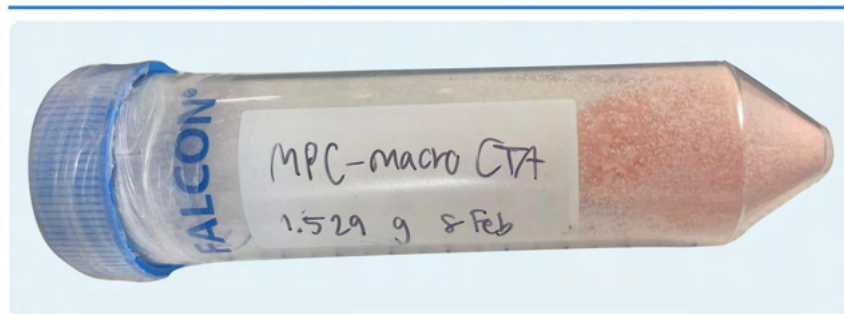


FIGURE 5.1: Synthesized MPC-macro CTA

5.1.1 Gel Permeation Chromatography (GPC) of MPC-macroCTA Results

The Gel Permeation Chromatography (GPC) analysis of the MPC-macroCTA sample yielded a number-average molecular weight (M_n) of 10,936 g/mol. This value was obtained following a rigorous preparation process where 1.5 grams of MPC, 36 milligrams of 4 Cyano-4-(phenylcarbonothioylthio)pentanoic acid (CTP), and 0.09 milligrams of 4,4'-Azobis(4-cyanovaleric acid) (ACVA) were polymerized in methanol at 67-70°C for 20 hours. The resulting polymer was purified through repeated precipitation in Tetrahydrofuran (THF) and characterized using GPC.

| Parameter | Value |
|----------------------------|--------------|
| Molecular Weight (M_n) | 10,936 g/mol |

TABLE 5.1: Nanogel Characterization Parameters

5.1.2 Synthesis of Copolymer Nanogel

The synthesis of the copolymer nanogel was successfully completed as outlined in the methodology, section 3.5.2. The key steps involved in the process included the preparation of the MPC-macroCTA via RAFT polymerization (section 3.5.2.1), followed

by the purification of the DEGMA monomer (Di(ethylene glycol) methyl ether methacrylate) using column filtration with alumina (section 3.5.2.2). The polymerization process was meticulously controlled, with the reaction mixture being purged with nitrogen and maintained at 75°C for 14 hours to ensure the proper formation of the polymer network. Post-polymerization, the product underwent extensive dialysis to remove any residual solvents and unreacted monomers, ensuring a pure final product. The resulting nanogel was then subjected to lyophilization, yielding a dry powder form that is suitable for further applications and analysis (section 3.5.2.3).



FIGURE 5.2: Synthesized Copolymer Nanogel

The purified nanogel, as depicted in the Figure 5.2, exhibits the expected physical characteristics and demonstrates the efficacy of the RAFT polymerization technique in producing a nanogel with specific properties. In the following sections, the nanogel will be tested for its function as a carrier, and its structure will be characterized using various techniques.

5.2 Encapsulation of SiQDs

This section presents the results of the encapsulation process for silicon quantum dots (SiQDs) within the synthesized copolymer nanogel. The analysis includes the encapsulation of both Acid-SiQDs and Acid-PEO-SiQDs, along with the efficiency assessment determined through fluorescence analysis. The results are structured according to the methodologies described in sections 3.6.1 and 3.6.2.

5.2.1 Encapsulation of Acid-SiQDs in the Nanogel

The encapsulation of Acid-SiQDs was performed following the procedure outlined in section 3.6.1.2. A nanogel solution was prepared in phosphate-buffered saline (PBS) to which the Acid-SiQDs were added, resulting in a final concentration of 3 mg/ml. The mixture was allowed to react at room temperature for 24 hours, followed by a freeze-drying process to obtain the final encapsulated product. This method ensures efficient encapsulation through electrostatic interactions.

In Figure 5.3, image (a) shows the nanogel with Acid-SiQDs still in the lyophilizer. This process is essential for ensuring the long-term stability and usability of the nanogel. Image (b) presents the visual fluorescence inspection of Acid-SiQDs encapsulated within the nanogel, confirming the encapsulation by displaying the characteristic fluorescence when exposed to a specific light source. A handheld ultraviolet (UV) flashlight was used for the visual fluorescence inspection.

This UV light source is crucial for the preliminary validation of the encapsulation process, as it allows for the direct observation of fluorescence emitted by the SiQDs within the nanogel. However, further characterization of the encapsulation efficiency and distribution of the SiQDs within the nanogel will be conducted in subsequent sections.



(a) Lyophilized Nanogel with Acid-SiQDs (b) Visual Fluorescence Inspection

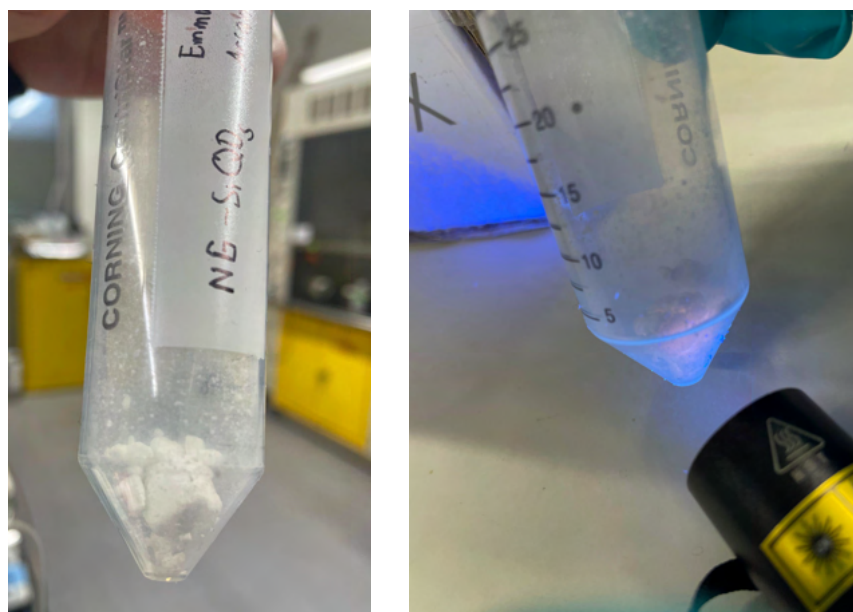
FIGURE 5.3: Encapsulation of Acid-SiQDs in the Nanogel

5.2.2 Encapsulation of Acid-PEO-SiQDs in the Nanogel

Similarly, Acid-PEO-SiQDs were encapsulated following the procedure in section 3.6.1.3. A nanogel solution in PBS was prepared, and the Acid-PEO-SiQDs were added to achieve a final concentration of 15 mg/ml. The reaction mixture was allowed to react at room temperature for 24 hours, followed by freeze-drying to obtain the encapsulated product. This process also relied on electrostatic interactions for effective encapsulation.

In Figure 5.4, image (a) shows the nanogel containing Acid-PEO-SiQDs after it has been removed from the lyophilizer, indicating the completion of the drying process which results in a stable, dry nanogel powder. This step is crucial for maintaining the integrity and usability of the nanogel in subsequent applications. Image (b) presents a visual fluorescence inspection of the Acid-PEO-SiQDs encapsulated within the nanogel, demonstrating the successful encapsulation by the characteristic light emission when exposed to a specialized UV light source. The fluorescence emitted by the SiQDs within

the nanogel, providing a preliminary indication of successful encapsulation, which will be confirmed later by characterization techniques.



(a) Lyophilized Nanogel with Acid-PEO-SiQDs (b) Visual Fluorescence Inspection

FIGURE 5.4: Encapsulation of Acid-PEO-SiQDs in the Nanogel

5.2.3 Fluorescence Analysis for Acid-SiQDs

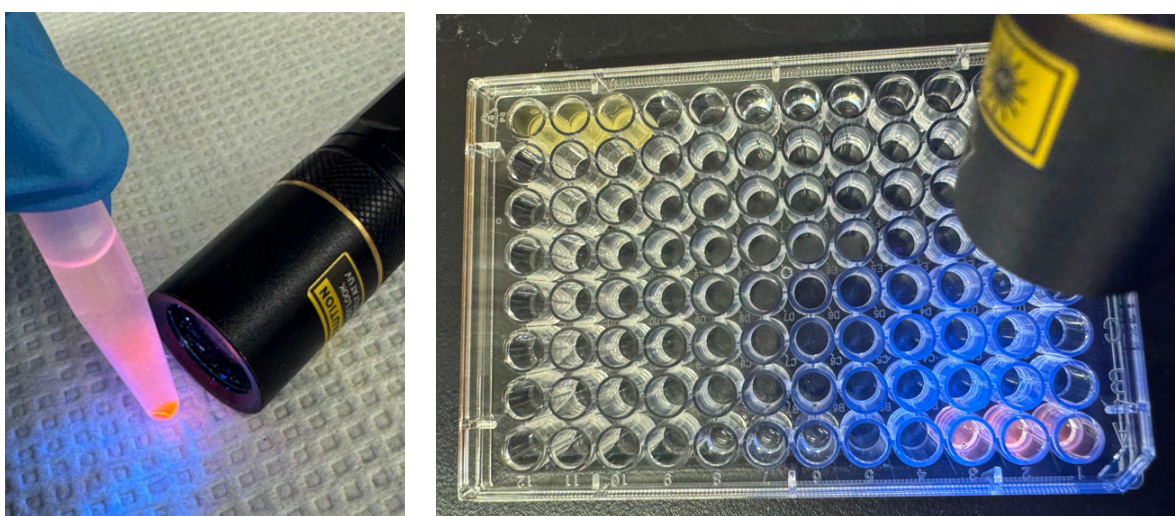
The encapsulation efficiency of Acid-SiQDs within the nanogel matrix was evaluated following a detailed protocol (section 3.6.2.1). The encapsulation process involved sonication of the Acid-SiQDs, dissolution of the nanogel in PBS, and subsequent mixing and stirring. After the encapsulation, unencapsulated SiQDs were removed through centrifugation, and the remaining solution was freeze-dried to obtain the final product.

Before lyophilization, a sample of the nanogel encapsulating Acid-SiQDs (supernatant) was taken to perform a fluorescence analysis, following the protocol outlined in

section 3.6.2.3. The purpose of this analysis was to determine the encapsulation efficiency by comparing the fluorescence intensity of the encapsulated SiQDs to that of the non-encapsulated SiQDs.

| Control | Sample |
|------------|---------------------------|
| Acid-SiQDs | Nanogel (NG) - Acid-SiQDs |

TABLE 5.2: Comparison of Fluorescence Intensities for Acid-SiQDs



(a) Acid-SiQDs Pellet

(b) NG-Acid-SiQDs vs. Acid-SiQDs in 96-Well Plate

FIGURE 5.5: Evaluation of Encapsulation Efficiency for Acid-SiQDs

The figure 5.5 (a) shows the visual inspection of the Acid-SiQDs pellet after the centrifugation process. The pellet consists of SiQDs that were not encapsulated within the nanogel. This separation into a pellet and supernatant highlights the fraction of SiQDs that failed to integrate into the nanogel matrix. The presence of the pellet is crucial for quantifying the amount of non-encapsulated SiQDs. To achieve this, a sample of the supernatant, presumed to contain the SiQDs encapsulated within the nanogel, is taken for analysis.

The figure 5.5 (b) illustrates the preparation of samples for fluorescence analysis. The 96-well plate contains both the NG-Acid-SiQDs (nanogel encapsulated Acid-SiQDs) and control Acid-SiQDs (non-encapsulated). This setup is essential for comparing the

fluorescence intensities of encapsulated and non-encapsulated SiQDs. The UV light is used here to visually highlight the presence of SiQDs, but the actual fluorescence analysis was conducted using a conventional absorbance equipment, which has an option for calculating the fluorescence spectrum.

The fluorescence intensity was measured over a range of wavelengths, from 400 nm to 800 nm. The fluorescence spectrum obtained will be shown below:

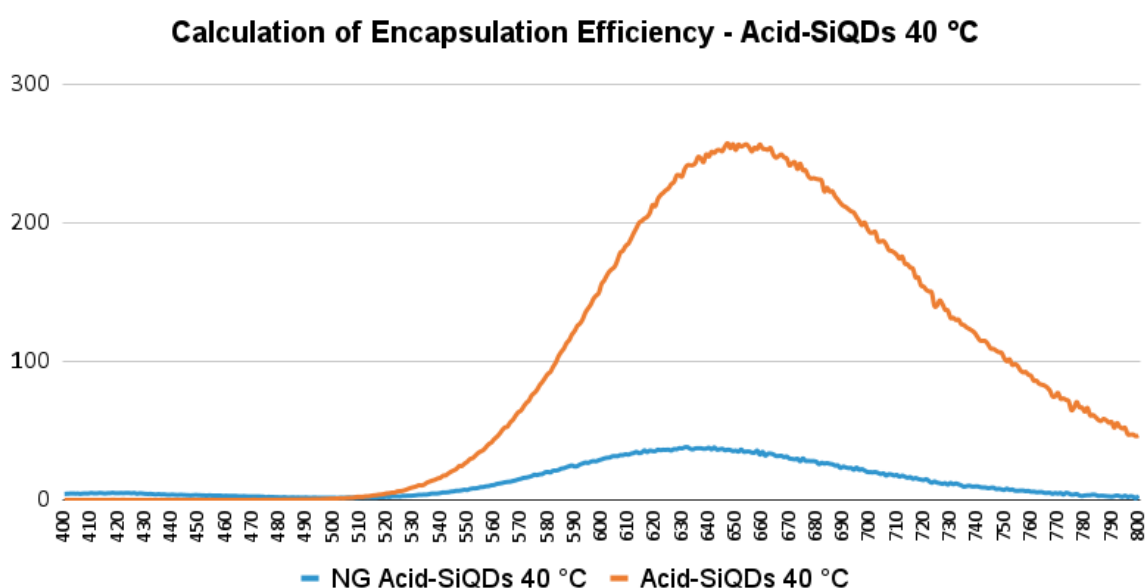


FIGURE 5.6: Fluorescence spectrum of NG-Acid-SiQDs and Acid-SiQDs at 40 °C

In Figure 5.6, the blue line represents the fluorescence intensity of the nanogel-encapsulated Acid-SiQDs (NG Acid-SiQDs 40°C), while the orange line represents the fluorescence intensity of free Acid-SiQDs at 40°C. From the graph, it can be observed that the nanogel-encapsulated Acid-SiQDs exhibit a lower fluorescence intensity compared to the free Acid-SiQDs, which is expected due to the encapsulation process. This decrease in intensity is indicative of successful encapsulation, as the nanogel matrix affects the optical properties of the SiQDs. Further quantitative analysis will provide the exact encapsulation efficiency percentage, confirming the effectiveness of the encapsulation protocol used.

5.2.3.1 Encapsulation Efficiency for Acid-SiQDs

The fluorescence intensity of the encapsulated Acid-SiQDs was compared to that of the control Acid-SiQDs (free) to calculate the encapsulation efficiency, following the protocol in section 3.6.2.3.

The encapsulation efficiency (EE) is determined by comparing the peak fluorescence intensity of the SiQDs before and after encapsulation. The encapsulation efficiency is calculated using the formula:

$$EE (\%) = \left(1 - \frac{I_{\text{encapsulated}}}{I_{\text{non-encapsulated}}} \right) \times 100 \quad (\text{V.1})$$

where:

- $I_{\text{encapsulated}}$ is the fluorescence intensity of the encapsulated Acid-SiQDs.
- $I_{\text{non-encapsulated}}$ is the fluorescence intensity of the non-encapsulated Acid-SiQDs.

| Wavelength (nm) | NG Acid-SiQDs 40°C | Acid-SiQDs 40°C |
|-----------------|--------------------|-----------------|
| 647 | 36.43 | 257.9 |

TABLE 5.3: Fluorescence Intensities at Peak Wavelength

Using the provided peak intensities at the wavelength of 647 nm:

$$I_{\text{encapsulated}} = 36.43, \quad I_{\text{non-encapsulated}} = 257.9$$

The encapsulation efficiency is calculated as:

$$EE (\%) = \left(1 - \frac{36.43}{257.9} \right) \times 100 = 85.9\%$$

The encapsulation efficiency of Acid-SiQDs within the nanogel is calculated to be 85.9%. This indicates that the fluorescence intensity of the SiQDs has been significantly altered upon encapsulation, signifying a successful encapsulation process.

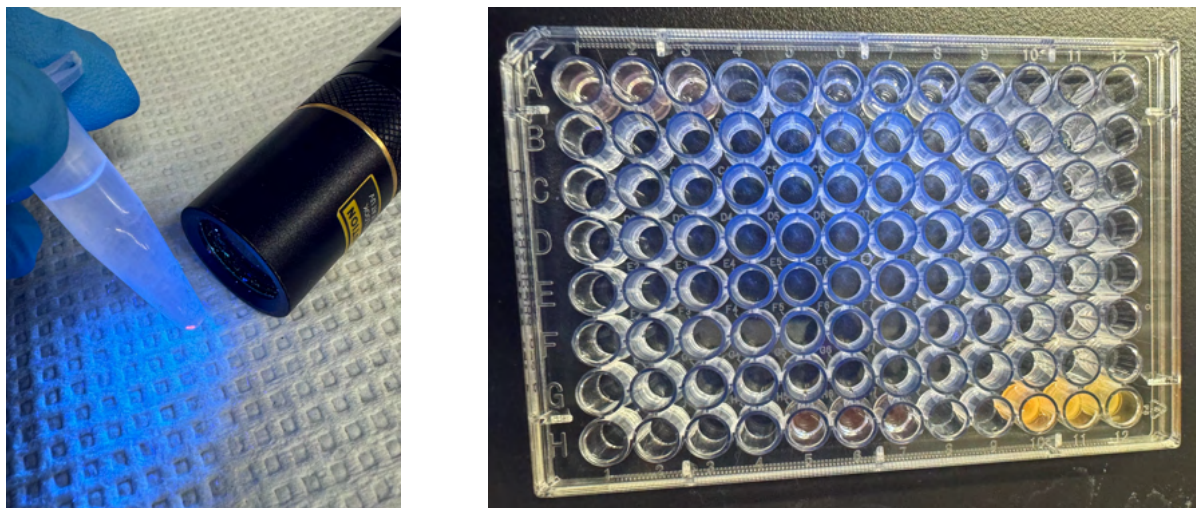
5.2.4 Fluorescence Analysis for Acid-PEO-SiQDs

The objective of the fluorescence analysis is to determine the encapsulation efficiency of Acid-PEO-SiQDs within the nanogel. To achieve this, an additional step of centrifugation was added to the initial encapsulation protocol. This step physically separates the non-encapsulated SiQDs from the encapsulated ones. Before lyophilization, a sample of the nanogel encapsulating Acid-PEO-SiQDs was taken to perform a fluorescence analysis, following the protocol outlined in section 3.6.2.3. The sample obtained from the centrifugation process, specifically the supernatant, was used for this analysis. The supernatant is assumed to contain the nanogel-encapsulated SiQDs, dissolved in PBS through electrostatic interactions.

| Control | Sample |
|----------------|---------------------|
| Acid-PEO-SiQDs | NG - Acid-PEO-SiQDs |

TABLE 5.4: Comparison of Fluorescence Intensities for Acid-PEO-SiQDs

Figure 5.7 provides a visual representation of the encapsulation efficiency evaluation for Acid-PEO-SiQDs. Image (a) shows the Acid-PEO-SiQDs pellet after centrifugation, indicating the quantum dots that were not encapsulated within the nanogel. This pellet is formed by the aggregation of non-encapsulated SiQDs, which settle at the bottom of the tube post-centrifugation. Image (b) displays the preparation of samples for fluorescence analysis in a 96-well plate. The plate includes both NG-Acid-PEO-SiQDs (nanogel encapsulated Acid-PEO-SiQDs) and control Acid-PEO-SiQDs (non-encapsulated). This setup is used to measure the fluorescence intensity in a conventional absorbance reader equipped with fluorescence detection capabilities, allowing for a quantitative comparison of encapsulated versus non-encapsulated SiQDs.



(a) Acid-PEO-SiQDs Pellet (b) NG-Acid-PEO-SiQDs vs. Acid-PEO-SiQDs in 96-Well Plate

FIGURE 5.7: Evaluation of Encapsulation Efficiency for Acid-PEO-SiQDs

The analysis comparing the fluorescence intensity (within a wavelength range of 400 nm to 800 nm) of encapsulated Acid-PEO-SiQDs to that of non-encapsulated Acid-PEO-SiQDs quantifies the encapsulation efficiency, providing insights into the nanogel's effectiveness in encapsulating SiQDs. The resulting fluorescence spectrum is shown in Figure 5.8.

Figure 5.8 illustrates the fluorescence spectrum of NG-Acid-PEO-SiQDs and Acid-PEO-SiQDs at 40°C. The blue line represents the fluorescence intensity of NG Acid-PEO-SiQDs (nanogel encapsulated Acid-PEO-SiQDs), while the yellow line represents the fluorescence intensity of Acid-PEO-SiQDs (non-encapsulated). In addition, the graph shows a significant difference in fluorescence intensity between the encapsulated (NG-Acid-PEO-SiQDs) and non-encapsulated (Acid-PEO-SiQDs) samples. The peak fluorescence intensity for Acid-PEO-SiQDs is markedly higher than that of the NG-Acid-PEO-SiQDs, indicating that the majority of the SiQDs have been successfully encapsulated within the nanogel because the fluorescence of the free SiQDs (control) is much higher.

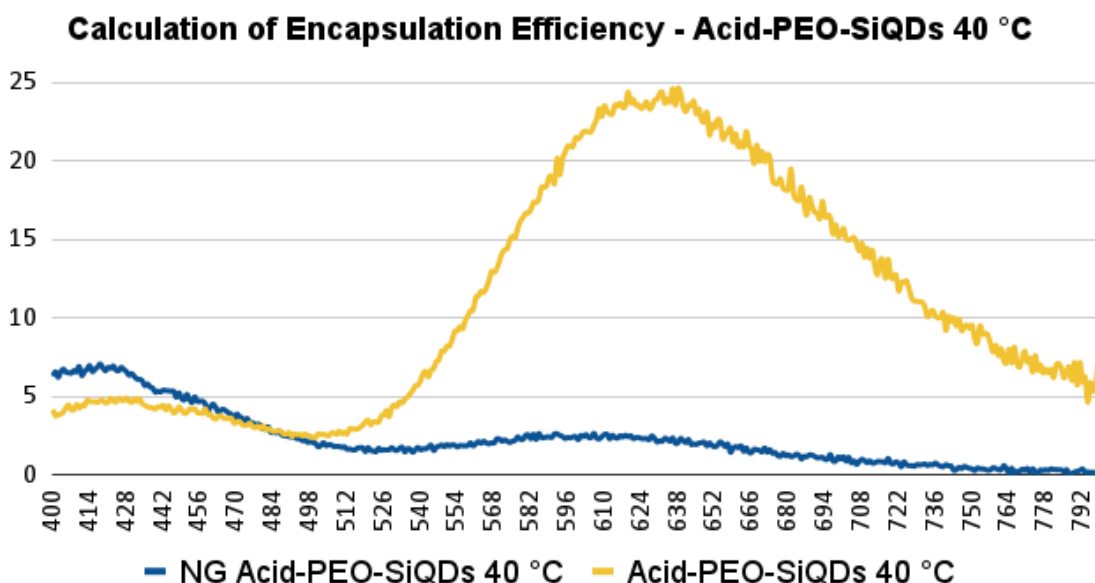


FIGURE 5.8: Fluorescence spectrum of NG-Acid-PEO-SiQDs and Acid-PEO-SiQDs at 40 °C

This difference in intensity is used to calculate the encapsulation efficiency, demonstrating the effectiveness of the nanogel in encapsulating the Acid-PEO-SiQDs and supporting the methodology employed for this purpose.

5.2.4.1 Encapsulation Efficiency for Acid-PEO-SiQDs

The encapsulation efficiency (EE) is determined by comparing the peak fluorescence intensity of the Acid-PEO-SiQDs before and after encapsulation. The encapsulation efficiency is calculated using the formula:

$$EE (\%) = \left(1 - \frac{I_{\text{encapsulated}}}{I_{\text{non-encapsulated}}} \right) \times 100 \tag{V.2}$$

where:

- $I_{\text{encapsulated}}$ is the fluorescence intensity of the encapsulated Acid-PEO-SiQDs.
- $I_{\text{non-encapsulated}}$ is the fluorescence intensity of the non-encapsulated Acid-PEO-SiQDs.

| Wavelength (nm) | NG Acid-PEO-SiQDs 40°C | Acid-PEO-SiQDs 40°C |
|-----------------|------------------------|---------------------|
| 638 | 2.046 | 24.64 |

TABLE 5.5: Fluorescence Intensities at Peak Wavelength

The peak fluorescence intensities were recorded at a wavelength of 638 nm, as shown in Table 5.5. Using the provided peak intensities at the wavelength of 638 nm:

$$I_{\text{encapsulated}} = 2.046$$

$$I_{\text{non-encapsulated}} = 24.64$$

The encapsulation efficiency is calculated as:

$$\text{EE (\%)} = \left(1 - \frac{2.046}{24.64} \right) \times 100 = 91.7\%$$

The encapsulation efficiency of Acid-PEO-SiQDs within the nanogel is calculated to be 91.7%. This indicates that the fluorescence intensity of the SiQDs has been significantly altered upon encapsulation, signifying a successful encapsulation process.

5.2.4.2 Comparison of Encapsulation Efficiencies for Acid-SiQDs and Acid-PEO-SiQDs

To evaluate the encapsulation efficiency of the nanogels with different types of silicon quantum dots (SiQDs), both Acid-SiQDs and Acid-PEO-SiQDs were subjected to fluorescence analysis. The encapsulation efficiency (EE) was calculated based on the

peak fluorescence intensities before and after encapsulation. The comparative results are summarized in Table 5.6.

| Type of SiQDs | Non-encapsulated | Encapsulated | EE (%) |
|----------------------|-------------------------|---------------------|---------------|
| Acid-SiQDs | 257.9 | 36.43 | 85.9 |
| Acid-PEO-SiQDs | 24.64 | 2.046 | 91.7 |

TABLE 5.6: Comparison of Encapsulation Efficiencies for Acid-SiQDs and Acid-PEO-SiQDs

The encapsulation efficiency of Acid-SiQDs within the nanogel was found to be 85.9%, while the encapsulation efficiency for Acid-PEO-SiQDs was higher, at 91.7%. These results indicate that both types of SiQDs were successfully encapsulated within the nanogel, with Acid-PEO-SiQDs exhibiting a slightly higher encapsulation efficiency. This comparative analysis highlights the effectiveness of the nanogel encapsulation process for different functionalized SiQDs, demonstrating the potential of these nanogels as a carrier.

5.3 Physicochemical Characterization of SiQDs-loaded Nanogel

In this section, the physicochemical properties of the synthesized nanogel and the nanogel encapsulating silicon quantum dots (SiQDs) are evaluated, focusing specifically on Acid-SiQDs. The characterization includes both the nanogel alone and the nanogel loaded with Acid-SiQDs to provide a comprehensive understanding of the system's properties. This analysis is essential as it lays the groundwork for understanding the behavior of Acid-PEO-SiQDs, given that Acid-SiQDs serve as the foundational form.

5.3.1 Particle Size Distribution

To assess the particle size distribution of the nanogel and the SiQDs-loaded nanogel, Dynamic Light Scattering (DLS) analysis was performed. This technique allows for the precise measurement of particle sizes, providing insight into the encapsulation efficiency

and the stability of the nanogel system. In the methodology section, we detailed the steps involved in preparing the samples and conducting the DLS measurements.

5.3.1.1 Dynamic Light Scattering (DLS) Results of the Nanogel at 25°C

The DLS analysis of the nanogel alone at 25°C was conducted to establish a baseline for comparison with the SiQDs-loaded nanogel. The results, including particle size distribution and polydispersity index (PDI), will be provided here to illustrate the nanogel's characteristics.

The lognormal distribution plot (Figure 5.9 (a)) and the accompanying data summary (Figure 5.9 (b)) detail the size and dispersion of the nanogel particles.

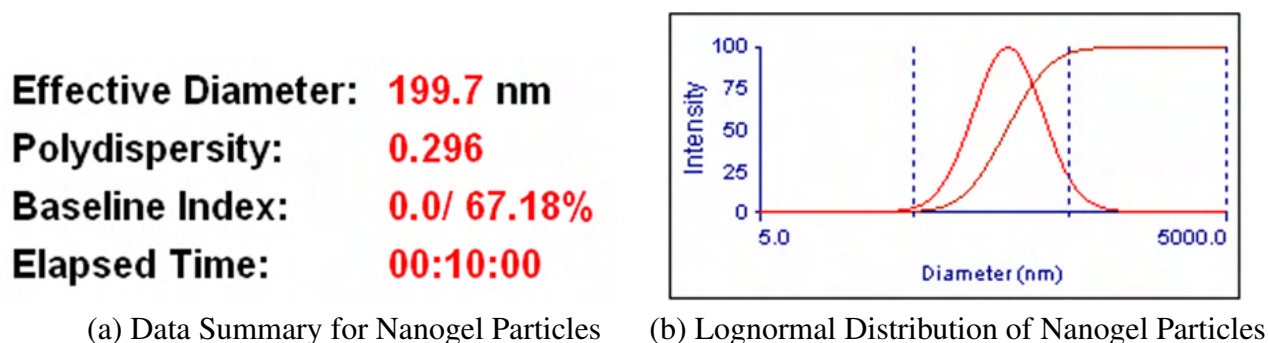


FIGURE 5.9: Dynamic Light Scattering (DLS) results for the synthesized copolymer nanogel at 25°C

The nanogel exhibited an effective diameter of 199.7 nm, indicating the presence of nano-sized particles suitable for biomedical use. The polydispersity index (PDI) was measured at 0.296, reflecting a moderately uniform particle size distribution with minimal heterogeneity. The analysis was stable over the 10-minute duration, as indicated by a baseline index of 67.18%. These findings confirm the successful synthesis of a nanogel with well-defined size and uniformity.

The lognormal distribution graph (Figure 5.9 (b)) shows the intensity versus diameter (nm) of the nanogel particles. The graph displays a bimodal distribution with two

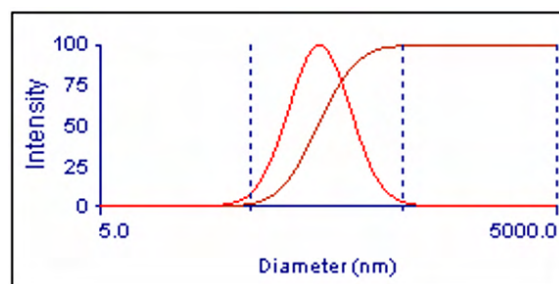
prominent peaks, indicating the presence of two distinct size populations within the sample. The majority of particles fall within the effective diameter range of approximately 199.7 nm. The graph highlights a well-defined particle size distribution with minimal aggregation, suggesting a successful synthesis process.

5.3.1.2 Dynamic Light Scattering (DLS) Results of the Nanogel at 37°C

To evaluate the physicochemical properties of the nanogel at physiological temperature, a sample of the nanogel was dissolved in PBS following the protocol outlined in section 3.7.1. The DLS measurements were then performed at 37°C. This temperature is crucial as it simulates the conditions within the human body, allowing for a more accurate characterization of the nanogel's behavior in biological environments. Understanding the particle size distribution and polydispersity at 37°C is essential for predicting the performance and stability of the nanogel in biomedical applications such as drug delivery.

Below are the visual representations of the DLS data for the nanogel at 37°C:

Effective Diameter: 140.2 nm
Polydispersity: 0.238
Baseline Index: 0.0/ 66.70%
Elapsed Time: 00:10:00



(a) DLS Data for Nanogel at 37°C

(b) Lognormal Distribution of Nanogel at 37°C

FIGURE 5.10: Dynamic Light Scattering (DLS) analysis of the nanogel at 37°C

The effective diameter of the nanogel particles at 37°C is 140.2 nm, indicating the average size of the nanoparticles. The figure 5.10 (b) shows the lognormal distribution of particle sizes for the nanogel at 37°C. The x-axis represents the diameter of the particles in nanometers (nm), ranging from 5 nm to 5,000 nm, while the y-axis indicates the intensity

of the scattered light. This graph provides a detailed view of the particle size distribution within the nanogel sample at physiological temperature.

The peak of the curve indicates the most common particle size, corresponding to the effective diameter identified in the DLS data. The shape of the curve shows the range of particle sizes present in the sample, with a significant concentration of particles around the effective diameter and fewer particles at the size extremes.

5.3.2 Comparison of DLS Results of Nanogel at Different Temperatures

The effective diameter and polydispersity index (PDI) of the nanogel were measured at two different temperatures: 25°C and 37°C. This comparison is crucial to understand the impact of temperature on the size distribution and uniformity of the nanogel particles, which is vital for their potential biomedical applications.

| Parameter | Nanogel at 25°C | Nanogel at 37°C |
|----------------------------|-----------------|-----------------|
| Effective Diameter (nm) | 199.7 | 140.2 |
| Polydispersity Index (PDI) | 0.296 | 0.238 |

TABLE 5.7: Comparison of Effective Diameter and Polydispersity Index of Nanogel at Different Temperatures

The table 5.7 provides a summary of the effective diameter and PDI of the nanogel at 25°C and 37°C. At 25°C, the nanogel has an effective diameter of 199.7 nm with a PDI of 0.296, indicating moderate polydispersity. At 37°C, the effective diameter decreases to 140.2 nm, and the PDI improves to 0.238, suggesting more uniform particle sizes at physiological temperature. This reduction in particle size and improved uniformity at 37°C can be attributed to the temperature-induced changes in the nanogel's physical properties, which may enhance its performance in biomedical applications. The effect of DEGMA on this thermoresponsive behavior will be further analyzed in the discussion.

The images in Figure 5.11 depict the nanogel samples prepared for Dynamic Light Scattering (DLS) analysis at two different temperatures. Image (a) shows the nanogel

sample dissolved in PBS at 25°C. This sample is in a liquid state, which is suitable for measuring the particle size distribution and polydispersity index under standard laboratory conditions.

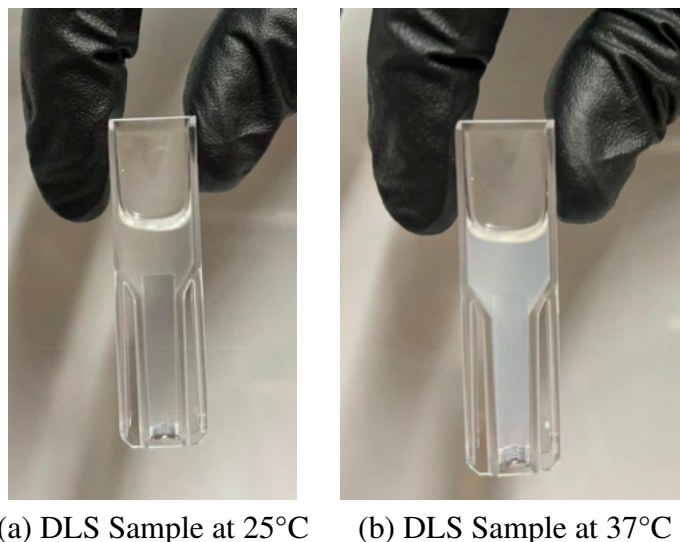


FIGURE 5.11: Nanogel sample dissolved in PBS after DLS analysis at 25°C and 37°C

Image (b) illustrates the nanogel sample dissolved in PBS at 37°C, representing physiological temperature. At this temperature, the nanogel exhibits a gelification state, indicating a potential thermo-responsive behavior. The comparison of DLS results at these two temperatures is essential for understanding the nanogel's behavior in different environments, particularly its stability and performance at body temperature.

The turbidity observed in thermoresponsive nanogel systems, such as the transition seen at 37°C compared to the clarity at 25°C, is primarily influenced by the LCST (Lower Critical Solution Temperature) behavior of the polymer. At 25°C, below the LCST, the DEGMA chains in the nanogel are hydrated due to hydrogen bonding with water molecules, leading to a swollen and transparent state. The hydrated polymer chains remain extended, maintaining a homogeneous dispersion in the solution.

As the temperature reaches and surpasses the LCST (approximately 32–37°C for DEGMA-based nanogels), the polymer undergoes a phase transition [149]. The DEGMA

chains lose hydration and collapse due to the breakdown of hydrogen bonds and the emergence of hydrophobic interactions among polymer segments. This deswelling reduces the nanogel's hydrodynamic size and creates a denser network within the matrix [150]. The collapse of the polymer chains results in light scattering, leading to an increase in turbidity and, in some cases, gelation. This turbidity acts as a visual marker of the nanogel's thermoresponsive behavior [151].

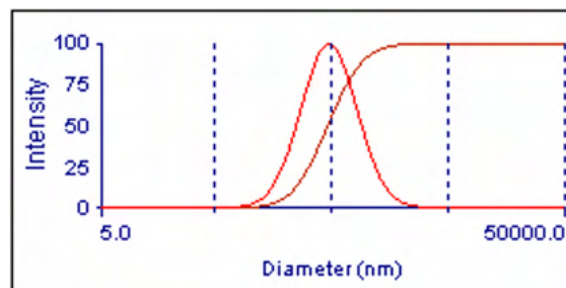
The presence of MPC in the polymer composition further influences this behavior. While MPC enhances colloidal stability by providing a zwitterionic hydration shell around the nanogel particles, it does not prevent the turbidity associated with the LCST transition [152]. Instead, it stabilizes the nanogel against irreversible aggregation, allowing the system to maintain reversible swelling and deswelling cycles. Environmental factors such as pH, ionic strength, and the specific interaction of MPC and DEGMA with surrounding media can modulate the degree of turbidity and the sharpness of the phase transition.

5.3.2.1 Dynamic Light Scattering (DLS) Results of Acid-SiQDs-loaded Nanogel at 25 °C

Following the encapsulation of Acid-SiQDs, DLS measurements were performed on the nanogel to evaluate changes in particle size distribution and PDI. These results are crucial for determining the impact of SiQDs encapsulation on the nanogel's physicochemical properties and for verifying the successful incorporation of SiQDs into the nanogel matrix.

DLS measurements were conducted on the nanogel encapsulating Acid-SiQDs at 25°C to determine the particle size distribution and polydispersity index (PDI). The results indicate the effective diameter, PDI, baseline index, and measurement time.

Effective Diameter: 469.4 nm
Polydispersity: 0.355
Baseline Index: 0.0/ 72.67%
Elapsed Time: 00:10:00



(a) DLS Data at 25°C

(b) Lognormal Distribution at 25°C

FIGURE 5.12: (a) DLS analysis data of Acid-SiQDs-loaded nanogel at 25°C

The effective diameter of the Acid-SiQDs-loaded nanogel at 25°C was measured to be 469.4 nm. The polydispersity index (PDI) was found to be 0.355, indicating moderate heterogeneity in particle size distribution. The baseline index was 0.0/72.67%, suggesting stable and consistent measurements. The total time taken for the DLS analysis was 10 minutes. This data provides insights into the size and distribution of the nanogel particles encapsulating Acid-SiQDs at room temperature, which is critical for understanding their behavior in different conditions.

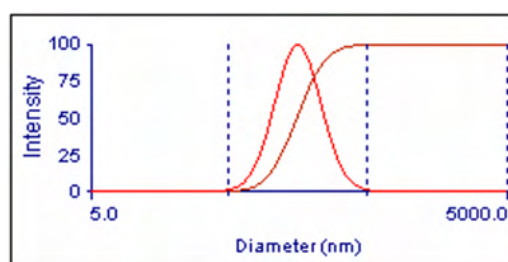
This lognormal distribution graph in Figure 5.12 (b) illustrates the particle size distribution of Acid-SiQDs-loaded nanogel at 25°C, showing the relationship between the intensity of scattered light and the particle diameter in nanometers (nm). The horizontal axis spans from 5.0 nm to 50,000 nm, while the vertical axis represents the intensity of scattered light as a percentage. The peak of the red curve, around 469.4 nm, indicates the most common particle size in the sample, suggesting successful encapsulation of Acid-SiQDs within the nanogel.

The width of the curve provides insight into the polydispersity of the sample, with a broader peak indicating a moderately polydisperse sample containing a variety of particle sizes. Higher intensity levels on the vertical axis correspond to a greater proportion of particles within that size range, essential for understanding the sample's composition and behavior.

5.3.2.2 Dynamic Light Scattering (DLS) Results of Acid-SiQDs-loaded Nanogel at 37 °C

DLS analysis was performed on the nanogel encapsulating Acid-SiQDs at 37°C to assess the particle size distribution and other relevant parameters. The results provide insights into the stability and uniformity of the nanogel at physiological temperature, which is critical for its potential biomedical applications.

Effective Diameter: 153.6 nm
Polydispersity: 0.113
Baseline Index: 5.4/ 73.50%
Elapsed Time: 00:02:00



(a) DLS Analysis Data

(b) Lognormal Distribution

FIGURE 5.13: DLS analysis data of Acid-SiQDs-loaded nanogel at 37°C

The DLS analysis data for the Acid-SiQDs-loaded nanogel at 37°C reveal an effective diameter of 153.6 nm, which indicates the average particle size. The polydispersity index (PDI) is 0.113, suggesting a relatively low degree of non-uniformity in the particle sizes, indicating that the nanogel particles are quite uniform in size. The baseline index, with values of 5.4/73.50%, reflects the stability and consistency of the measurement over the 2-minute duration.

The lognormal distribution graph further supports these findings by showing the intensity of particles at various diameters, with a peak around the effective diameter value. This data highlights the successful encapsulation and stability of the Acid-SiQDs within the nanogel at physiological temperature, making it suitable for potential biomedical applications.

At 37°C, no prominent change in turbidity was observed in the SiQD-loaded nanogel compared to the more noticeable turbidity shift seen during the DLS analysis

of the nanogel alone. This reduced turbidity change can be attributed to the presence of SiQDs within the poly(MPC-st-DEGMA) nanogel matrix, which likely modifies the nanogel's thermoresponsive behavior. The encapsulated SiQDs may partially hinder the complete collapse of DEGMA chains due to steric hindrance, leading to a less dramatic phase transition. Additionally, interactions between SiQDs and the DEGMA chains could slightly alter the LCST, softening the phase transition and minimizing the turbidity shift. Furthermore, the SiQDs may contribute to the system's colloidal stability, reducing large-scale aggregation and further limiting the increase in turbidity [109], [153]. Despite these modifications, the nanogel remains thermoresponsive, with the improved stability imparted by the SiQDs resulting in a more robust and reliable system.

5.3.2.3 Comparison of DLS Results for Acid-SiQDs-loaded Nanogel at Different Temperatures

To understand the impact of temperature on the nanogel encapsulating Acid-SiQDs, DLS analyses were conducted at both 25°C and 37°C. These temperatures were chosen to represent ambient conditions and physiological conditions, respectively. This analysis is essential to determine how the nanogel's particle size distribution, polydispersity, and overall structural integrity are affected by temperature changes, which is particularly relevant for biomedical applications where the nanogel may be exposed to body temperature. Understanding these changes is key to optimizing the nanogel's performance and ensuring its efficacy and safety in real-world applications.

The comparison between the DLS results at 25°C and 37°C, as shown in Table 5.8, reveals significant changes in the nanogel's properties with temperature. At 25°C, the effective diameter of the nanogel particles is 469.4 nm with a PDI of 0.355, indicating a higher degree of non-uniformity and larger particle size. The baseline stability is 72.67% over a 10-minute duration.

| Parameter | 25°C | 37°C |
|------------------------------|-------------|-------------|
| Effective Diameter (nm) | 469.4 | 153.6 |
| Polydispersity Index (PDI) | 0.355 | 0.113 |
| Baseline Index (% stability) | 72.67% | 73.50% |
| Elapsed Time (minutes) | 10 | 2 |

TABLE 5.8: Comparison of DLS Results for Acid-SiQDs-loaded Nanogel at 25°C and 37°C

In contrast, at 37°C, the effective diameter of the nanogel particles decreases to 153.6 nm with a PDI of 0.113, suggesting a much more uniform and smaller particle size distribution. The baseline stability at this temperature is slightly higher at 73.50%, over a shorter elapsed time of 2 minutes.

These results demonstrate that the nanogel particles become smaller and more uniform at physiological temperature (37°C), primarily due to the thermoresponsive nature of the poly(MPC-st-DEGMA) nanogel. This behavior is driven by DEGMA, which exhibits a lower critical solution temperature (LCST) of approximately 26-30°C. Below the LCST, DEGMA chains are hydrated and extended in water due to hydrogen bonding between water molecules and the ethylene glycol units of DEGMA [154]. However, at temperatures above the LCST, such as 37°C, these hydrogen bonds are disrupted, and DEGMA transitions into a hydrophobic state, causing the chains to collapse. This collapse leads to hydrophobic interactions between DEGMA segments, which result in a significant reduction in the nanogel's hydrodynamic size, as observed with the decrease in particle size from 469.4 nm at 25°C to 153.6 nm at 37°C.

This thermoresponsive behavior is further stabilized by MPC, which forms a hydrophilic, zwitterionic outer layer around the nanogel [155]. The MPC shell prevents excessive aggregation during the DEGMA collapse, ensuring colloidal stability and resistance to protein adsorption even at physiological conditions. Together, the dehydration and contraction of DEGMA chains and the stabilizing role of MPC result in a compact and uniform core-shell structure at 37°C, as reflected in the significant reduction in the

polydispersity index (PDI) from 0.355 to 0.113. These structural changes enhance the nanogel's stability, homogeneity, and suitability for biomedical applications, ensuring efficient and consistent delivery in physiological environments.

5.3.3 Thermal Stability

Understanding the thermal stability of the nanogel encapsulating Acid-SiQDs is crucial for determining its suitability for various biomedical applications, where thermal conditions can vary significantly. Thermal stability provides insight into the material's behavior under different temperatures, which can affect its structural integrity and functionality. To assess this, Thermogravimetric Analysis (TGA) was performed on both the nanogel alone and the nanogel encapsulating Acid-SiQDs. This analysis helps understand the fundamental thermal properties and stability of the nanogel system, which is the basis for further evaluations, including the encapsulation of Acid-PEO-SiQDs, given that Acid-PEO-SiQDs also contain the acid functional group.

5.3.3.1 Thermogravimetric Analysis (TGA) Results

Thermogravimetric Analysis (TGA) was conducted to evaluate the thermal stability of the nanogel both with and without the encapsulated Acid-SiQDs. The TGA results provide critical information about the thermal decomposition profile, stability, and degradation temperatures of the nanogel and the encapsulated system.

The TGA curves depicted in Figure 5.14 illustrate the thermal decomposition behavior of the nanogel and the Acid-SiQDs-loaded nanogel. The blue curve represents the weight loss profile of the neat nanogel, while the red curve corresponds to the nanogel encapsulating Acid-SiQDs. The weight loss stages and corresponding temperatures indicate the thermal stability and degradation characteristics of the materials. Comparing the thermal stability of both samples helps in understanding the influence of Acid-SiQDs

encapsulation on the nanogel's thermal properties, which is essential for its application in environments where thermal stability is a critical factor.

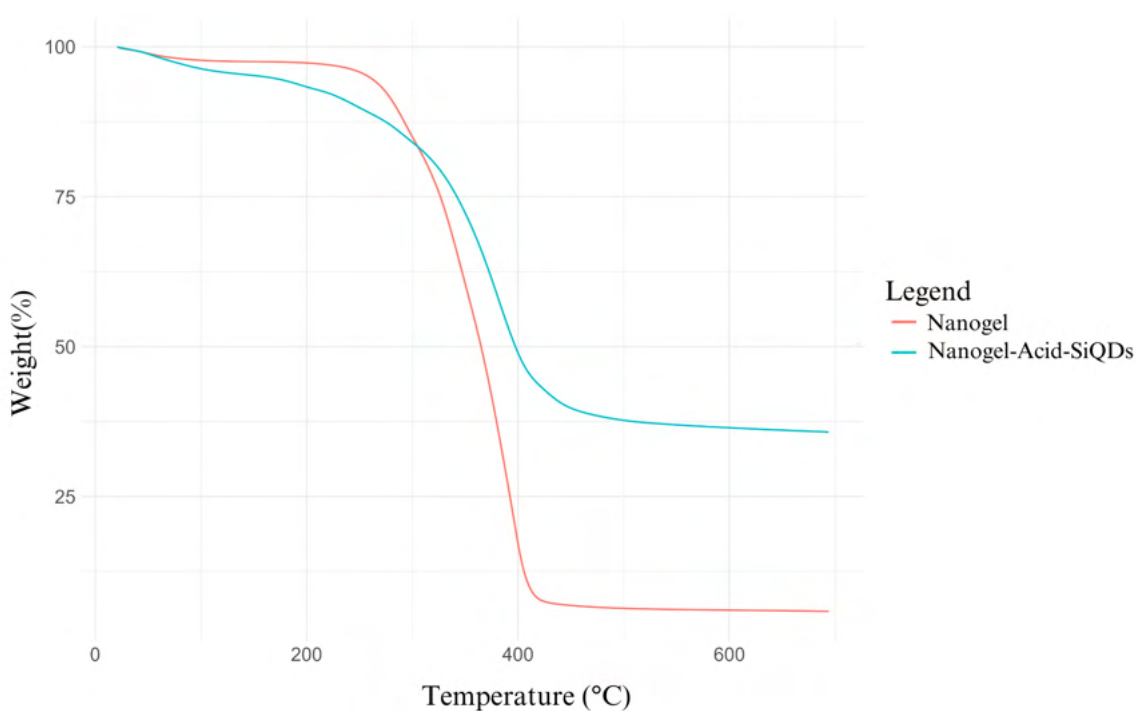


FIGURE 5.14: Thermogravimetric Analysis (TGA) curves for the nanogel alone and the nanogel encapsulating Acid-SiQDs

In the initial stages of heating, a gradual weight loss is observed for both samples, typically associated with the evaporation of residual solvents and water molecules. This is evident from the slight decrease in weight percentage at lower temperatures. As the temperature increases, more significant weight loss occurs, indicating the decomposition of organic components within the nanogel matrix.

A key observation is that the blue curve (Nanogel-SiQDs) shows a slower rate of weight loss compared to the red curve (Nanogel) as the temperature continues to rise. This suggests enhanced thermal stability imparted by the encapsulated Acid-SiQDs. The encapsulated nanogel does not reach as low a weight percentage as the unloaded nanogel,

indicating that the presence of SiQDs contributes to improved thermal stability. The Acid-SiQDs likely interact with the polymer matrix, providing additional resistance to thermal decomposition.

As the temperature reaches higher values, the primary decomposition phase occurs, marked by a sharp decline in weight percentage. The red curve shows a more pronounced and rapid decrease in weight, indicating a lower decomposition temperature for the unloaded nanogel. In contrast, the blue curve demonstrates a more gradual weight loss, suggesting that the nanogel with encapsulated Acid-SiQDs has a higher decomposition temperature and a more stable thermal profile.

Additionally, Annex 2 contains differential scanning calorimetry (DSC) data that provide more information about the thermal properties and transitions of the nanogel as a SiQD carrier system.

5.3.4 Chemical Structure Analysis

Nuclear Magnetic Resonance (NMR) is a powerful analytical technique used to determine the chemical structure of organic molecules. When a sample is placed in a strong magnetic field and irradiated with radio waves at the appropriate frequency, atomic nuclei with magnetic spin (such as ^1H and ^{13}C) absorb energy and enter resonance. The absorbed energy induces a transition in the nuclear spins, which is observed in an NMR spectrum. The position of the signals in the spectrum (chemical shift) depends on the chemical environment of the nucleus, allowing the elucidation of the molecular structure.

5.3.4.1 Nuclear Magnetic Resonance (NMR) of Nanogel (NG)

The synthesis and characterization of nanogels via RAFT polymerization involve meticulous evaluation of their chemical structure using ^1H NMR spectroscopy. The ^1H

NMR spectrum provides detailed insights into the chemical environments and molecular composition of the nanogels, confirming the successful incorporation of various monomers and the formation of the desired polymer network.

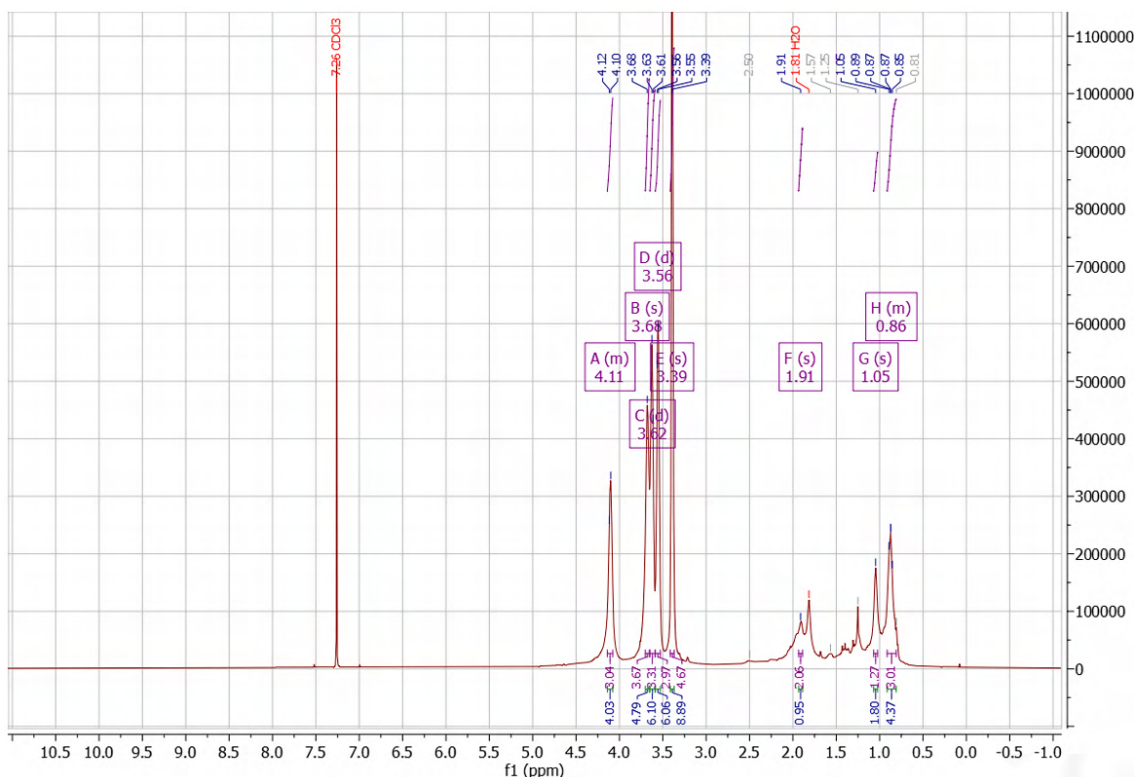


FIGURE 5.15: ^1H NMR spectrum of the synthesized nanogel (NG) showing distinct peaks corresponding to various proton environments in the polymer matrix

In Figure 5.15, the ^1H NMR spectrum of the nanogel (NG) is characterized by several distinct peaks, indicating various proton environments in the polymer matrix. The chemical shifts (δ) and integration values provide critical information about the polymer composition and the presence of specific functional groups: δ 4.14 – 4.08 (m, 3H), 3.68 (s, 4H), 3.62 (d, $J = 5.2$ Hz, 3H), 3.56 (d, $J = 5.2$ Hz, 3H), 3.39 (s, 5H), 1.91 (s, 2H), 1.05 (s, 1H), 0.91 – 0.81 (m, 3H).

The multiplet at δ 4.14 – 4.08, integrating for 3 protons, indicates the presence of protons in a complex chemical environment, likely due to the overlap of several proton signals. These could be attributed to the protons in the polymer backbone or side chains

that are in slightly different chemical environments. The singlet at δ 3.68 ppm, integrating for 4 protons, suggests the presence of a group of equivalent protons in a similar chemical environment, possibly methylene (-CH₂-) groups adjacent to oxygen or nitrogen atoms in the polymer network. The doublets at δ 3.62 and δ 3.56 ppm, each integrating for 3 protons with a coupling constant (J) of 5.2 Hz, indicate the presence of methylene protons in a distinct environment with adjacent protons causing the splitting, indicative of a more complex molecular structure.

The singlet at δ 3.39 ppm, integrating for 5 protons, likely corresponds to aromatic protons or those in a highly deshielded environment due to electron-withdrawing groups, such as oxygen or nitrogen atoms. The singlet at δ 1.91 ppm suggests the presence of aliphatic protons, likely from a methylene group adjacent to an electron-withdrawing group, such as a carbonyl or ester group. The singlet at δ 1.05 ppm indicates a proton in a shielded environment, possibly from a methyl group (-CH₃) in the polymer matrix. The multiplet at δ 0.91 – 0.81 ppm suggests the presence of protons in a varied chemical environment, likely due to overlapping signals from different proton groups in the polymer.

5.3.4.2 Nuclear Magnetic Resonance (NMR) of Acid-SiQDs

The ¹H NMR spectrum of acid-functionalized silicon quantum dots (SiQDs) with a carboxylic acid group (-COOH) at the end of an alkyl chain provides critical insights into the structural modifications and chemical environments of the functionalized SiQDs. This analysis is essential for understanding the impact of functionalization on the chemical structure of the SiQDs and confirming the successful incorporation of the carboxylic acid groups.

The Figure 5.16 shows several distinct peaks, indicating various proton environments resulting from the functionalization process. The chemical shifts (δ) and integration

values are as follows: δ 7.28 (s, 5H), 1.71 (s, 1H), 1.31 (d, $J = 4.4$ Hz, 1H), 1.28 (s, 7H), 1.04 (s, 2H), 0.91 (d, $J = 6.8$ Hz, 2H), 0.84 (d, $J = 6.5$ Hz, 15H), and 0.11 (s, 1H).

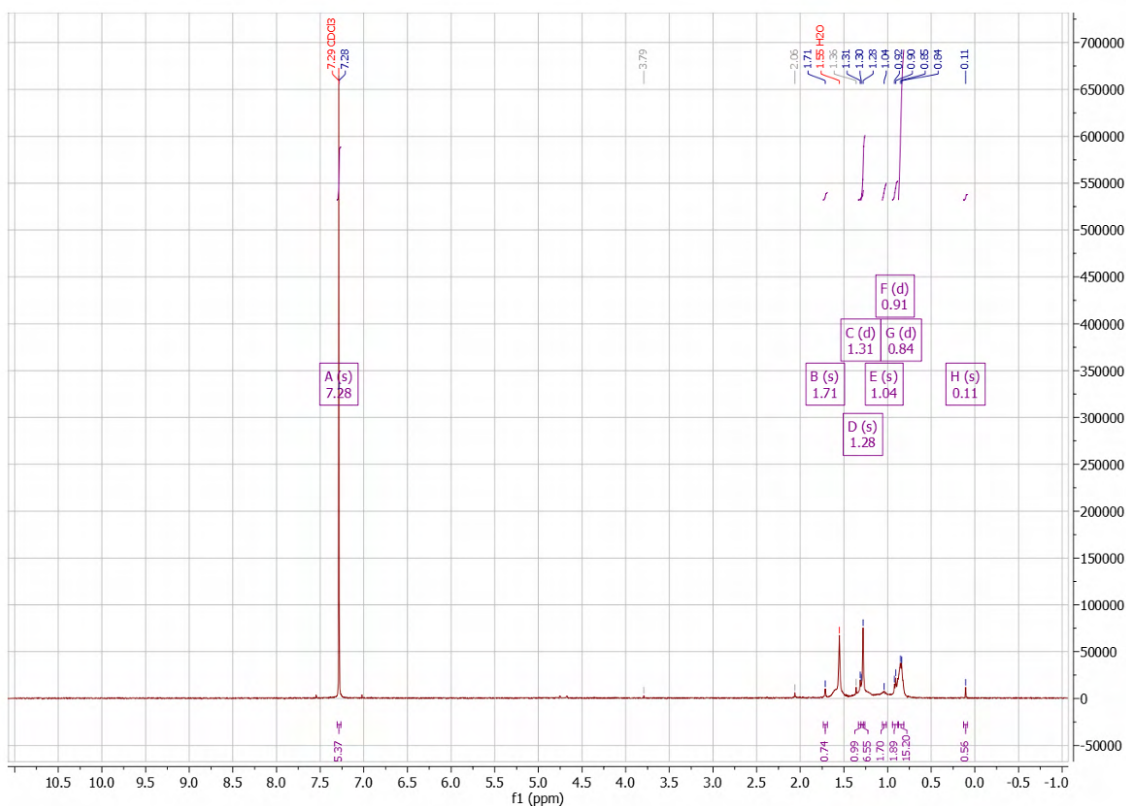


FIGURE 5.16: ^1H NMR spectrum of Acid-SiQDs showing distinct peaks corresponding to various proton environments

The singlet at δ 7.28 ppm, integrating for 5 protons, indicates the presence of aromatic protons or protons in a highly deshielded environment. This peak is characteristic of protons attached to an aromatic ring, suggesting that the functionalization process introduced aromatic groups into the structure of the SiQDs. The singlet at δ 1.71 ppm, integrating for 1 proton, suggests the presence of a unique proton environment, likely due to a proton adjacent to the carboxylic acid group.

The doublet at δ 1.31 ppm ($J = 4.4$ Hz, 1H) indicates a proton in a coupled environment, suggesting the presence of a methylene group adjacent to the carboxylic acid. The singlet at δ 1.28 ppm, integrating for 7 protons, represents aliphatic hydrogen atoms

in a similar chemical environment, possibly from the alkyl chains attached to the SiQDs. The reduced integration value compared to neat SiQDs suggests that some of the aliphatic protons are replaced or chemically modified during the functionalization process.

The singlet at δ 1.04 ppm, integrating for 2 protons, likely corresponds to protons in a distinct chemical environment, possibly near the carboxylic acid group. The doublet at δ 0.91 ppm ($J = 6.8$ Hz, 2H) and the doublet at δ 0.84 ppm ($J = 6.5$ Hz, 15H) reflect protons in coupled environments, indicating the presence of protons in the alkyl chain adjacent to the carboxylic acid group.

The singlet at δ 0.11 ppm, integrating for 1 proton, suggests a unique proton environment, likely associated with the terminal proton of the alkyl chain.

5.3.4.3 Nuclear Magnetic Resonance (NMR) of Nanogel Encapsulating Acid-Functionalized SiQDs

The ^1H NMR spectrum of the nanogel encapsulating silicon quantum dots (SiQDs) functionalized with a carboxylic acid group (-COOH) provides significant insights into the encapsulation mechanism and interactions within the system. In Figure 5.17, the chemical shifts observed at δ 4.13, 3.71, 3.65, 3.58, 3.42, 1.94, 1.04, and 0.90 have been carefully analyzed to confirm the presence and interaction of the Acid-SiQDs within the nanogel.

The identification of the encapsulated Acid-SiQDs was confirmed by the characteristic peaks at δ 1.04 and 0.90, which are also present in the ^1H NMR spectrum of the Acid-SiQDs. These peaks correspond to the hydrogen atoms on the alkyl chain and the carboxylic acid functional group, respectively. The preservation of these peaks indicates that the Acid-SiQDs are intact and retain their functional groups post-encapsulation, suggesting successful incorporation into the nanogel matrix.

The peaks at higher chemical shifts—specifically δ 4.13, 3.71, 3.65, 3.58, and 3.42—are indicative of the polymeric matrix of the nanogel. These shifts are not observed

in the spectra of the neat or Acid-SiQDs, indicating they arise from the polymer structure of the nanogel. These peaks suggest the presence of the nanogel's polymer backbone and possible interactions with the Acid-SiQDs.

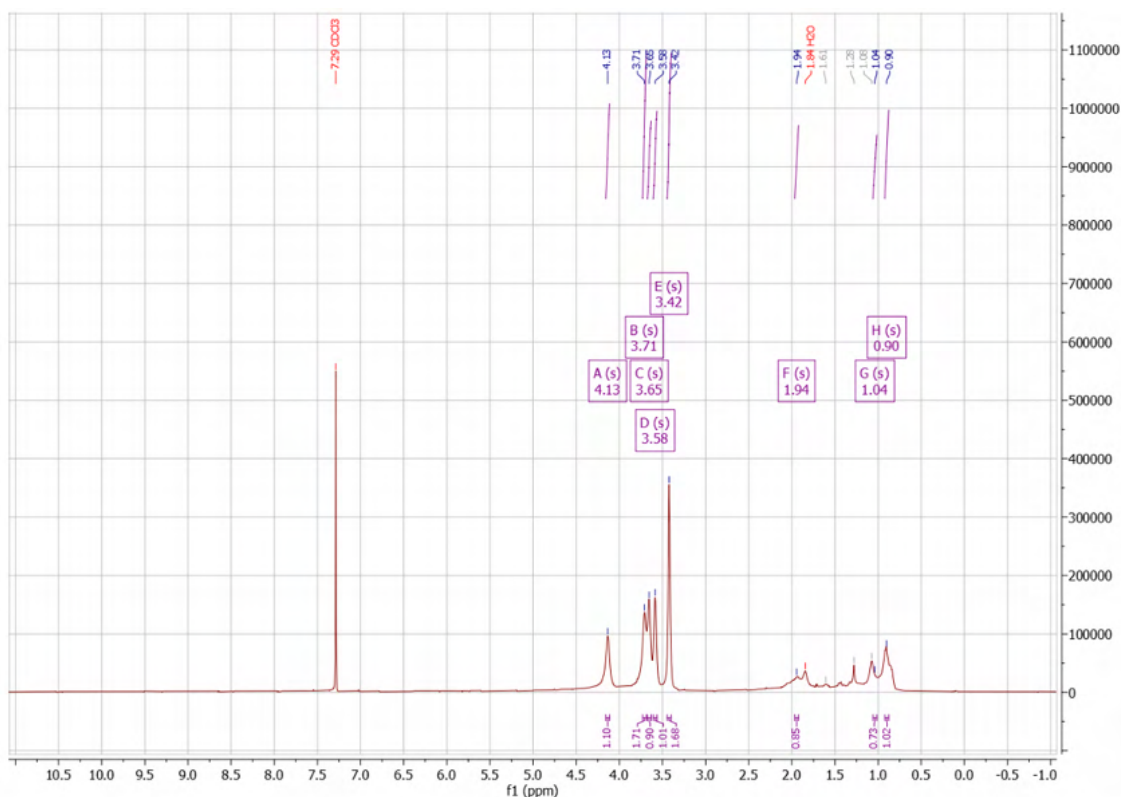


FIGURE 5.17: ^1H NMR spectrum of the nanogel encapsulating Acid-functionalized SiQDs showing distinct peaks corresponding to various proton environments

Importantly, the lack of new peaks that would indicate the formation of covalent bonds between the nanogel and the Acid-SiQDs suggests that the encapsulation is achieved through non-covalent interactions. The most plausible mechanism is through electrostatic interactions between the negatively charged carboxyl groups ($-\text{COOH}$) on the SiQDs and the positively charged or polar regions of the nanogel matrix. These interactions are critical for maintaining the stability and uniform distribution of the SiQDs within the nanogel.

The peak at δ 1.94, which corresponds to the carboxylic acid proton, supports the presence of Acid-SiQDs and suggests they are in a stable environment provided by the nanogel. The presence of peaks related to the polymer backbone (e.g., at δ 4.13) further confirms the encapsulation and stable integration of the SiQDs within the nanogel structure.

5.4 Cell Viability Assessment

The MTT assay, a widely recognized method, evaluates cellular metabolic activity as an indicator of cell health and proliferation. Healthy cell cultures are expected to maintain viability within the range of 80-95%, reflecting optimal conditions suitable for biomedical applications. For this study, a cell viability threshold above 80% was considered indicative of non-cytotoxicity, aligning with established criteria and ensuring compatibility with *in vitro* standards [156].

5.4.1 MTT Assay Results for HDFa Cells

Human dermal fibroblasts adult (HDFa) cells, representative of human skin cells, were chosen for the cytotoxicity assessment. This study tested a range of concentrations (0, 10, 25, 50, 100, 250, and 300 $\mu\text{g/ml}$) of NG-Acid-SiQDs and NG-Acid-PEO-SiQDs to evaluate their effects on cell viability. The selected range was designed to encompass low, medium, and high concentrations, providing a comprehensive analysis of cytotoxicity and potential therapeutic window. Concentrations up to 300 $\mu\text{g/ml}$ were included to simulate potential upper limits of dosage in applications like drug delivery or photodynamic therapy.

The Figure 5.18 shows the percentage of cell viability of HDFa cells treated with different concentrations of NG-Acid-SiQDs (blue columns) and NG-Acid-PEO-SiQDs (red columns). The results indicate that both NG-Acid-SiQDs and NG-Acid-PEO-SiQDs

maintain cell viability above the 80% threshold across all concentrations, suggesting low cytotoxicity and strong biocompatibility. Notably, at concentrations between 10 and 50 $\mu\text{g/ml}$, cell viability remained above 95%, which is ideal for ensuring minimal cytotoxicity while maintaining therapeutic efficacy. The slight decrease in viability at higher concentrations (250 and 300 $\mu\text{g/ml}$) is within acceptable limits for *in vitro* studies, highlighting the nanogels' safety for potential biomedical applications. For the primary objective of this study—targeted delivery and photodynamic therapy—concentrations between 50 and 300 $\mu\text{g/ml}$ are recommended.

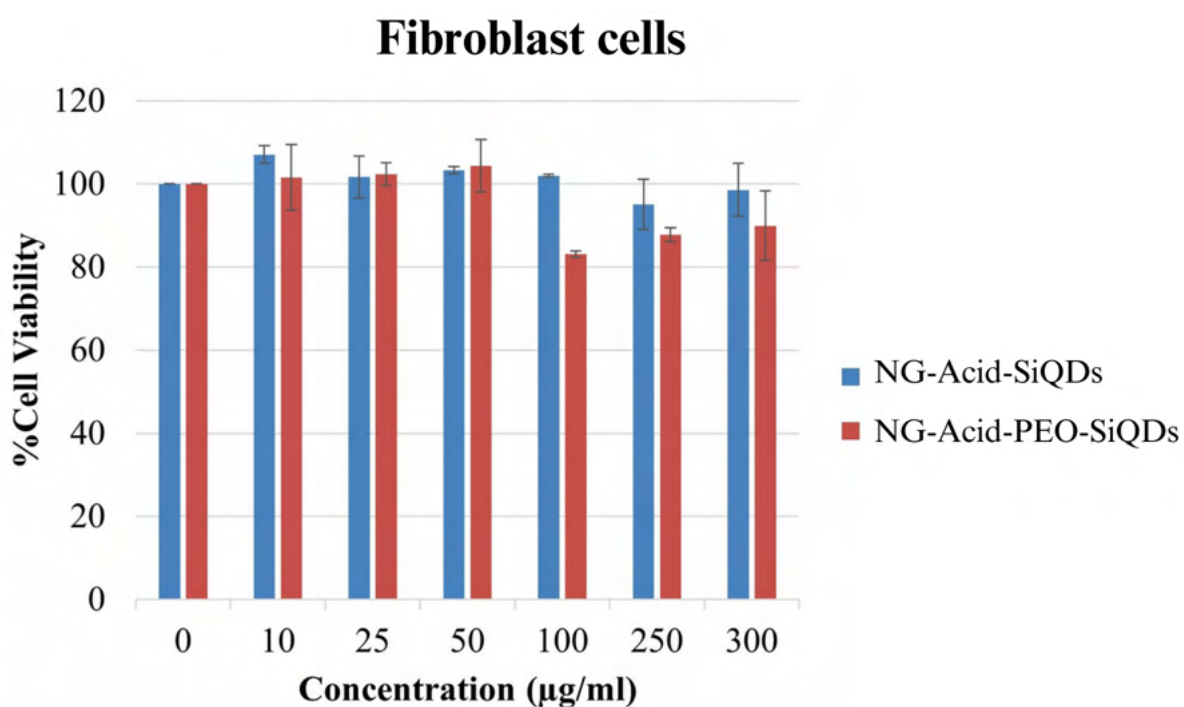


FIGURE 5.18: Cell viability of HDFa cells after 24 hours of treatment with various concentrations of NG-Acid-SiQDs and NG-Acid-PEO-SiQDs

5.5 *In Vitro* Delivery and Photodynamic Therapy Efficacy

PDT is an advanced treatment modality that utilizes a photosensitizing agent, light of a specific wavelength, and molecular oxygen to induce cytotoxic effects, primarily

through the production of ROS. The photosensitizing agents in this study are silicon quantum dots (SiQDs), specifically two types: NG-Acid-SiQDs and NG-Acid-PEO-SiQDs. Upon activation by a light source, these agents produce ROS, which target and destroy cancer cells. The efficacy of this therapy depends on the effective delivery of SiQDs to the target cells and their activation by light, leading to ROS generation and subsequent cell death. The cellular model used in this study to assess the efficacy of PDT is HeLa cells, a well-established cancer cell line.

5.5.1 MTT Assay Results for HeLa Cells

The MTT assay results for HeLa cells treated with NG-Acid-SiQDs and NG-Acid-PEO-SiQDs under light activation are presented to compare the photodynamic efficacy of these two types of SiQDs. This comparative analysis provides valuable insights into the performance of NG-SiQDs and NG-oxSiQDs in inducing cytotoxic effects through PDT.

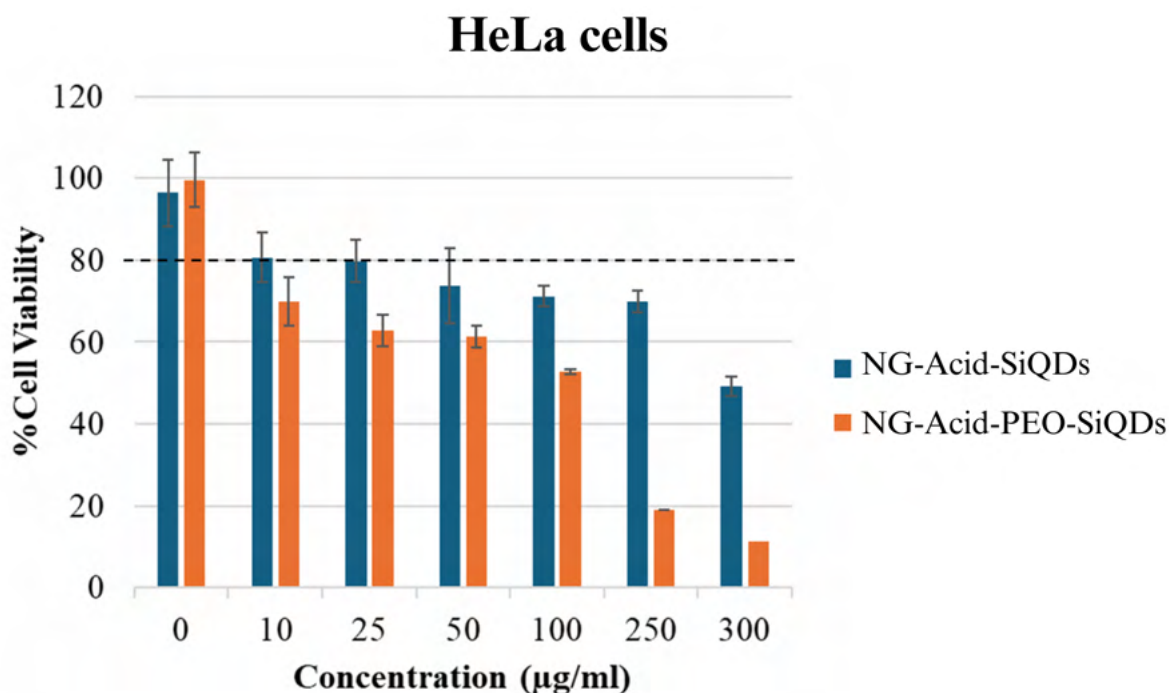


FIGURE 5.19: MTT Assay Results for HeLa Cells

The bar graph in Figure 5.19 presents the percentage of cell viability after treatment with varying concentrations (0, 10, 25, 50, 100, 250, and 300 $\mu\text{g/mL}$) of the photosensitizers. The blue bars represent NG-Acid-SiQDs, while the orange bars represent NG-Acid-PEO-SiQDs. A notable decrease in cell viability is observed with increasing concentrations, highlighting the effectiveness of PDT. NG-Acid-PEO-SiQDs exhibit a more significant reduction in cell viability compared to NG-Acid-SiQDs, suggesting higher photodynamic efficacy.

At the highest concentration tested (300 $\mu\text{g/mL}$), NG-Acid-SiQDs retained a viability of $49.24 \pm 0.00\%$, while NG-Acid-PEO-SiQDs showed a significantly lower viability of $11.22 \pm 2.37\%$. This trend is consistent across the tested concentrations, with NG-Acid-PEO-SiQDs showing consistently lower viability than NG-Acid-SiQDs: for example, at 100 $\mu\text{g/mL}$, the viability was $71.17 \pm 2.71\%$ for NG-Acid-SiQDs compared to $52.70 \pm 2.47\%$ for NG-Acid-PEO-SiQDs.

The comparative analysis of the photodynamic efficacy between NG-Acid-SiQDs and NG-Acid-PEO-SiQDs provides insights into the performance of the two photosensitizers under identical conditions. The observed differences in cell viability can be attributed to the distinct chemical structures and functional groups of the SiQDs, which influence their interaction with the nanogel matrix and the generation of ROS upon light activation. This analysis is critical for optimizing the design and application of SiQDs-based photosensitizers in photodynamic therapy, demonstrating that NG-Acid-PEO-SiQDs are more effective in inducing cell death through PDT mechanisms.

To further validate the observed differences in photodynamic efficacy between NG-Acid-SiQDs and NG-Acid-PEO-SiQDs, a statistical analysis was performed using a one-way ANOVA. The detailed results of this analysis are presented in Annex 3. This appendix includes the methodology, data, and Python code used for the analysis, which confirms that the differences in cell viability between the two treatments across the tested concentrations are statistically significant ($p < 0.05$).

CHAPTER VI

DISCUSSION

The synthesis of the nanogel via reversible addition-fragmentation chain transfer (RAFT) polymerization represents a significant advancement in the field of nanomedicine. RAFT polymerization is a controlled/living radical polymerization technique that allows for precise control over molecular weight, composition, and architecture of the polymer [157]. This method is particularly advantageous for synthesizing nanogels due to its ability to produce well-defined and uniform polymer networks, which are crucial for consistent drug delivery and therapeutic applications.

In this study, the nanogel was synthesized using 2-methacryloyloxyethyl phosphorylcholine (MPC) and diethylene glycol methyl ether methacrylate (DEGMA), both monomers selected for their biocompatibility. The RAFT polymerization process involves the use of a chain transfer agent (CTA) to mediate the polymerization, providing control over the molecular weight and distribution of the polymer chains. The RAFT agent used in this synthesis was 4-cyano-4-(phenylcarbonothioylthio) pentanoic acid (CPADB), a common CTA known for its efficiency and reliability in RAFT polymerizations. The polymerization was initiated by 4,4'-Azobis(4-cyanovaleric acid) (ACVA), which generates free radicals to propagate the polymerization.

The obtained M_n value of 10,936 g/mol for the MPC-macroCTA aligns with the range reported in the literature for similar MPC-based polymers. A study on poly(MPC-co-St) reported a number-average molecular weight (M_n) of approximately 10,000 g/mol, which is in close agreement with this result, suggesting that the polymerization and purification methods were effective and consistent with established techniques in the literature. This close similarity in M_n values indicates that the polymerization process achieved the

desired control over molecular weight, essential for maintaining specific properties of the MPC-based polymer [158].

A review on MPC polymers indicated that the M_n can be tuned from 10,000 to 100,000 g/mol by adjusting factors like monomer ratio, initiator concentration, and reaction time [158]. This tunability is crucial for customizing the polymer properties to meet specific application needs. In the context of a thermoresponsive nanogel application, an M_n of 10,936 g/mol is suitable as it ensures adequate chain length for achieving the desired thermoresponsive behavior while maintaining biocompatibility. Higher molecular weights are typically associated with enhanced mechanical properties, but for a nanogel system, the primary focus is on achieving responsive behavior and effective functionality. Thus, the M_n value obtained in this study is appropriate for the intended application, demonstrating that the synthesis conditions were well-controlled and suitable for producing the desired polymer characteristics.

Additionally, another study on MPC-BMA copolymers synthesized via a similar RAFT polymerization approach reported an M_n of 7,400 g/mol for a polymer with 29% MPC content. Although this value is somewhat lower than the result obtained here, it highlights the influence of monomer composition and polymerization conditions on the molecular weight of the final product. The higher M_n value of 10,936 g/mol suggests that the specific conditions used in this synthesis—such as the monomer ratio, initiator concentration, and reaction time—were optimized to produce longer polymer chains, which is beneficial for certain applications requiring higher molecular weights [159].

One of the critical advantages of RAFT polymerization in the synthesis of the nanogel is the ability to achieve a high degree of control over the polymer architecture. This control is evidenced by the narrow polydispersity indices (PDI) observed in the dynamic light scattering (DLS) results [160]. The nanogel synthesized via RAFT polymerization exhibited PDIs of 0.296 and 0.238 at 25°C and 37°C, respectively, indicating a uniform and well-defined polymer network. Such control over the polymer structure is

essential for ensuring consistent drug loading and release profiles, which are critical for effective therapeutic applications [151].

The comparative analysis of the nanogel at different temperatures, as shown in Figure 5.11, highlights the thermoresponsive nature of the nanogel. At 25°C, the nanogel exhibited an effective diameter of 469.4 nm with a PDI of 0.355, indicating a relatively larger and more polydisperse particle size distribution. Upon increasing the temperature to 37°C, which is closer to physiological conditions, the effective diameter significantly decreased to 153.6 nm with a PDI of 0.113, indicating a much smaller and more uniform particle size distribution. This change in size and uniformity is attributed to the thermoresponsive behavior of the DEGMA component, which causes the nanogel to collapse and become more compact at higher temperatures [161].

These findings align with prior research demonstrating that thermoresponsive nanogels, such as those synthesized using poly(N-isopropylacrylamide) (polyNIPAm), exhibit significant reductions in size when exposed to physiological temperatures [162]. Some nanogels utilize both temperature and reduction stimuli, enabling targeted delivery and degradation in specific environments, such as tumor microenvironments rich in reductive conditions [163]. Additionally, studies on the long-acting drug release capabilities of in situ forming implants have shown that tuning nanogel size can significantly impact drug release kinetics [164]. Smaller nanogels with tighter pore structures provide greater mechanical stability and sustained release profiles, which can enhance the controlled delivery of therapeutic agents in applications such as photodynamic therapy. The observed size reduction and uniformity at 37°C in this study suggest that the synthesized poly(MPC-st-DEGMA) nanogel may offer improved drug encapsulation and release efficiency, particularly for targeted therapies [161].

Experimental studies frequently use spectroscopic parameters, such as optical density and turbidity measurements, to correlate the phase behavior of nanogels with temperature changes. Bandyopadhyay et al. [162] demonstrated that volume phase transition temperature (VPTT) determination methods effectively capture the swelling-collapse behavior of poly(N-isopropylacrylamide) (pNIPAm)-based nanogels, with significant changes in hydrodynamic size and turbidity between 20°C and 50°C. These transitions highlight the shift from a hydrophilic to a hydrophobic state as temperature increases, a property essential for controlled drug delivery applications. Similarly, research on thermoresponsive pNIPAm systems has shown a marked increase in turbidity at the VPTT [164], indicating polymer network collapse and aggregation. These findings align with our observations, where the thermoresponsive behavior of the DEGMA component in our nanogel system exhibited a similar phase transition near 37°C.

The encapsulation capacity of nanogels is a critical factor influencing their functionality and effectiveness in biomedical applications, such as drug delivery and photodynamic therapy. At physiological temperatures (37°C), the thermoresponsive behavior of nanogels can significantly enhance their encapsulation efficiency. This behavior, demonstrated with DEGMA as a thermoresponsive component, results in a collapse of the polymer network, reducing particle size and improving uniformity. This structural change creates a more compact matrix ideal for encapsulating therapeutic agents or nanoparticles such as Silicon Quantum Dots (SiQDs).

Support for this concept comes from studies demonstrating the effective encapsulation of SiQDs in polymer matrices through techniques like miniemulsion polymerization. For instance, Harun et al. [165] successfully encapsulated SiQDs and Au nanoparticles (AuNPs) within polymer nanoparticles, achieving significant luminescence enhancement due to the proximity of the nanoparticles in a compact polymeric environment. This

indicates that a tightly packed structure, facilitated by temperature-induced collapse, enhances encapsulation and interactions between encapsulated components, leading to improved functional properties.

Additionally, the structural adaptation of nanogels at 37°C aligns with enhanced encapsulation efficiency. The reduction in nanogel size and increased uniformity at this temperature create a stable and efficient environment for entrapping SiQDs, reducing the loss of encapsulated material during further processes or applications. Encapsulation within a dense polymer matrix has also been shown to protect SiQDs from environmental degradation, enhancing their functional characteristics such as luminescence intensity and photostability [165].

On the other hand, considering the other key monomer of the nanogel, MPC emerges as an ideal candidate for enhancing the encapsulation of silicon quantum dots (SiQDs). The zwitterionic nature of MPC provides exceptional colloidal stability and resistance to non-specific protein adsorption [166], both of which are crucial for maintaining the functionality of encapsulated SiQDs in biological environments. Studies have shown that hydrogels functionalized with poly(MPC) exhibit high water retention (61.0%-68.3%) and outstanding optical transparency (> 90%) [167], features that significantly contribute to the stable and efficient encapsulation of SiQDs.

Furthermore, the zwitterionic properties of MPC enable a pH-responsive charge behavior, enhancing the accumulation of SiQDs in tumor tissues by responding to the acidic microenvironment [168]. This pH sensitivity facilitates targeted delivery while preserving the stability and dispersibility of the SiQDs. Additionally, the hydrophilic nature of MPC improves the dispersibility of SiQDs in aqueous media, as demonstrated in studies where encapsulated SiQDs exhibited improved hydrolytic stability and sustained fluorescence [109].

Moreover, the incorporation of silicon quantum dots (SiQDs) into the nanogel matrix was achieved without compromising the structural integrity of the nanogel. NMR

spectra confirmed the successful encapsulation, displaying characteristic peaks corresponding to both the nanogel and the SiQDs [169]. The preservation of the functional groups on the SiQDs post-encapsulation indicates that the process relied on non-covalent interactions, primarily electrostatic forces between the negatively charged carboxyl groups on the SiQDs and the polar regions of the nanogel.

Nanogel formulations encapsulating two types of functionalized SiQDs demonstrated varying biocompatibility and cytotoxicity profiles across different cell lines and concentrations. The selected concentration range (0, 10, 25, 50, 100, 250, and 300 $\mu\text{g/mL}$) follows established protocols for *in vitro* cytotoxicity testing of nanomaterials. This range is consistent with studies such as those by Peivandi et al. [170], which explored concentrations of 0, 1, 10, 50, 100, and 200 $\mu\text{g/mL}$, demonstrating a dose-dependent effect on cell survival.

For the HDFa cell line, the primary aim was to assess the safety and compatibility of the nanogel formulations. Examining a broad concentration spectrum enabled the determination of both non-cytotoxic doses (viability > 80%) and thresholds for potential cytotoxic effects. The high cell viability observed across all tested concentrations underscores the biocompatibility of the nanogels. Even at 300 $\mu\text{g/mL}$, NG-Acid-SiQDs and NG-Acid-PEO-SiQDs maintained viabilities of 98.6% and 89.9%, respectively. This indicates their suitability for applications in non-cancerous tissues such as skin regeneration. The slightly lower viability of NG-Acid-PEO-SiQDs compared to NG-Acid-SiQDs may reflect their higher encapsulation efficiency (91.7%), leading to greater cellular uptake and interactions, though remaining well within acceptable biocompatibility thresholds.

In the case of HeLa cells, the focus was on assessing the release dynamics of SiQDs from the nanogels and their photodynamic therapeutic potential. Higher concentrations (up to 100 $\mu\text{g/mL}$) were included to ensure sufficient release of SiQDs and to evaluate their effects under conditions that simulate therapeutic dosing. The inclusion of

intermediate concentrations provides a detailed understanding of dose-response relationships, ensuring both efficacy and safety in targeted photodynamic therapy applications. Therefore, the photodynamic response revealed significant cytotoxicity at higher concentrations. At 300 $\mu\text{g/mL}$, NG-Acid-SiQDs reduced cell viability to 49.2%, while NG-Acid-PEO-SiQDs achieved a dramatic reduction to 11.2%. This enhanced efficacy can be attributed to the optimized encapsulation and delivery properties of NG-Acid-PEO-SiQDs, driven by PEO functionalization. The increased intracellular concentration of NG-Acid-PEO-SiQDs facilitated greater ROS generation upon light activation, resulting in a potent photodynamic effect.

Achieving cell viabilities below 50%, as observed with NG-Acid-PEO-SiQDs (11.2%) and NG-SiQDs (49.2%) at 300 $\mu\text{g/mL}$, is a strong indicator of potent ROS activity and its cytotoxic effects. Such low viability levels signify a severe disruption of cellular redox balance, leading to oxidative damage and subsequent cell death [171]. Cancer cells, inherently more sensitive to elevated ROS due to their higher basal oxidative stress, are particularly vulnerable to these effects. Similarly, a study also identified a significant drop in viability below 50% as a critical threshold, correlating with elevated ROS production induced by increasing doses of aflatoxin B1 [172]. These findings strongly corroborate the role of ROS in enhancing the photodynamic efficacy of NG-Acid-PEO-SiQDs, establishing their capability to induce potent cytotoxic effects at therapeutic doses.

The activation of SiQDs as photosensitizers in this study was achieved using near-infrared (NIR) light, which offers superior tissue penetration compared to UV or visible light. SiQDs are highly effective for PDT due to their tunable absorption properties in the NIR region and their efficient generation of ROS. Upon NIR activation, SiQDs generate ROS through mechanisms such as direct photosensitization, where energy transfer to nearby oxygen molecules produces singlet oxygen ($^1\text{O}_2$), and electron transfer, which generates superoxide radicals ($\text{O}_2^{\bullet-}$) [173]. These ROS are highly reactive and induce oxidative damage to cellular components, ultimately causing apoptosis or necrosis in cancer

cells.

The superior photodynamic efficacy observed with NG-Acid-PEO-SiQDs can be attributed to their higher encapsulation efficiency and enhanced intracellular accumulation, resulting in greater ROS generation upon NIR activation. This aligns with previous studies that highlight SiQDs as biocompatible and efficient NIR-activated photosensitizers, with the added advantage of avoiding the heavy metal toxicity associated with traditional semiconductor quantum dots. The increased payload of Acid-PEO-SiQDs within the nanogel correlates with the significant reduction in HeLa cell viability, particularly at concentrations above 100 $\mu\text{g/mL}$, as evidenced by their pronounced photodynamic response [20], [174]. These findings underscore the importance of optimizing functionalization and dosing parameters to maximize ROS generation and therapeutic efficacy while maintaining selective cytotoxicity in PDT applications.

This photodynamic potential is further supported by the observed differences in encapsulation efficiencies and particle sizes between Acid-PEO-SiQDs and Acid-SiQDs, emphasizing the critical role of PEO functionalization in enhancing the properties of SiQDs. Acid-PEO-SiQDs achieved a significantly higher encapsulation efficiency of 91.7% within the nanogel, surpassing that of Acid-SiQDs. This higher efficiency allows for a greater payload of Acid-PEO-SiQDs, directly influencing their photodynamic efficacy by increasing the availability of SiQDs for ROS generation upon light activation.

PEO functionalization plays a pivotal role in this enhanced performance. By forming a stabilizing layer around SiQDs, PEO prevents agglomeration, reduces particle size, and ensures uniform distribution within the nanogel matrix [175]. Additionally, the hydrophilic nature of PEO improves the solubility and stability of SiQDs in physiological environments, minimizing nonspecific protein adsorption and reducing unwanted cellular interactions. This enhances the selectivity for target cells [176]. Furthermore, PEO surface modifications reduce immune responses and promote cellular uptake, as demonstrated by the comparative analysis of NG-SiQDs and NG-Acid-PEO-SiQDs.

The contrasting outcomes in HDFa and HeLa cells underscore the dual functionality of the nanogels: preserving biocompatibility in healthy cells while inducing significant cytotoxic effects in cancerous cells. The pronounced therapeutic effect observed at 300 $\mu\text{g}/\text{mL}$ in HeLa cells highlights the potential of these nanogels in targeted PDT, with NG-Acid-PEO-SiQDs demonstrating superior efficacy. This underscores the critical role of functionalization in enhancing the photodynamic properties of SiQDs, as the polyethylene oxide (PEO) modification not only improves encapsulation efficiency but also facilitates enhanced cellular uptake and ROS production under NIR activation.

These findings position NG-Acid-PEO-SiQDs as a promising therapeutic agent for PDT applications, combining high efficacy with excellent biocompatibility. Future research should focus on optimizing dosing parameters, including concentration and light exposure, while further investigating the mechanisms governing cellular uptake, ROS generation, and selective cytotoxicity. Advancing our understanding of the functionalization and behavior of SiQDs within nanogels will be crucial for their safe and effective integration into *in vivo* studies and, ultimately, clinical applications.

CONCLUSIONS

1. A copolymer nanogel was successfully synthesized using RAFT polymerization with 2-(Methacryloyloxy)ethyl phosphorylcholine (MPC) and Di(ethylene glycol) methyl ether methacrylate (DEGMA) as monomers. This method ensured precise control over polymer architecture.
2. The nanogel effectively encapsulated two types of functionalized silicon quantum dots (SiQDs): Acid-SiQDs and Acid-PEO-SiQDs. Encapsulation efficiencies reached 91.7% for Acid-PEO-SiQDs and 85.9% for Acid-SiQDs, demonstrating the nanogel's capacity to incorporate high payloads. The higher encapsulation efficiency of PEO-functionalized SiQDs further enhances their photodynamic potential, making them a promising candidate for therapeutic applications.
3. Characterization of the nanogel and SiQDs encapsulation confirmed the presence of functional groups through ^1H NMR and demonstrated thermoresponsive behavior via DLS analysis. At physiological temperatures, the nanogel exhibited reduced particle size, promoting stability, uniformity, and effective encapsulation, which are crucial for consistent therapeutic delivery.
4. Biocompatibility tests using HDFa cells revealed high cell viability (greater than 80%) across all tested concentrations of NG-SiQDs and NG-Acid-PEO-SiQDs, indicating minimal cytotoxic effects. These results confirm their suitability for applications in non-cancerous tissues, such as skin regeneration.
5. Photodynamic efficacy tests showed that NG-Acid-PEO-SiQDs had a significantly greater cytotoxic effect on HeLa cells compared to NG-SiQDs, reducing viability to 11.2% at 300 $\mu\text{g}/\text{mL}$. This enhanced therapeutic performance is attributed to the PEO functionalization, which improves ROS generation and cellular uptake under NIR light activation.

RECOMMENDATIONS

Although RAFT polymerization provides superior control over the molecular weight and architecture of the nanogel, the presence of residual chain transfer agents and other reagents could compromise the purity of the final product. It is essential to implement rigorous purification processes to remove these residuals, ensuring the safety and biocompatibility of the nanogel for biomedical applications. Future work should focus on optimizing these purification methods and employing advanced characterization techniques, such as Transmission Electron Microscopy (TEM), to analyze the structural integrity and purity of the nanogel.

While 2-(Methacryloyloxy)ethyl phosphorylcholine (MPC) and Di(ethylene glycol) methyl ether methacrylate (DEGMA) offer notable advantages in terms of biocompatibility and functionality, their scalability and cost could hinder widespread application. It is critical to develop cost-effective synthesis methods and scale-up production processes to make these advanced nanogels accessible for clinical use. Additionally, future research should explore alternative materials or synthesis strategies to reduce costs while preserving the nanogel's desirable properties.

The current study focused on *in vitro* analyses, which, while highly informative, cannot fully replicate the complexity of living organisms. *In vivo* studies are essential to validate the safety, efficacy, and biodistribution of the nanogel formulations in a physiological context. Future research should prioritize comprehensive *in vivo* testing to better understand the nanogel's therapeutic effects and behavior within biological systems.

Moreover, testing in biomimetic models, such as 3D-printed tumor microenvironments, could provide more accurate predictions of the nanogel's performance in clinical settings by replicating the complexities of tumor microenvironments.

It is also crucial to investigate the long-term stability and storage conditions of the nanogel to ensure consistent performance over time. Ensuring that the nanogel retains its structural integrity and functional properties during storage is vital for its successful translation into clinical use. Future studies should conduct accelerated aging tests and stability assessments under various environmental conditions to establish reliable storage protocols and shelf-life predictions.

The benefits of polyethylene oxide (PEO) functionalization observed in this study may have broader implications for other types of silicon quantum dots (SiQDs) and nanoparticles. Future research should investigate the generalizability of PEO modification to optimize its application across diverse nanoparticle systems. This includes exploring PEO's impact on stability, biocompatibility, and therapeutic efficacy when used with different nanoparticle cores, which will inform the design of versatile therapeutic platforms.

Finally, for more reliable and reproducible results, the MTT assay should be performed in triplicate to minimize variability. Statistical analyses beyond one-way ANOVA, such as post-hoc tests or multi-factorial analyses, should be considered to gain deeper insights into the data. These methods will enhance the robustness of conclusions and provide a stronger foundation for future developments in nanogel-based therapies.

ANNEXES

6.1 Annex 1. Protocol - Gel Permeation Chromatography (GPC) of MPC-macroCTA

Gel Permeation Chromatography (GPC) is a technique used to measure the molecular weight distribution of polymers. It separates molecules based on their size, with larger molecules eluting first and smaller molecules eluting later. This protocol outlines the steps for measuring a sample of MPC-macroCTA using GPC.

6.1.1 Steps for GPC Analysis

6.1.1.1 Sample Preparation

- Ensure the sample is dissolved in a solvent compatible with the column and detector. The solvent should not interact with the sample or the column packing material.

6.1.1.2 Column Selection

- Choose a column with the appropriate pore size to match the target molecular weight range of the sample. For wide molecular weight distributions, multiple columns can be used in series or a mixed gel type column can be employed.

6.1.1.3 Injection and Elution

- Inject the sample into the column and allow it to elute. The elution order is determined by the size of the molecules, with larger molecules eluting first.

6.1.1.4 Detection

- Use detectors such as refractometers, UV detectors, light scattering detectors, and viscometers to measure the molecular weight distribution. A triple detector approach (RI, UV, and light scattering) provides comprehensive data.

6.1.1.5 Data Analysis

- Process the data using software to calculate the molecular weight distribution and average molecular weights. The peak shape and width indicate the breadth of the molecular weight distribution.

6.2 Annex 2. Differential Scanning Calorimetry (DSC)

In Differential Scanning Calorimetry (DSC), exothermic peaks, represented as downward deflections in the thermogram, signify the release of heat due to structural changes such as crystallization or chemical reactions within the material. The rate of weight change ($\%/^{\circ}\text{C}$) in this analysis provides additional insight into the thermal decomposition dynamics of the nanogel and its encapsulated system.

The DSC thermogram presented in the figure reveals distinct thermal behavior for the two samples. The red curve, representing the neat nanogel, exhibits a pronounced exothermic peak at approximately 400.88°C . In contrast, the green curve, corresponding to the Acid-SiQDs-loaded nanogel, shows a similar exothermic peak at a slightly lower temperature, around 381.89°C . This shift indicates that the incorporation of silicon quantum dots alters the thermal stability of the nanogel matrix.

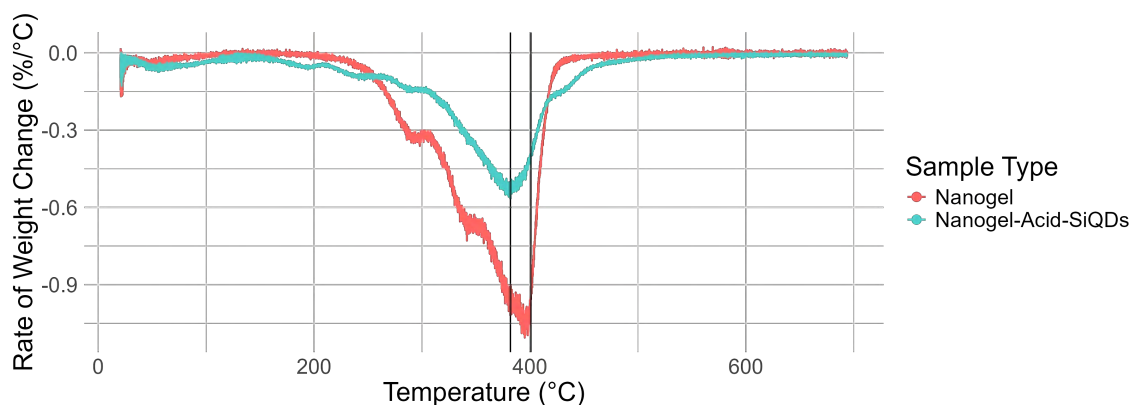


FIGURE 6.1: Differential Scanning Calorimetry (DSC) curves for the nanogel and Acid-SiQDs-loaded nanogel, showing heat flow against temperature. The blue line represents the nanogel without Acid-SiQDs, while the red line represents the nanogel with encapsulated Acid-SiQDs.

The sharper and more defined exothermic peak in the neat nanogel reflects a more abrupt thermal event, likely associated with the uniform decomposition of its polymer network. On the other hand, the slightly reduced intensity and lower peak temperature of the Acid-SiQDs-loaded nanogel suggest that the presence of silicon quantum dots disrupts the polymer structure, reducing its thermal resistance. These findings are consistent with the earlier TGA results, where the nanogel encapsulating Acid-SiQDs demonstrated enhanced stability at lower temperature ranges but began decomposing earlier compared to the neat nanogel.

This DSC analysis supports the TGA conclusion that embedding silicon quantum dots into the nanogel matrix affects its thermal stability. While the neat nanogel undergoes more abrupt thermal decomposition, the Acid-SiQDs-loaded nanogel shows a broader and more gradual thermal response, consistent with interactions between the silicon quantum dots and the polymer matrix. These interactions likely facilitate controlled thermal events, validating the compatibility of this system for applications requiring specific thermal behaviors.

6.3 Annex 3. Statistical Analysis (One-Way ANOVA)

The purpose of this analysis was to determine whether significant differences exist in the cell viability percentages (%) between the treatments (*NG-SiQDs* and *NG-Acid-PEO-SiQDs*) across the tested concentrations. A one-way ANOVA was used to assess statistical significance.

The concentrations tested and the corresponding cell viability (%) for each treatment are presented in Table 6.1.

TABLE 6.1: Cell Viability (%) for *NG-SiQDs* and *NG-Acid-PEO-SiQDs* under Different Concentrations

| Concentration ($\mu\text{g/mL}$) | <i>NG-SiQDs</i> (%) | <i>NG-Acid-PEO-SiQDs</i> (%) |
|------------------------------------|---------------------|------------------------------|
| 10 | 80.60 ± 6.65 | 69.93 ± 6.08 |
| 25 | 79.76 ± 6.02 | 62.80 ± 5.29 |
| 50 | 73.60 ± 3.78 | 61.32 ± 9.16 |
| 100 | 71.17 ± 2.71 | 52.70 ± 2.47 |
| 250 | 69.87 ± 0.65 | 19.03 ± 2.76 |
| 300 | 49.24 ± 0.00 | 11.22 ± 2.37 |

A one-way ANOVA was conducted to evaluate the differences in cell viability between the two treatments. The viability values (%) were treated as a continuous dependent variable, and the treatments (*NG-SiQDs* and *NG-Acid-PEO-SiQDs*) served as categorical independent variables.

The analysis was performed using Python with the `scipy.stats` library. The code snippet used for this analysis is provided below:

```
import pandas as pd
from scipy.stats import f_oneway

# Data
data = {
```

```

    "Concentration (µg/mL)": [10, 25, 50, 100, 250, 300],
    "NG-SiQDs NIR": [80.60, 79.76, 73.60, 71.17, 69.87, 49.24],
    "NG-oxSiQDs NIR": [69.93, 62.80, 61.32, 52.70, 19.03, 11.22]
}

# Convert to DataFrame
df = pd.DataFrame(data)

# Perform ANOVA
anova_result = f_oneway(df["NG-SiQDs NIR"], df["NG-oxSiQDs NIR"])
print(anova_result)

```

Results

The ANOVA analysis produced the following results:

- **F-statistic:** 19.57
- **p-value:** 0.00069

The p-value obtained ($p < 0.05$) indicates that the differences in cell viability between the two treatments are statistically significant. This confirms that the functionalization of SiQDs (*NG-SiQDs* vs. *NG-Acid-PEO-SiQDs*) has a meaningful impact on their cytotoxicity under the tested conditions.

The results of the ANOVA demonstrate that the differences in HeLa cell viability between *NG-SiQDs* and *NG-Acid-PEO-SiQDs* are not random. The significant decrease in cell viability observed with *NG-Acid-PEO-SiQDs*, especially at higher concentrations, can be attributed to their enhanced ROS generation and improved delivery properties, as discussed in the main text.

REFERENCES

- [1] S. Mosleh-Shirazi, M. Abbasi, M. r. Moaddeli, A. Vaez, M. Shafiee, S. R. Kasaei, A. M. Amani, and S. Hatam, “Nanotechnology Advances in the Detection and Treatment of Cancer: An Overview,” *Nanotheranostics*, vol. 6, no. 4, pp. 400–423, Aug. 2022. [Online]. Available: <https://www.ncbi.nlm.nih.gov/pmc/articles/PMC9428923/>
- [2] J. Wu, “Silicon quantum dots for optical applications,” Ph.D. dissertation, University of Minnesota, Minneapolis, MN, Aug. 2015. [Online]. Available: <https://hdl.handle.net/11299/175374>
- [3] A. Thiessen, M. Ha, R. Hooper, H. Yu, A. Oliynyk, J. Veinot, and V. Michaelis, “Silicon nanoparticles: Are they crystalline from the core to the surface?” *Chemistry of Materials*, vol. 31, 01 2019.
- [4] D. Sun, S. Wu, J. P. Martin, K. Tayutivutikul, G. Du, C. Combs, D. C. Darland, and J. X. Zhao, “Streamlined synthesis of potential dual-emissive fluorescent silicon quantum dots (siqds) for cell imaging,” *RSC Adv.*, vol. 13, pp. 26 392–26 405, Sep 2023. [Online]. Available: <http://dx.doi.org/10.1039/D3RA03669C>
- [5] A. A. H. Abdellatif, M. A. Younis, M. Alsharidah, O. Al Rugaie, and H. M. Tawfeek, “Biomedical Applications of Quantum Dots: Overview, Challenges, and Clinical Potential,” *International Journal of Nanomedicine*, vol. 17, pp. 1951–1970, May 2022. [Online]. Available: <https://www.ncbi.nlm.nih.gov/pmc/articles/PMC9076002/>

- [6] J. S. Brown, S. R. Amend, R. H. Austin, R. A. Gatenby, E. U. Hammarlund, and K. J. Pienta, “Updating the Definition of Cancer,” *Molecular Cancer Research*, vol. 21, no. 11, pp. 1142–1147, Nov. 2023. [Online]. Available: <https://www.ncbi.nlm.nih.gov/pmc/articles/PMC10618731/>
- [7] H. Sung, J. Ferlay, R. L. Siegel, M. Laversanne, I. Soerjomataram, A. Jemal, and F. Bray, “Global Cancer Statistics 2020: GLOBOCAN Estimates of Incidence and Mortality Worldwide for 36 Cancers in 185 Countries,” *CA: a cancer journal for clinicians*, vol. 71, no. 3, May. 2021. [Online]. Available: [10.3322/caac.21660](https://doi.org/10.3322/caac.21660)
- [8] Andean Health Organization – Hipólito Unanue Agreement, *Cancer Situation in the Andean Region*, 1st ed. Lima, Peru: Andean Health Organization – Hipólito Unanue Agreement, Feb. 2022. [Online]. Available: <http://www.orasconhu.org/>
- [9] Ministry of Health, “Technical guide: Clinical practice guidelines for the prevention and management of cervical cancer,” Directorate General of Strategic Health Interventions, Directorate of Cancer Prevention and Control, Lima, Peru, p. 29, Jun. 2017. [Online]. Available: <https://shorturl.at/FG9zE>
- [10] D. Debela, S. Muzazu, K. Heraro, M. Ndalama, B. Mesele, D. Haile, S. Kitui, and T. Manyazewal, “New approaches and procedures for cancer treatment: Current perspectives,” *SAGE Open Med*, vol. 9, Aug. 2021. [Online]. Available: <https://www.ncbi.nlm.nih.gov/pmc/articles/PMC8366192/>
- [11] M. E. Mejía-Rojas, A. Contreras-Rengifo, and M. Hernández-Carrillo, “Quality of life in women with breast cancer undergoing chemotherapy in Cali, Colombia,” vol. 40, no. 2, pp. 349–361, Jun. 2020. [Online]. Available: <https://revistabiomedica.org/index.php/biomedica/article/view/4971>
- [12] K. Kubota, “Recent advances and limitations of surgical treatment for pancreatic cancer,” *World Journal of Clinical Oncology*, vol. 2, no. 5, pp. 225–228, May. 2011. [Online]. Available: <https://www.ncbi.nlm.nih.gov/pmc/articles/PMC3100498/>

- [13] M. Shams, S. Abdallah, L. Alsadoun, Y. H. Hamid, R. Gasim, and A. Hassan, “Oncological horizons: The synergy of medical and surgical innovations in cancer treatment,” *Cureus*, vol. 15, no. 11, p. e49249, Nov. 2023. [Online]. Available: <https://www.cureus.com/articles/49249>
- [14] D. M. Ozog, A. M. Rkein, S. G. Fabi, M. H. Gold, M. P. Goldman, N. J. Lowe, G. M. Martin, and G. S. Munavalli, “Photodynamic Therapy: A Clinical Consensus Guide,” *Dermatologic Surgery: Official Publication for American Society for Dermatologic Surgery [et Al.]*, vol. 42, no. 7, pp. 804–827, Jul. 2016.
- [15] T. E. Kim and J.-E. Chang, “Recent Studies in Photodynamic Therapy for Cancer Treatment: From Basic Research to Clinical Trials,” *Pharmaceutics*, vol. 15, no. 9, p. 2257, Aug. 2023. [Online]. Available: <https://www.ncbi.nlm.nih.gov/pmc/articles/PMC10535460/>
- [16] X. Xu, C. Wang, P. Zhang, X. Gao, W. Guan, F. Wang, X. Li, J. Yuan, H. Dou, and G. Xu, “Enhanced Intracellular Reactive Oxygen Species by Photodynamic Therapy Effectively Promotes Chemoresistant Cell Death,” *International Journal of Biological Sciences*, vol. 18, no. 1, pp. 374–385, Jan. 2022. [Online]. Available: <https://www.ncbi.nlm.nih.gov/pmc/articles/PMC8692137/>
- [17] T. A. Debele, S. Peng, and H.-C. Tsai, “Drug Carrier for Photodynamic Cancer Therapy,” *International Journal of Molecular Sciences*, vol. 16, no. 9, pp. 22 094–22 136, Sep. 2015. [Online]. Available: <https://www.ncbi.nlm.nih.gov/pmc/articles/PMC4613299/>
- [18] N. Alvarez and A. Sevilla, “Current advances in photodynamic therapy (pdt) and the future potential of pdt-combinatorial cancer therapies,” *International Journal of Molecular Sciences*, vol. 25, no. 2, 2024. [Online]. Available: <https://www.mdpi.com/1422-0067/25/2/1023>

- [19] B. Uprety and H. Abrahamse, “Semiconductor quantum dots for photodynamic therapy: Recent advances,” *Frontiers in Chemistry*, vol. 10, Aug. 2022. [Online]. Available: <https://www.frontiersin.org/articles/10.3389/fchem.2022.946574>
- [20] F. Liu, J. Lin, Y. Luo, D. Xie, J. Bian, X. Liu, and J. Yue, “Sialic acid-targeting multi-functionalized silicon quantum dots for synergistic photodynamic and photothermal cancer therapy,” *Biomaterials Science*, vol. 11, no. 11, pp. 4009–4021, May 2023, publisher: The Royal Society of Chemistry. [Online]. Available: <https://pubs.rsc.org/en/content/articlelanding/2023/bm/d3bm00339f>
- [21] C. H. Rosmani, S. Abdullah, and M. Rusop, “Photoluminescence Characteristics of Silicon Quantum Dots Nanoparticles (SQDNs) Embedded on Glass Surface,” *Procedia Engineering*, vol. 56, pp. 750–754, Jan. 2013. [Online]. Available: <https://www.sciencedirect.com/science/article/pii/S1877705813005432>
- [22] L. Kong, J. Wang, Y. Zhang, K. Liang, J. Li, X. Xue, T. Chen, J. Ge, and P. Wang, “Lysosome-targeted silicon quantum dots theranostics for simultaneous fluorescent imaging and photodynamic therapy,” *Biomedical Materials (Bristol, England)*, vol. 18, no. 5, Jul. 2023. [Online]. Available: [10.1088/1748-605X/ace8dd](https://doi.org/10.1088/1748-605X/ace8dd)
- [23] Y. Zhang, N. Cai, and V. Chan, “Recent Advances in Silicon Quantum Dot-Based Fluorescent Biosensors,” *Biosensors*, vol. 13, no. 3, p. 311, Feb. 2023. [Online]. Available: <https://www.ncbi.nlm.nih.gov/pmc/articles/PMC10046568/>
- [24] D. Sun, S. Wu, J. P. Martin, K. Tayutivutikul, G. Du, C. Combs, D. C. Darland, and J. X. Zhao, “Streamlined synthesis of potential dual-emissive fluorescent silicon quantum dots (SiQDs) for cell imaging,” *RSC Advances*, vol. 13, no. 38, pp. 26392–26405. [Online]. Available: <https://www.ncbi.nlm.nih.gov/pmc/articles/PMC10476025/>
- [25] J. Wang, Y. Liu, F. Peng, C. Chen, Y. He, H. Ma, L. Cao, and S. Sun, “A general route to efficient functionalization of silicon quantum dots for high-performance

- fluorescent probes,” *Small (Weinheim an Der Bergstrasse, Germany)*, vol. 8, no. 15, pp. 2430–2435, Aug. 2012.
- [26] M. Mohkam, M. Sadraeian, A. Lauto, A. Gholami, S. H. Nabavizadeh, H. Esmailzadeh, and S. Alyasin, “Exploring the potential and safety of quantum dots in allergy diagnostics,” *Microsystems & Nanoengineering*, vol. 9, no. 1, pp. 1–23, Nov. 2023, publisher: Nature Publishing Group. [Online]. Available: <https://www.nature.com/articles/s41378-023-00608-x>
- [27] M. Abdelhameed, D. R. Martir, S. Chen, W. Z. Xu, O. O. Oyeneye, S. Chakrabarti, E. Zysman-Colman, and P. A. Charpentier, “Tuning the Optical Properties of Silicon Quantum Dots via Surface Functionalization with Conjugated Aromatic Fluorophores,” *Scientific Reports*, vol. 8, no. 1, p. 3050, Feb. 2018, publisher: Nature Publishing Group. [Online]. Available: <https://www.nature.com/articles/s41598-018-21181-8>
- [28] F. Erogbogbo, K.-T. Yong, I. Roy, G. Xu, P. N. Prasad, and M. T. Swihart, “Biocompatible Luminescent Silicon Quantum Dots for Imaging of Cancer Cells,” *ACS nano*, vol. 2, no. 5, pp. 873–878, May. 2008. [Online]. Available: <https://www.ncbi.nlm.nih.gov/pmc/articles/PMC2676166/>
- [29] L. Sun, H. Liu, Y. Ye, Y. Lei, R. Islam, S. Tan, R. Tong, Y.-B. Miao, and L. Cai, “Smart nanoparticles for cancer therapy,” *Signal Transduction and Targeted Therapy*, vol. 8, no. 1, pp. 1–28, Nov. 2023, publisher: Nature Publishing Group. [Online]. Available: <https://www.nature.com/articles/s41392-023-01642-x>
- [30] P. Kumari, B. Ghosh, and S. Biswas, “Nanocarriers for cancer-targeted drug delivery,” *Journal of Drug Targeting*, vol. 24, no. 3, pp. 179–191, 2016.
- [31] D. Fan, Y. Cao, M. Cao, Y. Wang, Y. Cao, and T. Gong, “Nanomedicine in cancer therapy,” *Signal Transduction and Targeted Therapy*, vol. 8, no. 1, p. 293, Aug. 2023. [Online]. Available: <https://doi.org/10.1038/s41392-023-01536-y>

- [32] S. Hanada, K. Fujioka, Y. Futamura, N. Manabe, A. Hoshino, and K. Yamamoto, “Evaluation of anti-inflammatory drug-conjugated silicon quantum dots: Their cytotoxicity and biological effect,” *International Journal of Molecular Sciences*, vol. 14, no. 1, pp. 1323–1334, 2013. [Online]. Available: <https://www.mdpi.com/1422-0067/14/1/1323>
- [33] S. S. Dhilip Kumar and H. Abrahamse, “Recent advances in the development of biocompatible nanocarriers and their cancer cell targeting efficiency in photodynamic therapy,” *Frontiers in Chemistry*, vol. 10, Aug. 2022, publisher: Frontiers. [Online]. Available: <https://www.frontiersin.org/articles/10.3389/fchem.2022.969809>
- [34] —, “Recent advances in the development of biocompatible nanocarriers and their cancer cell targeting efficiency in photodynamic therapy,” *Frontiers in Chemistry*, vol. 10, 2022. [Online]. Available: <https://www.frontiersin.org/articles/10.3389/fchem.2022.969809>
- [35] S. Shah, N. Rangaraj, K. Laxmikeshav, and S. Sampathi, “Nanogels as drug carriers - Introduction, chemical aspects, release mechanisms and potential applications,” *International Journal of Pharmaceutics*, vol. 581, p. 119268, May. 2020. [Online]. Available: <https://pubmed.ncbi.nlm.nih.gov/32240803/>
- [36] F. Jiao, “Mechanism of cross-linking, self-assembly, controlled release, and applications of nanogels in drug delivery system,” *Highlights in Science, Engineering and Technology*, vol. 40, p. 326–331, Mar. 2023. [Online]. Available: <https://drpress.org/ojs/index.php/HSET/article/view/6695>
- [37] M. A. Ward and T. K. Georgiou, “Thermoresponsive polymers for biomedical applications,” *Polymers*, vol. 3, no. 3, pp. 1215–1242, Aug. 2011. [Online]. Available: <https://www.mdpi.com/2073-4360/3/3/1215>

- [38] S. Ghaeini-Hesaroeiye, H. Razmi Bagtash, S. Boddohi, E. Vasheghani-Farahani, and E. Jabbari, “Thermoresponsive Nanogels Based on Different Polymeric Moieties for Biomedical Applications,” *Gels*, vol. 6, no. 3, p. 20, Jul. 2020. [Online]. Available: <https://www.ncbi.nlm.nih.gov/pmc/articles/PMC7559285/>
- [39] —, “Thermoresponsive nanogels based on different polymeric moieties for biomedical applications,” *Gels*, vol. 6, no. 3, p. 20, Jul. 2020, PMID: 32635573; PMCID: PMC7559285. [Online]. Available: <https://doi.org/10.3390/gels6030020>
- [40] H. Cao, F. Guo, Z. Chen, and X. Z. Kong, “Preparation of Thermoresponsive Polymer Nanogels of Oligo(Ethylene Glycol) Diacrylate-Methacrylic Acid and Their Property Characterization,” *Nanoscale Research Letters*, vol. 13, no. 1, p. 209, Jul. 2018. [Online]. Available: <https://doi.org/10.1186/s11671-018-2610-6>
- [41] A. Almohsin, B. Bai, A. Imqam, M. Wei, W. Kang, M. Delshad, and K. Sepehrnoori, *Transport of Nanogel through Porous Media and Its Resistance to Water Flow*, ser. SPE Improved Oil Recovery Conference, Apr. 2014, vol. All Days, eprint: <https://onepetro.org/SPEIOR/proceedings-pdf/14IOR/All-14IOR/SPE-169078-MS/1519033/spe-169078-ms.pdf>. [Online]. Available: <https://doi.org/10.2118/169078-MS>
- [42] V. Manimaran, R. P. Nivetha, T. Tamilanban, J. Narayanan, S. Vetriselvan, N. K. Fuloria, S. V. Chinni, M. Sekar, S. Fuloria, L. S. Wong, A. Biswas, G. Ramachawolran, and S. Selvaraj, “Nanogels as novel drug nanocarriers for CNS drug delivery,” *Frontiers in Molecular Biosciences*, vol. 10, Aug. 2023, publisher: Frontiers. [Online]. Available: <https://www.frontiersin.org/articles/10.3389/fmolb.2023.1232109>
- [43] X. Du, Y. Gao, Q. Kang, and J. Xing, “Design and applications of tumor microenvironment-responsive nanogels as drug carriers,” *Frontiers*

- in *Bioengineering and Biotechnology*, vol. 9, 2021. [Online]. Available: <https://www.frontiersin.org/journals/bioengineering-and-biotechnology/articles/10.3389/fbioe.2021.771851>
- [44] Y. Liu, L. Chen, Q. Shi, Q. Zhao, and H. Ma, “Tumor microenvironment-responsive polypeptide nanogels for controlled antitumor drug delivery,” *Frontiers in Pharmacology*, vol. 12, p. 748102, Oct. 2021, pMID: 34776965; PMCID: PMC8578677. [Online]. Available: <https://doi.org/10.3389/fphar.2021.748102>
- [45] K. Deng, Y. Wang, L. Wang, X. Fan, Z. Wu, X. Wen, W. Xie, H. Wang, Z. Zhou, P. Chen, and X. Chen, “Phase transition behaviors of poly(n-isopropylacrylamide) nanogels with different compositions induced by (-)-epigallocatechin-3-gallate and ethyl gallate,” *Molecules*, vol. 28, no. 23, Nov. 2023. [Online]. Available: <https://www.mdpi.com/1420-3049/28/23/7823>
- [46] D. Lipowska-Kur, Otulakowski, B. Trzebicka, A. Utrata-Wesołek, and A. Dworak, “Thermoresponsive Nanogels of Modified Poly((di(ethylene glycol) methyl ether methacrylate)-co-(2-aminoethyl methacrylate)s),” *Polymers*, vol. 12, no. 8, p. 1645, Jul. 2020. [Online]. Available: <https://www.ncbi.nlm.nih.gov/pmc/articles/PMC7463910/>
- [47] A. Vashist, G. Perez Alvarez, V. Andion Camargo, A. D. Raymond, A. Y. Arias, N. Kolishetti, A. Vashist, P. Manickam, S. Aggarwal, and M. Nair, “Recent advances in nanogels for drug delivery and biomedical applications,” *Biomater. Sci.*, vol. 12, pp. 6006–6018, 2024. [Online]. Available: <http://dx.doi.org/10.1039/D4BM00224E>
- [48] Q. Wang, Y. Bao, J. Ahire, and Y. Chao, “Co-encapsulation of Biodegradable Nanoparticles with Silicon Quantum Dots and Quercetin for Monitored Delivery,” *Advanced Healthcare Materials*, vol. 2, no. 3, pp. 459–466, 2013, eprint:

- <https://onlinelibrary.wiley.com/doi/pdf/10.1002/adhm.201200178>. [Online]. Available: <https://onlinelibrary.wiley.com/doi/abs/10.1002/adhm.201200178>
- [49] J. A. Kemp and Y. J. Kwon, “Cancer nanotechnology: current status and perspectives,” *Nano Convergence*, vol. 8, no. 1, p. 34, Nov. 2021. [Online]. Available: <https://doi.org/10.1186/s40580-021-00282-7>
- [50] M. H. Aziz, M. Fakhar-e Alam, M. Fatima, F. Shaheen, S. Iqbal, M. Atif, M. Talha, S. M. Ali, M. Afzal, A. Majid, T. S. AlHarbi, M. Ismail, Z. M. Wang, M. S. AlSalhi, and Z. A. Alahmed, “Photodynamic effect of ni nanotubes on an hela cell line,” *PLOS ONE*, vol. 11, no. 3, p. e0150295, Mar. 2016. [Online]. Available: <https://doi.org/10.1371/journal.pone.0150295>
- [51] P. Acedo, J. C. Stockert, M. Cañete, and A. Villanueva, “Two combined photosensitizers: a goal for more effective photodynamic therapy of cancer,” *Cell Death Disease*, vol. 5, no. 3, p. e1122, Mar. 2014. [Online]. Available: <https://doi.org/10.1038/cddis.2014.77>
- [52] S. Perrier, “50th anniversary perspective: Raft polymerization—a user guide,” *Macromolecules*, vol. 50, no. 19, pp. 7433–7447, Sep. 2017. [Online]. Available: <https://doi.org/10.1021/acs.macromol.7b00767>
- [53] L. G. Weaver, R. Stockmann, A. Postma, and S. H. Thang, “Multi-responsive (diethylene glycol)methyl ether methacrylate (DEGMA)-based copolymer systems,” *RSC Advances*, vol. 6, no. 93, pp. 90 923–90 933, Sep. 2016. [Online]. Available: <https://pubs.rsc.org/en/content/articlelanding/2016/ra/c6ra14425j>
- [54] A. Ramírez-Jiménez, C. Alvarez-Lorenzo, A. Concheiro, and E. Bucio, “Temperature-responsiveness and biocompatibility of DEGMA/OEGMA radiation-grafted onto PP and LDPE films,” *Radiation Physics and Chemistry*, vol. 99, pp. 53–61, Jun. 2014. [Online]. Available: <https://www.sciencedirect.com/science/article/pii/S0969806X14000589>

- [55] K. Ikeya, M. Fukunishi, F. Iwasa, Y. Inoue, K. Ishihara, and K. Baba, “2-Methacryloyloxyethyl Phosphorylcholine Polymer Treatment of Complete Dentures to Inhibit Denture Plaque Deposition,” *Journal of Visualized Experiments* : *JoVE*, no. 118, p. 54965, Dec. 2016. [Online]. Available: <https://www.ncbi.nlm.nih.gov/pmc/articles/PMC5226458/>
- [56] X. Tian, J. Ding, B. Zhang, F. Qiu, X. Zhuang, and Y. Chen, “Recent Advances in RAFT Polymerization: Novel Initiation Mechanisms and Optoelectronic Applications,” *Polymers*, vol. 10, no. 3, p. 318, Mar. 2018. [Online]. Available: <https://www.ncbi.nlm.nih.gov/pmc/articles/PMC6415088/>
- [57] M. Ghomi, E. N. Zare, H. Alidadi, N. Pourreza, A. Sheini, N. Rabiee, V. Mattoli, X. Chen, and P. Makvandi, “A multifunctional bioresponsive and fluorescent active nanogel composite for breast cancer therapy and bioimaging,” *Advanced Composites and Hybrid Materials*, vol. 6, no. 1, p. 51, Jan. 2023. [Online]. Available: <https://doi.org/10.1007/s42114-022-00613-0>
- [58] B. N. H. M. Neerooa, L.-T. Ooi, K. Shameli, N. A. Dahlan, J. M. M. Islam, J. Pushpamalar, and S.-Y. Teow, “Development of Polymer-Assisted Nanoparticles and Nanogels for Cancer Therapy: An Update,” *Gels*, vol. 7, no. 2, p. 60, Jun. 2021, number: 2 Publisher: Multidisciplinary Digital Publishing Institute. [Online]. Available: <https://www.mdpi.com/2310-2861/7/2/60>
- [59] D. Roy, K. Majhi, M. K. Mondal, S. K. Saha, S. Sinha, and P. Chowdhury, “Silicon Quantum Dot-Based Fluorescent Probe: Synthesis Characterization and Recognition of Thiocyanate in Human Blood,” *ACS Omega*, vol. 3, no. 7, pp. 7613–7620, Jul. 2018, publisher: American Chemical Society. [Online]. Available: <https://doi.org/10.1021/acsomega.8b00844>
- [60] D. Öztürk, Ömeroğlu, and M. Durmuş, “14 - Quantum dots in photodynamic therapy,” in *Nanomaterials for Photodynamic Therapy*, ser. Woodhead Publishing

- Series in Biomaterials, P. Kesharwani, Ed. Woodhead Publishing, Jan. 2023, pp. 401–439. [Online]. Available: <https://www.sciencedirect.com/science/article/pii/B9780323855952000098>
- [61] D. Beri, M. Jakoby, D. Busko, B. S. Richards, and A. Turshatov, “Enhancing Singlet Oxygen Generation in Conjugates of Silicon Nanocrystals and Organic Photosensitizers,” *Frontiers in Chemistry*, vol. 8, Jul. 2020, publisher: Frontiers. [Online]. Available: <https://www.frontiersin.org/journals/chemistry/articles/10.3389/fchem.2020.00567/full>
- [62] L. A. Osminkina, M. B. Gongalsky, A. V. Motuzuk, V. Y. Timoshenko, and A. A. Kudryavtsev, “Silicon nanocrystals as photo- and sono-sensitizers for biomedical applications,” *Applied Physics B*, vol. 105, no. 3, pp. 665–668, Nov. 2011. [Online]. Available: <https://doi.org/10.1007/s00340-011-4562-8>
- [63] R.-g. Wang, M.-y. Zhao, D. Deng, X. Ye, F. Zhang, H. Chen, and J.-l. Kong, “An intelligent and biocompatible photosensitizer conjugated silicon quantum dots–MnO₂ nanosystem for fluorescence imaging-guided efficient photodynamic therapy,” *Journal of Materials Chemistry B*, vol. 6, no. 28, pp. 4592–4601, Jul. 2018, publisher: The Royal Society of Chemistry. [Online]. Available: <https://pubs.rsc.org/en/content/articlelanding/2018/tb/c8tb00931g>
- [64] N. G. Özbilgin, T. Yamazaki, J. Watanabe, H.-T. Sun, N. Hanagata, and N. Shirahata, “Water-Soluble Silicon Quantum Dots toward Fluorescence-Guided Photothermal Nanotherapy,” *Langmuir: the ACS journal of surfaces and colloids*, vol. 38, no. 17, pp. 5188–5196, May 2022.
- [65] A. A. Attama, P. O. Nnamani, O. B. Onokala, A. A. Ugwu, and A. L. Onugwu, “Nanogels as target drug delivery systems in cancer therapy: A review of the last decade,” vol. 13, 2022. [Online]. Available: <https://www.frontiersin.org/articles/10.3389/fphar.2022.874510>

- [66] R. Rajput, J. Narkhede, and J. Naik, "Nanogels as nanocarriers for drug delivery: A review," *ADMET DMPK*, vol. 8, no. 1, pp. 1–15, Dec 21 2019.
- [67] L. Chambre, A. Degirmenci, R. Sanyal, and A. Sanyal, "Multi-Functional Nanogels as Theranostic Platforms: Exploiting Reversible and Nonreversible Linkages for Targeting, Imaging, and Drug Delivery," *Bioconjugate Chemistry*, vol. 29, no. 6, pp. 1885–1896, Jun. 2018, publisher: American Chemical Society. [Online]. Available: <https://doi.org/10.1021/acs.bioconjchem.8b00085>
- [68] R. Ganguly, P. Saha, L. A. Kringe, A. Pich, and N. K. Singha, "Thermoresponsive Microgels with High Loading of Zwitterions Exhibiting Superior Performance: A Macromonomer Approach," *Macromolecular Chemistry and Physics*, vol. 224, no. 1, p. 2200349, 2023, eprint: <https://onlinelibrary.wiley.com/doi/pdf/10.1002/macp.202200349>. [Online]. Available: <https://onlinelibrary.wiley.com/doi/abs/10.1002/macp.202200349>
- [69] Y. Yin, B. Hu, X. Yuan, L. Cai, H. Gao, and Q. Yang, "Nanogel: A versatile nano-delivery system for biomedical applications," vol. 12, no. 3, p. 290. [Online]. Available: <https://www.ncbi.nlm.nih.gov/pmc/articles/PMC7151186/>
- [70] E. Anooj, M. Charumathy, V. Sharma, B. V. Vibala, S. T. Gopukumar, S. I. B. Jainab, and S. Vallinayagam, "Nanogels: An overview of properties, biomedical applications, future research trends and developments," *Journal of Molecular Structure*, vol. 1239, p. 130446, Sep. 2021. [Online]. Available: <https://www.sciencedirect.com/science/article/pii/S0022286021005792>
- [71] T. Kaewruethai, C. Laomeephol, Y. Pan, and J. A. Luckanagul, "Multifunctional polymeric nanogels for biomedical applications," *Gels*, vol. 7, no. 4, 2021. [Online]. Available: <https://www.mdpi.com/2310-2861/7/4/228>
- [72] Y. Yuan, H. Zhao, Y. Guo, J. Tang, C. Liu, L. Li, C. Yao, and D. Yang, "A Programmable Hybrid DNA Nanogel for Enhanced Photodynamic Therapy of

- Hypoxic Glioma,” *Transactions of Tianjin University*, vol. 26, no. 6, pp. 450–457, Dec. 2020. [Online]. Available: <https://doi.org/10.1007/s12209-020-00260-w>
- [73] J. Yang, M.-H. Yao, L. Wen, J.-T. Song, M.-Z. Zhang, Y.-D. Zhao, and B. Liu, “Multifunctional quantum dot–polypeptide hybrid nanogel for targeted imaging and drug delivery,” *Nanoscale*, vol. 6, no. 19, pp. 11 282–11 292, Sep. 2014, publisher: The Royal Society of Chemistry. [Online]. Available: <https://pubs.rsc.org/en/content/articlelanding/2014/nr/c4nr03058c>
- [74] B. Love, *Biomaterials: A Systems Approach to Engineering Concepts*. London, United Kingdom: Academic Press is an imprint of Elsevier, 2017. [Online]. Available: <https://search.ebscohost.com/login.aspx?direct=true&scope=site&db=nlebk&db=nlabk&AN=1145081>
- [75] National Cancer Institute. Tumor grade, Aug. 2022. [Online]. Available: <https://www.cancer.gov/espanol/tipos/grados-del-tumor>
- [76] Cleveland Clinic Medical Professional. (2022, Aug.) What is cancer? symptoms, signs, types & causes. [Online]. Available: <https://my.clevelandclinic.org/health/diseases/12194-cancer>
- [77] Cleveland Clinic Medical Professional. Chemotherapy: Types & how they work. Oct. 2022. [Online]. Available: <https://my.clevelandclinic.org/health/treatments/16859-chemotherapy>
- [78] National Cancer Institute. Chemotherapy to treat cancer. National Cancer Institute, 2015. [Online]. Available: <https://www.cancer.gov/espanol/cancer/tratamiento/tipos/quimioterapia>
- [79] Cleveland Clinic Medical Professional. Radiation therapy for cancer: How does it work?, Jul. 2022. [Online]. Available: <https://my.clevelandclinic.org/health/treatments/17637-radiation-therapy>

- [80] National Cancer Institute. Radiotherapy for cancer. 2019. [Online]. Available: <https://www.cancer.gov/espanol/cancer/tratamiento/tipos/radioterapia>
- [81] R. P. Gale. Surgery for cancer. MSD Manual Consumer Version, Sep. 2022. [Online]. Available: <https://www.msdmanuals.com/home/cancer/prevention-and-treatment-of-cancer/surgery-for-cancer>
- [82] American Cancer Society. How surgery is used for cancer - curative surgery. Sep. 2019. [Online]. Available: <https://www.cancer.org/cancer/managing-cancer/treatment-types/surgery/how-surgery-is-used-for-cancer.html>
- [83] T. Li and L. Yan, “Functional Polymer Nanocarriers for Photodynamic Therapy,” *Pharmaceuticals*, vol. 11, no. 4, p. 133, Dec. 2018, number: 4 Publisher: Multidisciplinary Digital Publishing Institute. [Online]. Available: <https://www.mdpi.com/1424-8247/11/4/133>
- [84] J. Song, X. Gao, M. Yang, W. Hao, and D.-K. Ji, “Recent Advances of Photoactive Near-Infrared Carbon Dots in Cancer Photodynamic Therapy,” *Pharmaceutics*, vol. 15, no. 3, p. 760, Feb. 2023. [Online]. Available: <https://www.ncbi.nlm.nih.gov/pmc/articles/PMC10051950/>
- [85] A. Marconi, E. J. Mattioli, F. Ingargiola, G. Giugliano, T. D. Marforio, L. Prodi, M. Di Giosia, and M. Calvaresi, “Dissecting the Interactions between Chlorin e6 and Human Serum Albumin,” *Molecules*, vol. 28, no. 5, p. 2348, Mar. 2023. [Online]. Available: <https://www.ncbi.nlm.nih.gov/pmc/articles/PMC10005744/>
- [86] Q. Gao, D. Huang, Y. Deng, W. Yu, Q. Jin, J. Ji, and G. Fu, “Chlorin e6 (Ce6)-loaded supramolecular polypeptide micelles with enhanced photodynamic therapy effect against *Pseudomonas aeruginosa*,” *Chemical Engineering Journal*, vol. 417, p. 129334, Aug. 2021. [Online]. Available: <https://www.sciencedirect.com/science/article/pii/S1385894721009220>

- [87] R. Shrestha, S. K. Mallik, J. Lim, P. Gurung, T. B. T. Magar, and Y.-W. Kim, “Efficient Synthesis of Chlorin e6 and Its Potential Photodynamic Immunotherapy in Mouse Melanoma by the Abscopal Effect,” *International Journal of Molecular Sciences*, vol. 24, no. 4, p. 3901, Feb. 2023. [Online]. Available: <https://www.ncbi.nlm.nih.gov/pmc/articles/PMC9963834/>
- [88] K. Pyrzynska, K. Kilian, and M. Pegier, “Porphyrins as chelating agents for molecular imaging in nuclear medicine,” *Molecules*, vol. 27, no. 10, 2022. [Online]. Available: <https://www.mdpi.com/1420-3049/27/10/3311>
- [89] B. Chilukuri, U. Mazur, and K. W. Hipps, “Structure, Properties, and Reactivity of Porphyrins on Surfaces and Nanostructures with Periodic DFT Calculations,” *Applied Sciences*, vol. 10, no. 3, p. 740, Jan. 2020, number: 3 Publisher: Multidisciplinary Digital Publishing Institute. [Online]. Available: <https://www.mdpi.com/2076-3417/10/3/740>
- [90] S. Bardhan, S. Roy, and S. Das, “Carbon Dots: Fundamental Concepts and Biomedical Applications,” in *Nanotechnology for Biomedical Applications*, S. Gopi, P. Balakrishnan, and N. M. Mubarak, Eds. Singapore: Springer, 2022, pp. 83–108. [Online]. Available: https://doi.org/10.1007/978-981-16-7483-9_5
- [91] L. Cui, X. Ren, M. Sun, H. Liu, and L. Xia, “Carbon Dots: Synthesis, Properties and Applications,” *Nanomaterials*, vol. 11, no. 12, p. 3419, Dec. 2021. [Online]. Available: <https://www.ncbi.nlm.nih.gov/pmc/articles/PMC8705349/>
- [92] B. Domingo-Tafalla, E. Martínez-Ferrero, F. Franco, and E. Palomares-Gil, “Applications of Carbon Dots for the Photocatalytic and Electrocatalytic Reduction of CO₂,” *Molecules*, vol. 27, no. 3, p. 1081, Jan. 2022, number: 3 Publisher: Multidisciplinary Digital Publishing Institute. [Online]. Available: <https://www.mdpi.com/1420-3049/27/3/1081>

- [93] G. Gunaydin, M. E. Gedik, and S. Ayan, “Photodynamic Therapy for the Treatment and Diagnosis of Cancer—A Review of the Current Clinical Status,” *Frontiers in Chemistry*, vol. 9, Aug. 2021, publisher: Frontiers. [Online]. Available: <https://www.frontiersin.org/journals/chemistry/articles/10.3389/fchem.2021.686303/full>
- [94] F. Fan, Y. Yu, F. Zhong, M. Gao, T. Sun, J. Liu, H. Zhang, H. Qian, W. Tao, and X. Yang, “Design of Tumor Acidity-Responsive Sheddable Nanoparticles for Fluorescence/Magnetic Resonance Imaging-Guided Photodynamic Therapy,” *Theranostics*, vol. 7, no. 5, pp. 1290–1302, 2017. [Online]. Available: <https://doi.org/10.7150%2Fthno.18557>
- [95] “Realtime pdt dosimetry,” Division of Atomic Physics, 2023. [Online]. Available: <https://www.atomic.physics.lu.se/biophotonics/research/photodynamic-therapy/realtime-pdt-dosimetry/>
- [96] M. M. Kim and A. Darafsheh, “Light Sources and Dosimetry Techniques for Photodynamic Therapy,” *Photochemistry and Photobiology*, vol. 96, no. 2, pp. 280–294, 2020, eprint: <https://onlinelibrary.wiley.com/doi/pdf/10.1111/php.13219>. [Online]. Available: <https://onlinelibrary.wiley.com/doi/abs/10.1111/php.13219>
- [97] A. Bessi re, J.-O. Durand, and C. No s, “Persistent luminescence materials for deep photodynamic therapy,” *Nanophotonics*, vol. 10, no. 12, pp. 2999–3029, Sep. 2021, publisher: De Gruyter. [Online]. Available: <https://www.degruyter.com/document/doi/10.1515/nanoph-2021-0254/html>
- [98] G. Shafirstein, D. Bellnier, E. Oakley, S. Hamilton, M. Potasek, K. Beeson, and E. Parilov, “Interstitial Photodynamic Therapy—A Focused Review,” *Cancers*, vol. 9, no. 2, p. 12, Jan. 2017. [Online]. Available: <https://www.ncbi.nlm.nih.gov/pmc/articles/PMC5332935/>

- [99] P. J. Worsfold, A. Townshend, and C. F. Poole, Eds., *Encyclopedia of Analytical Science*, 2nd ed. Elsevier, Dec. 2004. [Online]. Available: <https://shop.elsevier.com/books/encyclopedia-of-analytical-science/worsfold/978-0-08-092662-9>
- [100] A. Mouahid, "Infrared thermography used for composite materials," *MATEC Web of Conferences*, vol. 191, p. 00011, 2018, publisher: EDP Sciences. [Online]. Available: https://www.matec-conferences.org/articles/mateconf/abs/2018/50/mateconf_ndecs2017_00011/mateconf_ndecs2017_00011.html
- [101] A. J. P. O. de Almeida, J. C. P. L. de Oliveira, L. V. da Silva Pontes, J. F. de Souza Júnior, T. A. F. Gonçalves, S. H. Dantas, M. S. de Almeida Feitosa, A. O. Silva, and I. A. de Medeiros, "ROS: Basic Concepts, Sources, Cellular Signaling, and its Implications in Aging Pathways," *Oxidative Medicine and Cellular Longevity*, vol. 2022, p. 1225578, Oct. 2022. [Online]. Available: <https://www.ncbi.nlm.nih.gov/pmc/articles/PMC9605829/>
- [102] H. Sies, C. Berndt, and D. P. Jones, "Oxidative stress," *Annual Review of Biochemistry*, vol. 86, no. Volume 86, 2017, pp. 715–748, 2017. [Online]. Available: <https://www.annualreviews.org/content/journals/10.1146/annurev-biochem-061516-045037>
- [103] A. Abdal Dayem, M. K. Hossain, S. B. Lee, K. Kim, S. K. Saha, G.-M. Yang, H. Y. Choi, and S.-G. Cho, "The Role of Reactive Oxygen Species (ROS) in the Biological Activities of Metallic Nanoparticles," *International Journal of Molecular Sciences*, vol. 18, no. 1, p. 120, Jan. 2017, number: 1 Publisher: Multidisciplinary Digital Publishing Institute. [Online]. Available: <https://www.mdpi.com/1422-0067/18/1/120>
- [104] K. Das and A. Roychoudhury, "Reactive oxygen species (ROS) and response of antioxidants as ROS-scavengers during environmental stress in plants," *Frontiers in Environmental Science*, vol. 2, Dec. 2014, publisher: Frontiers. [Online].

Available: <https://www.frontiersin.org/journals/environmental-science/articles/10.3389/fenvs.2014.00053/full>

- [105] B. Halliwell, “Reactive Species and Antioxidants. Redox Biology Is a Fundamental Theme of Aerobic Life,” *Plant Physiology*, vol. 141, no. 2, pp. 312–322, Jun. 2006. [Online]. Available: <https://doi.org/10.1104/pp.106.077073>
- [106] E. Pinto, T. C. S. Sigaud-Kutner, M. A. S. Leitao, O. K. Okamoto, D. Morse, and P. Colepicolo, “Heavy metal-induced oxidative stress in algae,” *Journal of Phycology*, vol. 39, no. 6, pp. 1008–1018, 2003. [Online]. Available: <https://doi.org/10.1111/j.0022-3646.2003.02-193.x>
- [107] A. Krieger-Liszkay, C. Fufezan, and A. Trebst, “Singlet oxygen production in photosystem ii and related protection mechanism,” *Photosynthesis Research*, vol. 98, no. 1, pp. 551–564, 2008. [Online]. Available: <https://doi.org/10.1007/s11120-008-9349-3>
- [108] M. L. Mastronardi, F. Hennrich, E. J. Henderson, F. Maier-Flaig, C. Blum, J. Reichenbach, U. Lemmer, C. Kübel, D. Wang, M. M. Kappes, and G. A. Ozin, “Preparation of Monodisperse Silicon Nanocrystals Using Density Gradient Ultracentrifugation,” *Journal of the American Chemical Society*, vol. 133, no. 31, pp. 11 928–11 931, Aug. 2011, publisher: American Chemical Society. [Online]. Available: <https://doi.org/10.1021/ja204865t>
- [109] S. Morozova, M. Alikina, A. Vinogradov, and M. Pagliaro, “Silicon quantum dots: Synthesis, encapsulation, and application in light-emitting diodes,” *Frontiers in Chemistry*, vol. 8, 2020. [Online]. Available: <https://www.frontiersin.org/journals/chemistry/articles/10.3389/fchem.2020.00191>
- [110] D. Beri, “Silicon quantum dots: surface matter, what next?” *Materials Advances*, vol. 4, no. 16, pp. 3380–3398, Mar. 2023. [Online]. Available: <https://pubs.rsc.org/en/content/articlelanding/2023/ma/d2ma00984f>

- [111] P. Hernández Abril, J. Iriqui, E. Leon, S. Leal-Soto, E. Álvarez, D. Berman-Mendoza, and H. Higuera, “Synthesis of silicon quantum dots using chitosan as a novel reductor agent,” *Revista Mexicana de Fisica*, vol. 67, pp. 249–254, 03 2021.
- [112] F. Erogbogbo, J. May, M. Swihart, P. N. Prasad, K. Smart, S. E. Jack, D. Korczyk, M. Webster, R. Stewart, I. Zeng, M. Jullig, K. Bakeev, M. Jamieson, N. Kasabov, B. Gopalan, L. Liang, R. Hu, S. Schliebs, S. Villas-Boas, and P. Gladding, “Bioengineering silicon quantum dot theranostics using a network analysis of metabolomic and proteomic data in cardiac ischemia,” *Theranostics*, vol. 3, no. 9, pp. 719–728, 2013. [Online]. Available: <https://doi.org/10.7150/thno.5010>
- [113] H. Yukawa, K. Sato, and Y. Baba, “Theranostics applications of quantum dots in regenerative medicine, cancer medicine, and infectious diseases,” *Advanced Drug Delivery Reviews*, vol. 200, p. 114863, Sep. 2023. [Online]. Available: <https://linkinghub.elsevier.com/retrieve/pii/S0169409X23001783>
- [114] A. Hamidu, W. G. Pitt, and G. A. Hussein, “Recent Breakthroughs in Using Quantum Dots for Cancer Imaging and Drug Delivery Purposes,” *Nanomaterials*, vol. 13, no. 18, p. 2566, Jan. 2023. [Online]. Available: <https://www.mdpi.com/2079-4991/13/18/2566>
- [115] M. Abdelhameed, S. Aly, J. T. Lant, X. Zhang, and P. Charpentier, “Energy/Electron Transfer Switch for Controlling Optical Properties of Silicon Quantum Dots,” *Scientific Reports*, vol. 8, no. 1, p. 17068, Nov. 2018, publisher: Nature Publishing Group. [Online]. Available: <https://www.nature.com/articles/s41598-018-35201-0>
- [116] X. Wang, C. Hu, Z. Gu, and L. Dai, “Understanding of catalytic ROS generation from defect-rich graphene quantum-dots for therapeutic effects in tumor microenvironment,” *Journal of Nanobiotechnology*, vol. 19, no. 1, p. 340, Oct. 2021. [Online]. Available: <https://doi.org/10.1186/s12951-021-01053-6>

- [117] X. Dou, Q. Zhang, S. N. A. Shah, M. Khan, K. Uchiyama, and J.-M. Lin, “Mos2-quantum dot triggered reactive oxygen species generation and depletion: responsible for enhanced chemiluminescence,” *Chem. Sci.*, vol. 10, pp. 497–500, 2019. [Online]. Available: <http://dx.doi.org/10.1039/C8SC03511C>
- [118] R. L. Ferreira, W. M. Jr, L. E. A. Souza, H. M. C. Navarro, L. R. de Mello, V. R. Mastelaro, T. O. Sales, C. D. A. E. S. Barbosa, A. S. Ribeiro, E. R. da Silva, M. F. Landell, and I. N. de Oliveira, “Harnessing Efficient ROS Generation in Carbon Dots Derived from Methyl Red for Antimicrobial Photodynamic Therapy,” *ACS applied bio materials*, vol. 6, no. 10, pp. 4345–4357, Oct. 2023. [Online]. Available: <https://doi.org/10.1021/acsabm.3c00541>
- [119] K. S. Soni, S. S. Desale, and T. K. Bronich, “Nanogels: An overview of properties, biomedical applications and obstacles to clinical translation,” vol. 240, pp. 109–126, 2016. [Online]. Available: <https://doi.org/10.1016/j.jconrel.2015.11.009>
- [120] X. Tian, J. Ding, B. Zhang, F. Qiu, X. Zhuang, and Y. Chen, “Recent advances in raft polymerization: Novel initiation mechanisms and optoelectronic applications,” *Polymers*, vol. 10, no. 3, 2018. [Online]. Available: <https://www.mdpi.com/2073-4360/10/3/318>
- [121] I. Neamtu, A. Rusu, A. Diaconu, L. Nita, and A. Chiriac, “Basic concepts and recent advances in nanogels as carriers for medical applications,” *Drug Deliv*, vol. 24, no. 1, pp. 539–557, Nov. 2017. [Online]. Available: <https://doi.org/10.1080%2F10717544.2016.1276232>
- [122] A. Ullah and S. I. Lim, “Nanogels: Update on the methods of synthesis and applications for cardiovascular and neurological complications,” *Journal of Drug Delivery Science and Technology*, vol. 77, p. 103879, Nov. 2022. [Online]. Available: <https://www.sciencedirect.com/science/article/pii/S1773224722007900>

- [123] S. Kalaiarasi, P. Arjun, S. Nandhagopal, J. Brijitta, A. M. Iniyan, S. G. P. Vincent, and R. R. Kannan, “Development of biocompatible nanogel for sustained drug release by overcoming the blood brain barrier in zebrafish model,” *Journal of Applied Biomedicine*, vol. 14, no. 2, pp. 157–169, Apr. 2016, publisher: Journal of Applied Biomedicine. [Online]. Available: <https://doi.org/10.1016/j.jab.2016.01.004>
- [124] A. A. K. P. R. S. S. K. Ankita Sharma, Tarun Garg and T. Markandeywar, “Nanogel—an advanced drug delivery tool: Current and future,” *Artificial Cells, Nanomedicine, and Biotechnology*, vol. 44, no. 1, pp. 165–177, 2016, PMID: 25053442. [Online]. Available: <https://doi.org/10.3109/21691401.2014.930745>
- [125] N. Rabiee, S. Hajebi, M. Bagherzadeh, S. Ahmadi, M. Rabiee, H. Roghani-Mamaqani, M. Tahriri, L. Tayebi, and M. R. Hamblin, “Stimulus-Responsive Polymeric Nanogels as Smart Drug Delivery Systems,” *Acta biomaterialia*, vol. 92, pp. 1–18, Jul. 2019. [Online]. Available: <https://www.ncbi.nlm.nih.gov/pmc/articles/PMC6661071/>
- [126] H. Kang, D. E. Suich, J. F. Davies, A. D. Wilson, J. J. Urban, and R. Kostecki, “Molecular insight into the lower critical solution temperature transition of aqueous alkyl phosphonium benzene sulfonates,” *Communications Chemistry*, vol. 2, no. 1, pp. 1–11, May 2019, publisher: Nature Publishing Group. [Online]. Available: <https://www.nature.com/articles/s42004-019-0151-2>
- [127] P. I. Siafaka, E. Özcan Bülbül, M. E. Okur, I. D. Karantas, and N. Üstündağ Okur, “The application of nanogels as efficient drug delivery platforms for dermal/transdermal delivery,” *Gels*, vol. 9, no. 9, 2023. [Online]. Available: <https://www.mdpi.com/2310-2861/9/9/753>
- [128] M. Semsarilar and V. Abetz, “Polymerizations by raft: Developments of the technique and its application in the synthesis of tailored (co)polymers,”

- Macromolecular Chemistry and Physics*, vol. 222, no. 1, p. 2000311, 2021. [Online]. Available: <https://onlinelibrary.wiley.com/doi/abs/10.1002/macp.202000311>
- [129] H. Zhang, Y. Zhai, J. Wang, and G. Zhai, “New progress and prospects: The application of nanogel in drug delivery,” *Materials Science and Engineering: C*, vol. 60, pp. 560–568, Mar. 2016. [Online]. Available: <https://www.sciencedirect.com/science/article/pii/S0928493115305749>
- [130] J. A. Brydson, “7 - Additives for Plastics,” in *Plastics Materials (Seventh Edition)*, J. A. Brydson, Ed. Oxford: Butterworth-Heinemann, Jan. 1999, pp. 124–157. [Online]. Available: <https://www.sciencedirect.com/science/article/pii/B9780750641326500486>
- [131] D.-J. Lim, “Cross-Linking Agents for Electrospinning-Based Bone Tissue Engineering,” *International Journal of Molecular Sciences*, vol. 23, no. 10, p. 5444, Jan. 2022, number: 10 Publisher: Multidisciplinary Digital Publishing Institute. [Online]. Available: <https://www.mdpi.com/1422-0067/23/10/5444>
- [132] G. C. Eastmond, “Group Transfer Polymerization,” in *Encyclopedia of Materials: Science and Technology*, K. H. J. Buschow, R. W. Cahn, M. C. Flemings, B. Ilschner, E. J. Kramer, S. Mahajan, and P. Veysière, Eds. Oxford: Elsevier, Jan. 2001, pp. 3658–3665. [Online]. Available: <https://www.sciencedirect.com/science/article/pii/B0080431526006537>
- [133] M. E. Díaz-García and A. Fernández-González, “MOLECULARLY IMPRINTED POLYMERS,” in *Encyclopedia of Analytical Science (Second Edition)*, P. Worsfold, A. Townshend, and C. Poole, Eds. Oxford: Elsevier, Jan. 2005, pp. 172–182. [Online]. Available: <https://www.sciencedirect.com/science/article/pii/B0123693977007007>

- [134] V. K. Dhote, K. Dhote, S. P. Pandey, T. Shukla, R. Maheshwari, D. K. Mishra, and R. K. Tekade, "Chapter 3 - Fundamentals of Polymers Science Applied in Pharmaceutical Product Development," in *Basic Fundamentals of Drug Delivery*, ser. Advances in Pharmaceutical Product Development and Research, R. K. Tekade, Ed. Academic Press, Jan. 2019, pp. 85–112. [Online]. Available: <https://www.sciencedirect.com/science/article/pii/B9780128179093000030>
- [135] A. Bradford, "What is a polymer?" *livescience.com*, Oct. 2017. [Online]. Available: <https://www.livescience.com/60682-polymers.html>
- [136] M. E. García, S. R. Woodruff, E. Hellemann, N. V. Tsarevsky, and R. R. Gil, "Di(ethylene glycol) methyl ether methacrylate (DEGMEMA)-derived gels align small organic molecules in methanol," *Magnetic resonance in chemistry: MRC*, vol. 55, no. 3, pp. 206–209, Mar. 2017. [Online]. Available: <https://doi.org/10.1002/mrc.4400>
- [137] S. Chatterjee and T. Ooya, "Copolymers Composed of 2-(Methacryloyloxy)ethyl Phosphorylcholine and Methacrylated Polyhedral Oligomeric Silsesquioxane as a Simple Modifier for Liposomes," *ACS Applied Polymer Materials*, vol. 2, no. 5, pp. 1909–1916, May 2020, publisher: American Chemical Society. [Online]. Available: <https://doi.org/10.1021/acsapm.0c00129>
- [138] National Center for Biotechnology Information, "Pubchem compound summary for cid 128934, 2-methacryloyloxyethyl phosphorylcholine," 2024, retrieved June 25, 2024 from <https://pubchem.ncbi.nlm.nih.gov/compound/2-Methacryloyloxyethyl-phosphorylcholine>.
- [139] S. Fujii, S. Kozuka, K. Yokota, K. Ishihara, and S.-i. Yusa, "Preparation of biocompatible poly(2-(methacryloyloxy)ethyl phosphorylcholine) hollow particles using silica particles as a template," *Langmuir*, vol. 38, no. 18, pp. 5812–5819, 2022. [Online]. Available: <https://doi.org/10.1021/acs.langmuir.2c00423>

- [140] J. G. Speight, “Chapter 14 - Monomers, Polymers, and Plastics,” in *Handbook of Industrial Hydrocarbon Processes*, J. G. Speight, Ed. Boston: Gulf Professional Publishing, Jan. 2011, pp. 499–537. [Online]. Available: <https://www.sciencedirect.com/science/article/pii/B9780750686327100143>
- [141] K. Shoyama, S. Yamaguchi, S. Ogawa, T. Takamuku, H. Kawakita, K. Ohto, and S. Morisada, “Poly(*N*-isopropylacrylamide) copolymer nanogels with thermogelling ability prepared by a single step of dispersion polymerization,” *Advanced Powder Technology*, vol. 33, no. 5, p. 103553, May 2022. [Online]. Available: <https://www.sciencedirect.com/science/article/pii/S0921883122001315>
- [142] H. F. Giles, J. R. Wagner, and E. M. Mount, “18 - Polymer Overview and Definitions,” in *Extrusion*, ser. *Plastics Design Library*, H. F. Giles, J. R. Wagner, and E. M. Mount, Eds. Norwich, NY: William Andrew Publishing, Jan. 2005, pp. 165–177. [Online]. Available: <https://www.sciencedirect.com/science/article/pii/B9780815514732500192>
- [143] M. Ghasemi, T. Turnbull, S. Sebastian, and I. Kempson, “The MTT Assay: Utility, Limitations, Pitfalls, and Interpretation in Bulk and Single-Cell Analysis,” *International Journal of Molecular Sciences*, vol. 22, no. 23, p. 12827, Nov. 2021. [Online]. Available: <https://www.ncbi.nlm.nih.gov/pmc/articles/PMC8657538/>
- [144] Merck, “MTT assay protocol for cell viability and proliferation,” Merck — Germany, n.d. [Online]. Available: <https://www.sigmaaldrich.com/CA/en/technical-documents/protocol/cell-culture-and-cell-culture-analysis/cell-counting-and-health-analysis/cell-proliferation-kit-i-mtt>
- [145] M. Ahmed, K. Ishihara, and R. Narain, “Calcium mediated formation of phosphorylcholine-based polyplexes for efficient knockdown of epidermal growth factor receptors (EGFR) in HeLa cells,” *Chemical Communications*, vol. 50, no. 22,

- pp. 2943–2946, Feb. 2014, publisher: The Royal Society of Chemistry. [Online]. Available: <https://pubs.rsc.org/en/content/articlelanding/2014/cc/c4cc00181h>
- [146] R. Narain, Y. Wang, M. Ahmed, B. F. Lai, and J. N. Kizhakkedathu, “Blood Components Interactions to Ionic and Nonionic Glyconanogels,” *Biomacromolecules*, vol. 16, no. 9, pp. 2990–2997, Sep. 2015, publisher: American Chemical Society. [Online]. Available: <https://doi.org/10.1021/acs.biomac.5b00890>
- [147] N. P. Truong, G. R. Jones, K. G. E. Bradford, D. Konkolewicz, and A. Anastasaki, “A comparison of RAFT and ATRP methods for controlled radical polymerization,” *Nature Reviews Chemistry*, vol. 5, no. 12, pp. 859–869, Dec. 2021, publisher: Nature Publishing Group. [Online]. Available: <https://www.nature.com/articles/s41570-021-00328-8>
- [148] M. Szewczyk-Łagodzińska, A. Plichta, M. Debowski, S. Kowalczyk, A. Iuliano, and Z. Florjańczyk, “Recent advances in the application of atp in the synthesis of drug delivery systems,” *Polymers*, vol. 15, no. 5, 2023. [Online]. Available: <https://www.mdpi.com/2073-4360/15/5/1234>
- [149] L. G. Weaver, R. Stockmann, A. Postma, and S. H. Thang, “Multi-responsive (diethylene glycol)methyl ether methacrylate (degma)-based copolymer systems,” *RSC Adv.*, vol. 6, pp. 90923–90933, 2016. [Online]. Available: <http://dx.doi.org/10.1039/C6RA14425J>
- [150] A. Ramírez-Jiménez, K. A. Montoya-Villegas, A. Licea-Claverie, and M. A. González-Ayón, “Tunable thermo-responsive copolymers from degma and oegma synthesized by raft polymerization and the effect of the concentration and saline phosphate buffer on its phase transition,” *Polymers*, vol. 11, no. 10, 2019. [Online]. Available: <https://www.mdpi.com/2073-4360/11/10/1657>

- [151] Y. Yuan, K. Raheja, N. B. Milbrandt, S. Beilharz, S. Tene, S. Oshabaheebwa, U. A. Gurkan, A. C. S. Samia, and M. Karayilan, “Thermoresponsive polymers with LCST transition: synthesis, characterization, and their impact on biomedical frontiers,” *RSC Applied Polymers*, vol. 1, no. 2, pp. 158–189, 2023, publisher: Royal Society of Chemistry. [Online]. Available: <https://pubs.rsc.org/en/content/articlelanding/2023/lp/d3lp00114h>
- [152] X. Huang, J. Li, Y. Araki, T. Wada, Y. Xu, and M. Takai, “Enzyme stability in polymer hydrogel–enzyme hybrid nanocarrier containing phosphorylcholine group,” *RSC Adv.*, vol. 14, pp. 18 807–18 814, 2024. [Online]. Available: <http://dx.doi.org/10.1039/D4RA02436B>
- [153] Z. Li, W. Xu, Y. Wang, B. R. Shah, C. Zhang, Y. Chen, Y. Li, and B. Li, “Quantum dots loaded nanogels for low cytotoxicity, ph-sensitive fluorescence, cell imaging and drug delivery,” *Carbohydrate Polymers*, vol. 121, pp. 477–485, 2015. [Online]. Available: <https://www.sciencedirect.com/science/article/pii/S0144861714011990>
- [154] A. Christopoulou, C. Kazamiakis, Z. Iatridi, and G. Bokias, “Controlled amphiphilicity and thermo-responsiveness of functional copolymers based on oligo(ethylene glycol) methyl ether methacrylates,” *Polymers*, vol. 16, no. 11, 2024. [Online]. Available: <https://www.mdpi.com/2073-4360/16/11/1456>
- [155] M. Ukawa, H. Akita, T. Masuda, Y. Hayashi, T. Konno, K. Ishihara, and H. Harashima, “2-methacryloyloxyethyl phosphorylcholine polymer (mpc)-coating improves the transfection activity of gala-modified lipid nanoparticles by assisting the cellular uptake and intracellular dissociation of plasmid dna in primary hepatocytes,” *Biomaterials*, vol. 31, no. 24, pp. 6355–6362, August 2010.
- [156] K. M. Eder, A. Marzi, A. M. Wågbø, J. P. Vermeulen, L. J. J. de la Fonteyne-Blankestijn, M. Rösslein, R. Ossig, G. Klinkenberg, R. J. Vandebriel, and J. Schnekenburger, “Standardization of an *in vitro* assay matrix to assess

- cytotoxicity of organic nanocarriers: a pilot interlaboratory comparison,” *Drug Delivery and Translational Research*, vol. 12, no. 9, pp. 2187–2206, Sep. 2022, epub: July 6, 2022; PMID: 35794354; PMCID: PMC9360155. [Online]. Available: <https://doi.org/10.1007/s13346-022-01203-9>
- [157] Z. An, Q. Qiu, and G. Liu, “Synthesis of architecturally well-defined nanogels via RAFT polymerization for potential bioapplications,” *Chemical Communications*, vol. 47, no. 46, pp. 12 424–12 440, Nov. 2011, publisher: The Royal Society of Chemistry. [Online]. Available: <https://pubs.rsc.org/en/content/articlelanding/2011/cc/c1cc13955j>
- [158] S. Sakaki, Y. Iwasaki, N. Nakabayashi, and K. Ishihara, “Water-soluble 2-methacryloyloxyethyl phosphorylcholine copolymer as a novel synthetic blocking reagent in immunoassay system,” *Polymer Journal*, vol. 32, no. 8, pp. 637–641, Aug. 2000. [Online]. Available: <https://doi.org/10.1295/polymj.32.637>
- [159] O. Nazarova, E. Chernova, A. Dobrodumov, Y. Zolotova, M. Bezrukova, T. Nekrasova, E. Vlasova, and E. Panarin, “New water-soluble copolymers of 2-methacryloyloxyethyl phosphorylcholine for surface modification,” *Journal of Applied Polymer Science*, vol. 138, no. 17, p. 50272, 2021, eprint: <https://onlinelibrary.wiley.com/doi/pdf/10.1002/app.50272>. [Online]. Available: <https://onlinelibrary.wiley.com/doi/abs/10.1002/app.50272>
- [160] G. Gardoni, N. Manfredini, G. Bagnato, M. Sponchioni, and D. Moscatelli, “Role of the Polymer Microstructure in Controlling Colloidal and Thermo-Responsive Properties of Nano-Objects Prepared Via RAFT Polymerization in a Non-polar Medium,” *Langmuir*, vol. 39, no. 29, pp. 10 133–10 144, Jul. 2023, publisher: American Chemical Society. [Online]. Available: <https://doi.org/10.1021/acs.langmuir.3c01065>

- [161] S.-I. Yamamoto, J. Pietrasik, and K. Matyjaszewski, “The effect of structure on the thermoresponsive nature of well-defined poly(oligo(ethylene oxide) methacrylates) synthesized by ATRP,” *Journal of Polymer Science Part A: Polymer Chemistry*, vol. 46, no. 1, pp. 194–202, 2008, eprint: <https://onlinelibrary.wiley.com/doi/pdf/10.1002/pola.22371>. [Online]. Available: <https://onlinelibrary.wiley.com/doi/abs/10.1002/pola.22371>
- [162] S. Bandyopadhyay, A. Sharma, M. A. A. Alvi, R. Raju, and W. R. Glomm, “A robust method to calculate the volume phase transition temperature (vp_{tt}) for hydrogels and hybrids,” *RSC Advances*, vol. 7, pp. 53 192–53 202, 2017, received: 15th September 2017; Accepted: 13th November 2017; First published: 17th November 2017. [Online]. Available: <https://doi.org/10.1039/C7RA10258E>
- [163] W. Gao, Z. Wang, F. Song, Y. Fu, Q. Wu, and S. Liu, “Temperature/reduction dual response nanogel is formed by in situ stereocomplexation of poly (lactic acid),” *Polymers (Basel)*, vol. 13, no. 20, p. 3492, Oct. 2021, pMID: 34685251; PMCID: PMC8540984. [Online]. Available: <https://doi.org/10.3390/polym13203492>
- [164] A. R. Town, J. Taylor, K. Dawson, E. Niezabitowska, N. M. Elbaz, A. Corker, E. Garcia-Tuñón, and T. O. McDonald, “Tuning HIV drug release from a nanogel-based in situ forming implant by changing nanogel size,” *Journal of Materials Chemistry B*, vol. 7, pp. 373–383, 2019, received: 17th June 2018; Accepted: 27th November 2018; First published: 20th December 2018. [Online]. Available: <https://doi.org/10.1039/C8TB01597J>
- [165] N. A. Harun, M. J. Benning, B. R. Horrocks, and D. A. Fulton, “Gold nanoparticle-enhanced luminescence of silicon quantum dots co-encapsulated in polymer nanoparticles,” *Nanoscale*, vol. 5, pp. 3817–3827, 2013. [Online]. Available: <http://dx.doi.org/10.1039/C3NR00421J>

- [166] M. Nagao, J. Sengupta, D. Diaz-Dussan, M. Adam, M. Wu, J. Acker, R. Ben, K. Ishihara, H. Zeng, Y. Miura, and R. Narain, “Synthesis of Highly Biocompatible and Temperature-Responsive Physical Gels for Cryopreservation and 3D Cell Culture,” *ACS Applied Bio Materials*, vol. 1, no. 2, pp. 356–366, Aug. 2018, publisher: American Chemical Society. [Online]. Available: <https://doi.org/10.1021/acsabm.8b00096>
- [167] T. P. Vales, J.-P. Jee, W. Y. Lee, S. Cho, G. M. Lee, H.-J. Kim, and J. S. Kim, “Development of poly(2-methacryloyloxyethyl phosphorylcholine)-functionalized hydrogels for reducing protein and bacterial adsorption,” *Materials*, vol. 13, no. 4, 2020. [Online]. Available: <https://www.mdpi.com/1996-1944/13/4/943>
- [168] S. Peng, Y. Men, R. Xie, Y. Tian, and W. Yang, “Biodegradable phosphorylcholine-based zwitterionic polymer nanogels with smart charge-conversion ability for efficient inhibition of tumor cells,” *Journal of Colloid and Interface Science*, vol. 539, pp. 19–29, 2019. [Online]. Available: <https://www.sciencedirect.com/science/article/pii/S0021979718314693>
- [169] S. Pandey and D. Bodas, “High-quality quantum dots for multiplexed bioimaging: A critical review,” *Advances in Colloid and Interface Science*, vol. 278, p. 102137, Apr. 2020. [Online]. Available: <https://www.sciencedirect.com/science/article/pii/S0001868619302969>
- [170] Z. Peivandi, F. H. Shirazi, S. Teimourian, G. Farnam, V. Babaei, N. Mehrparvar, N. Koohsari, and A. Ashtarinezhad, “Silica nanoparticles-induced cytotoxicity and genotoxicity in A549 cell lines,” *Scientific Reports*, vol. 14, no. 1, p. 14484, Jun. 2024. [Online]. Available: <https://doi.org/10.1038/s41598-024-65333-5>
- [171] S. J. Kim, H. S. Kim, and Y. R. Seo, “Understanding of ROS-Inducing strategy in anticancer therapy,” *Oxidative Medicine and Cellular Longevity*, vol. 2019,

- p. 5381692, Dec. 2019, pMID: 31929855; PMCID: PMC6939418. [Online]. Available: <https://doi.org/10.1155/2019/5381692>
- [172] C. E. P. Zimmermann, A. K. Machado, F. C. Cadoná, J. A. S. Jaques, K. B. Schlemmer, C. Lautert, I. B. M. Cruz, R. A. Zanette, D. B. R. Leal, and J. M. Santurio, “In-vitro cytotoxicity of aflatoxin b1 to broiler lymphocytes of broiler chickens,” *Brazilian Journal of Poultry Science*, vol. 16, no. 3, pp. 307–312, Sep. 2014. [Online]. Available: <https://doi.org/10.1590/1516-635x1603307-312>
- [173] L. Zhang, C. Zhu, R. Huang, Y. Ding, C. Ruan, and X.-C. Shen, “Mechanisms of reactive oxygen species generated by inorganic nanomaterials for cancer therapeutics,” *Frontiers in Chemistry*, vol. 9, p. 630969, Mar. 2021, pMID: 33816437; PMCID: PMC8012804. [Online]. Available: <https://doi.org/10.3389/fchem.2021.630969>
- [174] A. Escudero, C. Carrillo-Carrión, M. Carmen Castillejos, E. Romero-Ben, C. Rosales-Barrios, and N. Khir, “Photodynamic therapy: photosensitizers and nanostructures,” *Materials Chemistry Frontiers*, vol. 5, no. 10, pp. 3788–3812, 2021, publisher: Royal Society of Chemistry. [Online]. Available: <https://pubs.rsc.org/en/content/articlelanding/2021/qm/d0qm00922a>
- [175] L. Gibot, M. Demazeau, V. Pimienta, A.-F. Mingotaud, P. Vicendo, F. Collin, N. Martins-Froment, S. Dejean, B. Nottelet, C. Roux, and B. Lonetti, “Role of Polymer Micelles in the Delivery of Photodynamic Therapy Agent to Liposomes and Cells,” *Cancers*, vol. 12, no. 2, p. 384, Feb. 2020. [Online]. Available: <https://www.ncbi.nlm.nih.gov/pmc/articles/PMC7072360/>
- [176] U. Nagarajan, S. Chandra, T. Yamazaki, N. Shirahata, and F. M. Winnik, “Analysis of Silicon Quantum Dots and Serum Proteins Interactions Using Asymmetrical Flow Field-Flow Fractionation,” *Langmuir*, vol. 39, no. 22,

pp. 7557–7565, Jun. 2023, publisher: American Chemical Society. [Online].
Available: <https://doi.org/10.1021/acs.langmuir.3c00109>